Chelating innovative nanomaterials : elaboration, characterization and potential

Abdel Wahab Mouhamad

université PARIS-SACLAY

Chelating innovative nanomaterials: elaboration, characterization and potential

Nanomatériaux innovants chélatants : élaboration, caractérisation et potentiels

Thèse de doctorat de l'université Paris-Saclay

École doctorale n° 571 : Sciences Chimiques : Molécules, Matériaux, Instrumentation et Biosystèmes (2MIB)
Spécialité de doctorat : Chimie
Graduate School : Chimie. Référent : Faculté des sciences d'Orsay

Thèse préparée dans l'unité de recherche : Institut de Chimie Moléculaire et des Matériaux d'Orsay (Université Paris-Saclay, CNRS), sous la direction de **Philippe ROGER**, Professeur, Université Paris Saclay, sous le co-endradrement de **Nadine AUBRY-BARROCA,** maître de conférences**,** Université Paris Saclay, **Tamara ELZEIN**, directeur de recherche, CNRS-Liban

Thèse soutenue à Paris-Saclay, le 21 juillet 2022, par

Abdel Wahab MOUHAMAD

Composition du Jury

Jean-Maurice MALLET Directeur de recherche, Université PSL	Président
Philippe MIELE Professeur, Université de Montpellier	Rapporteur & Examinateur
François STOFFELBACH Maître de conférences, HDR, Sorbonne Université	Rapporteur & Examinateur
Gilles PONCHEL Professeur, Université Paris-Saclay	Examinateur
Philippe ROGER Professeur, Université Paris-Saclay	Directeur de thèse

THÈSE DE DOCTORAT

NNT : 2022UPASF052

université PARIS-SACLAY
ÉCOLE DOCTORALE
Sciences Chimiques: Molécules, Matériaux, Instrumentation et Biosystèmes (2MIB)

Titre : Nanomatériaux innovants chélatants : élaboration, caractérisation et potentiels.

Mots clés : Polymérisation contrôlée, nanoparticules, polymère en étoile, décontamination d'effluents aqueux.

Résumé : Les métaux lourds (radionucléides et terres rares) jouent un rôle crucial dans le mode de vie contemporain, en particulier dans les technologies tournées vers les énergies vertes et propres. Les propriétés physiques, chimiques, magnétiques et luminescentes de ces éléments sont uniques, ces « vitamines de l'industrie moderne » sont utilisées dans divers secteurs tels que les véhicules électriques et hybrides, les aimants, les batteries rechargeables et la catalyse. Jour après jour, la concentration élevée de ces métaux dans l'eau due aux activités naturelles et anthropiques, entraîne une augmentation sur l'impact environnemental et la contamination de l'eau. Dans ce contexte, l'objectif de ce projet est de proposer de nouveaux matériaux polymères innovants, capables de décontaminer les milieux aqueux des métaux lourds.

Au cours de cette thèse, deux systèmes polymères différents ont été préparés : des nanoparticules de type cœur-couronne et des polymères en étoile. Ces nouveaux matériaux ont été obtenus à partir d'un monomère dérivé de l'acide dipicolinique par polymérisation radicalaire contrôlée. Les nanoparticules ont été formées suite à l'auto-assemblage d'une série de nouveaux copolymères diblocs polystyrène-b-poly(acide 4-vinyldipicolinique) en solution aqueuse. Les polymères en forme d'étoile ont pour leur part été synthétisés à partir d'amorceurs multifonctionnels de type calix[6]arene. Le succès de ces nouveaux matériaux dans le piégeage d'europium dans un milieu aqueux a été confirmé et quantifié *via* de nombreuse technique de caractérisatiosn.

Title: Chelating innovative nanomaterials: elaboration, characterization and potential.

Keywords: Controlled polymerization, nanoparticles, star polymer, water decontamination.

Abstract: Heavy metals (radionuclide and rare earth metals) play crucial roles in the contemporary lifestyle, particularly in green and clean energy technologies. Since they have unique physical, chemical, magnetic and luminescent proprieties, these "vitamins of modern industry" are used in variety of sectors such as electric and hybrid vehicles, super magnets, rechargeable batteries, and catalysis. Day-by-day, the increase of the concentration of these metals in water due to natural and anthropogenic activities, led to an increased environmental impact and water pollution. In this context, the aim of this project was to come up with new innovative polymeric materials, capable of decontaminate aqueous media from heavy metals.

During this thesis, two different polymeric systems have been prepared: Core-shell nanoparticles and star polymers. These new materials have been synthesized from a monomer derived from dipicolinic acid, using controlled radical polymerization. The present approach includes a study of the self-assembly of a series of a new amphiphilic polystyrene-b-poly(4-vinyldipicolinic acid) diblock copolymers in aqueous solution. Beside, novel star-shaped polymers, with multifunctional calix[6]arene-type initiators were synthesized in the same aim. The success of these new materials in europium trapping in aqueous medium has been confirmed and quantified by using different characterization techniques .

Acknowledgement

First and foremost, I would like to express my most sincere gratitude and thanks to my supervisor Prof. **Philippe ROGER** for his patient guidance, vision encouragement and his support. I have been extremely lucky to have a kind, clever and unique supervisor who cared so much for my work.

Sincere gratitude also to my co-supervisor Dr. **Tamara ELZEIN** who made this collaboration possible with the CNRS-Lebanon. I am grateful for her encouragement, and expert advice even the distance that separates us. The completion of this study could not have been possible without the expertise of Dr. **Nadine Aubry-Barroca**, the funniest and the smartest supervisor I have ever had.

Secondly, I'm deeply acknowledged the rest of my thesis committee Prof. **Gilles PONCHEL**, Prof**. Philippe MIELE**, Dr. **François STOFFELBACH** and Dr. **Jean-Maurice MALLET** for accepting being in my defense committee and to evaluate my work.

I would like to address my deepest thanks to Dr. **Caroline AYMES-CHODUR** for being always there to support and to advice. I am extremely grateful to her motherly kindness. My sincere thanks also go to Dr. **Hanène Salmi** and Mr. **Ludovic COSTA**. I thank Prof. **Eric SIMONI** for scientific conversations. Also, I express my sincere gratitude to all Postdocs, PhD students and interns for the great and happiest moments we spent. Their friendships and their support did a lot for me.

I would also like to send my deepest acknowledgement to my Lebanese friends at ICMMO for their presence, their support, and their encouragement. A special thanks to all my friends here and overseas. Thank you for always bringing a smile to my face.

I would like to thank the Lebanese CNRS, the EIFFEL EXCELLENCE program, and the university of Paris Saclay for funding this project.

My endless gratitude is given to my family, who always support and respect my decisions. Without their sacrifices and their encouragement, I could have never come this far, done this much and become the person I am today. I will be always grateful.

Lastly, to me of today, thank you for never giving up because no matter where life will lead us to, we will certainly never regret this!

Table of contents

List of abbreviations

ACN	Acetonitrile
AFM	Atomic force microscopy
ATR-FTIR	Attenuated total reflection fourier transform infrared spectroscopy
ATRP	Atom Transfer Radical Polymerization
BnCl	Benzyl chloride
Calix	Calixarene
CMC	Critical micelle concentration
CRP	Controlled radical polymerization
D	Diffusion coefficient
Đ	Polymer dispersity
Dh	Hydrodynamic diameter
DP	Degree of polymerization
DCM	Dichloromethane
DLS	Dynamic light scattering
DMF	*N,N*-dimethyl formamide
	Dimethyl sulfoxide
DMSO	Inductively coupled plasma atomic emission spectroscopy
ICP-AES	Isothermal titration calorimetry
ITC	
Ln	Lanthanide
NPs	Nanoparticles
NMP	Nitroxide mediated polymerization
NMR	Nuclear magnetic resonance spectroscopy
PMMA	Poly(methyl methacrylate)
PS	Polystyrene
PVDPA	4-vinyl dipicolinic acid
PVDPM	4-vinyl dimethyl dipicolinate
PS-b-PVDPA	Polystyrene-block-poly(4-vinyl dipicolinic acid)

PS-b-PVDPM	Polystyrene-block-poly(4-vinyl dimethyl dipicolinate)
RDRP	Reversible-deactivation radical polymerization
REEs	Rare-earth elements
RT	Room temperature
SARA ATRP	Supplemental Activation Reducing Agent Atom Transfer Radical Polymerization
SEC	Size exclusion chromatography
SEM	Scanning electron microscopy
$\mathbf{T_d}$	Degradation temperature
TEM	Transmission electron microscopy
TGA	Thermogravimetric analysis
THF	Tetrahydrofuran
TPMA	Tris(2-pyridylmethyl)amine
TRLFS	Time-Resolved Laser-induced Fluorescence Spectroscopy
$\boldsymbol{\tau}$	Lifetime
$\boldsymbol{\lambda}$	Wavelength
ζ	Zeta potential

General introduction

General introduction

Production of energy and environmental remediation resemble to the two major focuses of researchers worldwide [1]. Aqueous environment, especially seawater can become a long sustainable resource for energy. For example, the recovery of uranium (U) from seawater has been investigated for over six decades in efforts to secure uranium sources for future energy production. Additionally, the increase in industrial effluents is causing serious environmental contamination. For example, the direct discharge of toxic organic compounds and metallic ions (non-biodegradable, highly toxic, and potentially carcinogenic) into seawater may seriously damage and contaminate environments.

Polymer materials play a key role for sustainable solution of both problems. However, the use of these materials should meet several strict requirements to be feasible for such processes. They should be simple, efficient, eco-friendly, non-toxic, and not expensive, which implies that they should be prepared from earth-abundant elements via environmentally friendly synthetic routes. In our lab, many studies in the last years have demonstrated promising results on the lanthanides and uranium trapping capacity in aqueous media using a novel synthesized polymer named poly(4-vinyldipicolinic acid) (PVDPA) as a new highly promising polymer [2]. Even though this functionalized material was able to successfully capture the metals in simulated water, it represents some limitation for the cleaning of large volume of water. On that matter, amphiphilic block copolymer forming self-assembly, and star polymers based on PVDPA attracted our interest.

Hazardous heavy metal pollution of wastewater is one of the most important environmental problems throughout the world. The removal of heavy metals from waste effluents has therefore become a special concern. It is evident from the literature survey of thousands of articles that various methods of removal have been extensively studied as summarized in Figure 1. A wide range of treatment technologies such as adsorption, biological process, chemical reactions, coagulation, flocculation, electrochemical techniques, flotation, filtration, ion exchange, membrane processes, precipitation, and sedimentation have been

applied with varying levels of success and these processes have also accelerated progress in the scientific community for the removal or extraction of metal.

Adsorption by chelating polymers appears to be the most promising method for heavy metals recovery from wastewater in terms of simplicity of operation, operating cost, environmental risk, and uptake capacity.

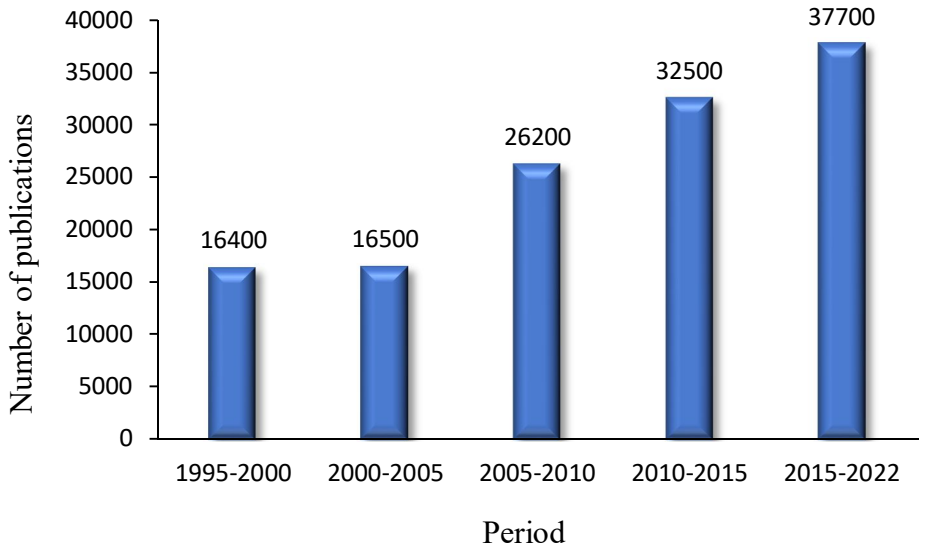

Figure 1. The increasing trend in research involving the removal of heavy metals from waste effluents, data retrieved from Google Scholar.

Standing from those points of view, this project has been implemented in several stages which are going to be presented and discussed in the three chapters of this dissertation, as presented in the general scheme (Figure 2).

Chapter **I** cover an overview of the general context of this study, state of the art in the natural and anthropogenic sources of heavy metals, its economic and environmental benefits and the technologies used for the recovery of these metals, and finally a brief discussion on controlled polymerization

Chapter **II** is divided into two main sections: the first sub-chapter deals with the synthesis of a new class of diblock copolymer polystyrene-b-poly(4-vinyldipicolinic acid), PS-b-

PVDPM via SARA-ATRP. Nanoprecipitation was used to prepare core-shell nanoparticles in aqueous solution using the prepared copolymer. The second sub-chapter presents the interactions of nanoparticles with different metal species. The structural, chemical and optical properties of the as-prepared complexes are studied using several analytical techniques.

Chapter **III** focuses on the synthesis of star polymers. Herein, two hexafunctional calixarenes derivatives were synthesized and used to initiate the ATRP of 4-vinyl dimethyl dipicolinate (VDPM) by the core-first method called. The effects of the structure of the initiator on the kinetic of the polymers are studied. In the sub-chapter, some of these obtained star polymers have been tested for their complexation properties which are also going to be discussed.

Finally, we summarize achievements of this research as well as perspectives for future work

The complete study brings new results regarding the synthesis of new polymers *via* novel routes. Amphiphilic diblock copolymers, hexafunctional star polymers have been synthesized and characterized. These new materials have been proved to be highly performing in heavy metals trapping.

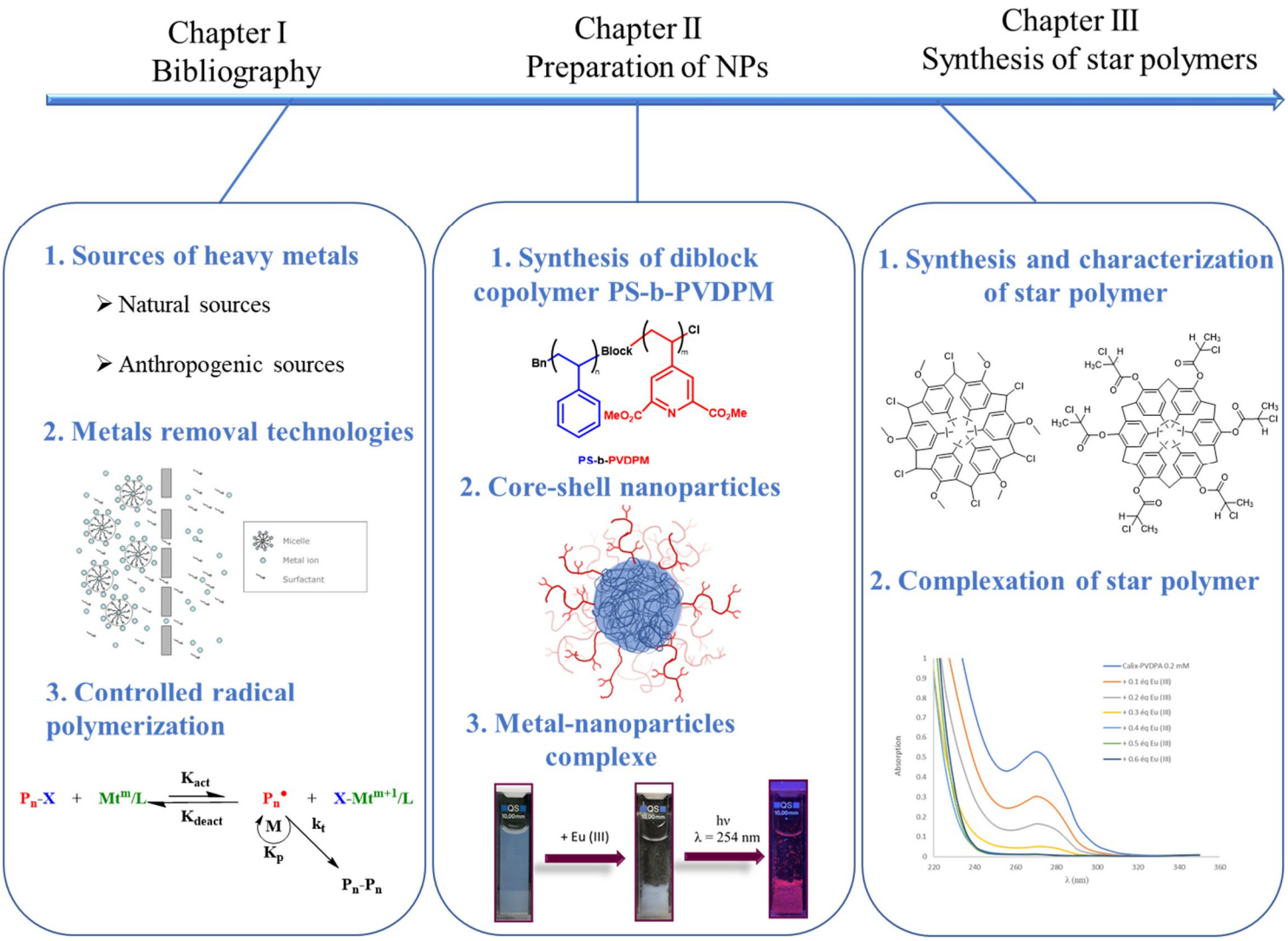

Figure 2. General organization of the manuscript.

Chapter I. State of the art

This chapter is an introduction presenting an overview on different aspects of the research; it includes major knowledge about sources, distribution, toxicological and economical effects of heavy metals. In addition, this chapter will focus on the different prospects for heavy metals removal technologies and the advancement and revolution of these techniques. A special attention will be paid to the controlled radical polymerization methods: Atom Transfer Radical Polymerization (ATRP) and Supplemental activator and reducing agent (SARA-ATRP) as it will be used to prepare star polymer and amphiphilic copolymers respectively in this manuscript.

I.1. Heavy metal

During the last hundred years, industrialization has grown at a fast rate. It has thus increased the demand for exploitation of the earth's natural resources at a careless speed. Heavy metals are one of the most important compounds, which are relatively scarce in the earth's crust but are present in many aspects of modern life, used in many applications for their admirable physical and chemical properties. The heavy metals can be defined as having a high atomic number, atomic weight with a density greater than 5.0 g/cm^3, they are good heat and electricity conductor and its compounds are colored and have high stability which is not quickly affected by the weather, they include some metalloids, transition metals, basic metals, lanthanides and actinides. Some heavy metals are either essential nutrients usually iron, cobalt, and zinc or relatively harmless such as ruthenium, silver, and indium. Other heavy metals like cadmium, mercury, uranium and lead are considered highly toxic.

I.1.1. Lanthanides

According to IUPAC (International Union of Pure and Applied Chemistry), the lanthanide series, whose generic symbol is Ln, comprises the fifteen chemical elements between lanthanum (Z=57) and lutetium (Z=71) in the periodic table, are often collectively known as the rare-earth elements “REE” or rare-earth metals which designates the series of lanthanides as follows: lanthanum (La), cerium (Ce), praseodymium (Pr), neodymium (Nd), promethium (Pm), samarium (Sm), europium (Eu), gadolinium (Gd), terbium (Tb),

dysprosium (Dy), holmium (Ho), erbium (Er), thulium (Tm), ytterbium (Yb), and lutecium (Lu), in addition to the elements scandium (Sc, Z=21) and yttrium (Y, Z=39), All of them can be found in nature, in form of compounds, except promethium, which is obtained by synthetic methods [3].

Lanthanides have similar physical and chemical properties. Their electrons of valence are found in the 4f orbitals. Because the electrons of the 4f orbitals are strongly shielded by electrons of the upper layers 5s and 5p [4], they participate weakly in chemical bonds and are not affected by the environment of the ion. The most common oxidation state for lanthanides is Ln^{3+}. However, thanks to coordination chemistry, a wide variety of complexes can be obtained. The coordination numbers of lanthanides vary from 6 to 12, the most frequent values being 8 and 9. Ln^{3+} ions have a preference for ligands donors O and F, but can form complexes with other ligands as Lewis base type.

Lanthanides are known for their emission spectrum with narrow emission peaks whose spectral positions do not vary according to the matrix. Ions with a higher luminous intensity are samarium, dysprosium, europium and terbium (Sm^{3+} 643 nm, Dy^{3+} 574 nm, Eu^{3+} 615 nm, Tb^{3+} 545 nm). The lanthanum, lutetium and gadolinium are not luminescent, while all the others lanthanides have an intermediate intensity.

During the past years, a lot of investments are made in order to find exploitable regions for the extraction of rare earths. The resurgence of prospecting comes from the fact that, recently, China is limiting its exports of rare earths. So, several large companies, especially in the electronics and automotive sector, are looking for another source supply for these metals. Lanthanides are critical elements for a wide range of application in different industries, as well as in agriculture, medicine and consumer products such as nuclear, petroleum, electronic (e.g., mobile phones, color TV sets), military and automotive sectors [5].

I.1.2. Actinides

The known radioactive nuclides are distributed among the 15 elements approximately as follows: actinium (Ac), thorium (Th), protactinium (Pa), uranium (U), neptunium (Np),

plutonium (Pu), americium (Am), curium (Cm), californium (Cf), einsteinium (Es), and fermium (Fm), berkelium (Bk), mendelevium (Md), nobelium (No) and lawrencium (Lr). Because the two sets of atomic orbitals, the 5f and 6d, are very close in energy and both capable of contributing to bonding, the actinides are of particular interest. This near degeneracy is most apparent in the early members of the actinide series, where atomic ground states can occupy both 5f and 6d orbitals. For example, the ground state configuration of the thorium atom is $6d^2\ 7s^2$ [6]. Each of the actinide elements has a number of isotopes, all radioactive and some of which can be obtained in isotopic pure form [3]. Their ability to form stable complexes is preferable with ligands bearing softer donors (Cl, N, S) as defined by the Pearson theory [7]. Recent studies frequently focus on ligands containing mixed N,O-donors [8]. 2,6-bis(5,6-dipropyl-1,2,4-triazin-3-yl)pyridine (BTP) and its derivatives whose have become the most powerful extractants, separating actinides (An) and lanthanides (Ln) from nuclear waste. This success was partly attributed to the soft donor nitrogen atoms in an aromatic environment [9][10].

Ever since their discovery, the fundamental properties of the actinides have been of substantial interest to scientists [11]. For example, 10.2 % of electricity produced by nuclear in 2020. Hence, the nuclear electrical generating capacity is projected to increase by about 20% by 2030 and more than the double by 2050 compared with 2020 capacity [12].

David S. Sholl and Ryan P. Lively were reported in Nature article/2016, “Seven chemical separations to change the world” [13]. We have focused on two chemical separations of this list: Uranium and rare earth metals. Due to the increasing demand of nuclear energy, and the fact that conventional uranium reserves could be depleted within a century, uranium recovery from seawater considered one of chemical that will change the word. Similarly, lanthanides are used in magnets, in renewable-energy technologies and as catalysts in petroleum refining, etc. Which make them indispensable chemical in our life.

I.2. Sources of heavy metals

I.2.1. Natural sources

The studies have shown that the bedrock mineralogy and lithology largely contribute to the heavy metals distribution patterns of soils, sediments, waters, and plants. However, REE are naturally found in very low concentration in the environment, they are widely presented in mineral deposits such as silicates (about 43% of all REE minerals), carbonates (23%), oxides (14%), phosphates, and related hydroxy salts (14%) [14]. Moreover, surficial waters (rivers, lakes ..) play an important role in the transport and distribution of REE between environmental compartments. For example, the concentrations of REE in about 500 stream waters of Eastern Canada varied from < 0.005 to 11.540 µg/L, with an average of 0.253 µg/L [15], whereas very low concentration of REE in natural fresh water from the tropical Terengganu River basin, Malaysia. Similarly, Actinide elements are ubiquitous in nature [16]. The world's oceans for example contain 99.9 % of the earth's uranium, with over 4 billion tons. It was proposed shortly after World War II to extract some of this uranium. However, due to the rapidly increasing demand, it was decided that efforts should be directed toward the then-known ores, owing to the enormous economic and technical challenges of extracting the extremely diluted uranium (3.3 ppb) from natural waters [17].

Table 1 shows the vast amounts of trace metals at low concentrations in the seawater.

Element	Concentration (ppb)	Element	Concentration (ppb)
Cl	1.91×10^7	Fe	1-2
Na	1.08×10^7	Ni	0.5-1.7
Mg	1.33×10^6	V	1.5
Ca	4.22×10^5	Ti	1
K	3.8×10^5	Cu	0.6
Li	170	Mn	0.25
Zn	4	Co	0.05
U	3-3.3	Pb	0.03
Al	2		

Table 1. Various elements in seawater [18].

I.2.2. Anthropogenic sources

The increase of the concentration of heavy metals in water is usually due to anthropogenic activities, such as industrial and mining wastes. Due to the mining activities and processing of metal ores, large amounts of metals are released into natural water bodies in two ways: the direct discharge of industrial wastewater which contains high levels of metals and the leaching process in soils which are enriched in heavy metals. Recent studies have shown that fossil fuel combustion and metallurgic processes greatly contribute to the REE emissions to soils, waters, air, and biota [19]. As a result, concentrations of heavy metals in water bodies have been significantly enhanced.

Liang et al. summarized the biogeochemical cycle of REEs in Chinese REE mining areas [20]. Figure 3, shows the range of total REE contents in various environmental media varied significantly. For example, the distribution patterns and transportation characteristics of REEs of different soil profiles and of different parts (4 soil layers were observed at the profile: A (0 ± 20 cm depth), B (20 ± 150 cm depth), C (150 ± 400 cm depth), and D (rock) were studied. It is worth mentioning that, the levels of REEs in REE mining areas of China are obviously higher than those in non-mining areas.

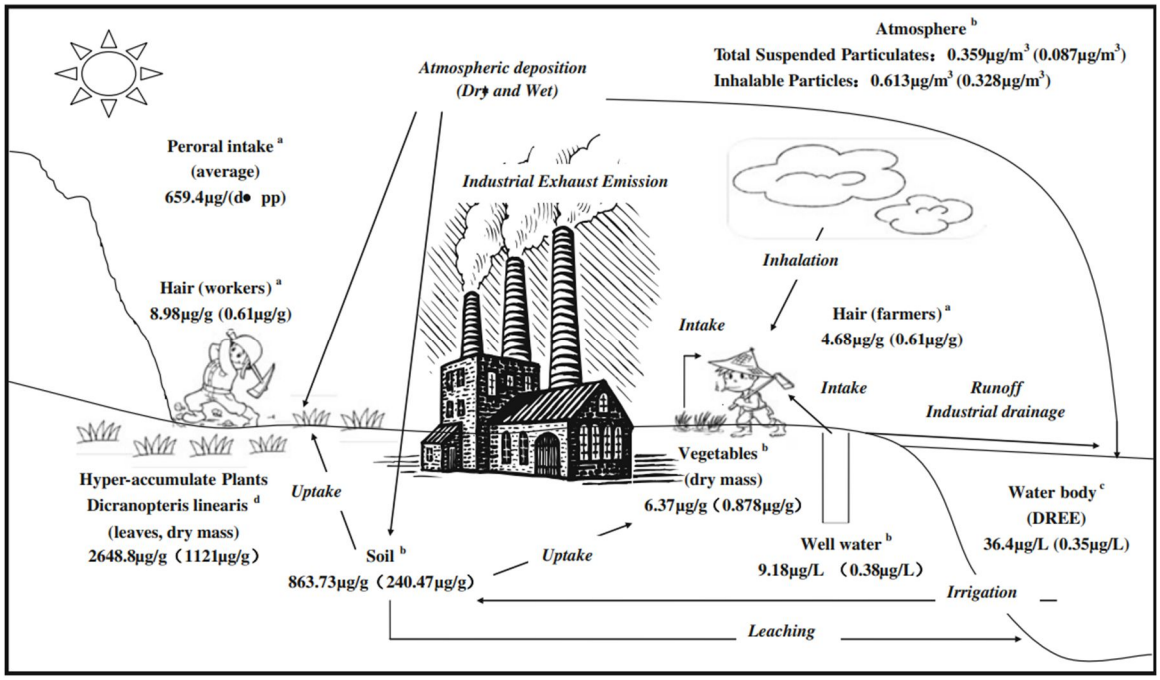

Figure 3. The average contents of REEs in Chinese REE mining area [20].

For more than 50 years, nuclear weapons production, testing, and energy generation have polluted the environment around the world. In other words, development of the nuclear energy applications has resulted in a significant environmental contamination because of both the regulated discharges and several accidents. Furthermore, the disposal of man-made radionuclides from nuclear waste or spent nuclear fuel in geological media, which has been implemented in a number of countries, is a potential source of environmental contamination.

In the other hand, after the severe accident at the Fukushima nuclear power plant (NPP), thousands of tons of seawater were injected to cool the high-temperature reactor cores after the Tokyo Electric Power Company (TEPCO) Fukushima Daiichi Nuclear Power Station (NPS) station blackout [21] resulting high water contamination by the radioactive materials [22].

Many studies have been proved the sorption of radionuclides to colloid particles [23][24]. In this aim, Novikov et al [25] have investigated the colloidal actinide speciation depending on the geochemical. Several groundwater samples chosen for the experiments were taken at the depth of 80–100 m in the Karachay pollution zone adjacent to the Production Association "Mayak" (PAM) nuclear facility in Russia and at the depth of 350–400 m near the Siberian Chemical Combine (SCC) liquid radioactive waste repository in Tomsk region.

Figure 4 depicts the association of actinides with colloids of different sizes for both groundwater samples. Three types of colloids were recognized as follows: aquatic colloids, real colloids, and carrier colloids. Aquatic colloids were represented by mineral particles, hydrolyzed metal ion precipitates, high-molecular weight organic substances etc. Real colloids were typical for some low-soluble radionuclides, e.g. tetravalent actinides or Tc(IV), which produced aggregates of hydrolyzed species through oxo- or hydroxyl bridge formation. When radionuclides were absorbed by aquatic colloids, the so-called "carrier colloids" were generated. It is not surprising that soluble uranium U (VI) and neptunium Np (V) are found in the filtrate for samples collected under oxidizing conditions, while plutonium and americium are found in colloids. The fraction of actinides and other elements bound to colloids decreased in the following sequence: Pu > Zr ≥ Am ≥ Eu » Np

> U. The share of U and Pu bound to nanocolloids increased upon dilution of waste with groundwater.

The reverse is seen under reducing conditions where all actinides are predominantly associated with colloids. For groundwater samples from Anoxic Zone, the following sequence of radionuclide inclusion into colloidal particles was observed: U > Np > Pu ≥ Am ≥ Zr ≥ Zn ≥ Eu.

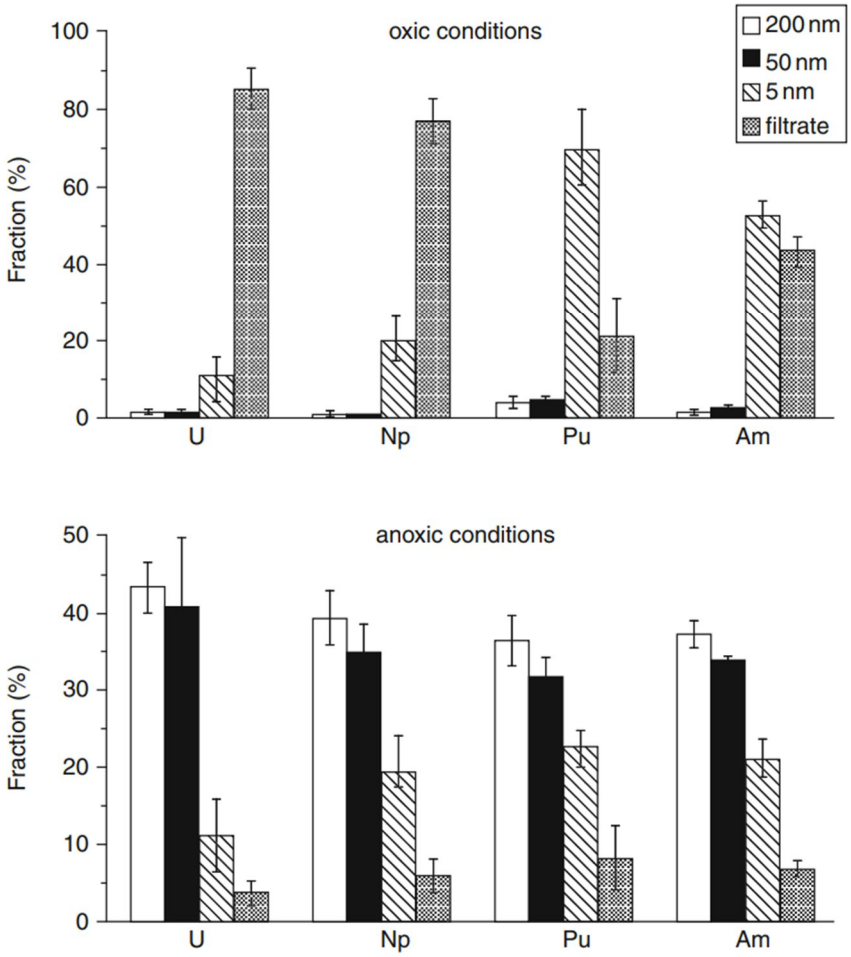

Figure 4. Association of actinides with colloid particles of different size in groundwater samples collected in oxic zone (top) and in anoxic zone (bottom). Average values and uncertainties [25].

I.3. Heavy metals toxicity

REEs have widespread use and importance for industrial applications due to their metallurgical, optical and electronic properties. This growing demand for the REEs have also led to an increased environmental impact and water pollution from numerous REE commercial products and rare earth (RE) metal mines. The increasing use of REE in different areas of human activity has led to environmental contamination and bioaccumulation in food chain. However, exposure to heavy metals, even at trace level, is believed to be a risk for human beings [26][27]. Inhalation is considered as the most frequent mode of contamination in the industry. For example, due to extremely similarity between the ionic radius of Gd^{3+} and Ca^{2+} this chemical property making Gd^{3+} a toxic ion that disturbs calcium homeostasis in the organism. The inhibition of Ca^{2+} activated enzymes have negatively affects to the nervous system and other Ca-related physiological processes [28]. On the other hand, external exposure of some metals can be dangerous such as uranium and plutonium. Their different isotopes are considered as the most dangerous contaminants, contamination occurs mainly through inhalation or skin exposure with subsequent absorption and distribution of the radionuclides in the blood then different tissues where they induce damaging effects [29]. In other words, the report published in 2007, has been proved the frequencies of contamination that can occur in French nuclear plants or research centers using Calcium diethylenetriamine pentaacetate (Ca-DTPA) as an efficient tool in the treatment of internal plutonium and americium contamination [30].

I.4. Economic value of heavy metals

The increase in industrial usage, economic and environmental benefits of the REEs have resulted in an increased demand and price. Recovery of rare earth elements has become an attractive process owing to the high costs and limited availabilities of REEs. The global REE market's demand-supply balance has always been unstable. Because of changing mining restrictions, the prices of rare earth elements have fluctuated over the last decade. The global demand for REEs is increasing [31]. The most significant increase of prices took place during the years 2009-2011 [5]. The total demand for REEs have continuously

increased, and it is expected to reach 200,000 tons/ year in the next few years [32], Elbashier et al. [33] have summarized the most significant increase of prices of rare earth metal oxides took place during the years 2016-2020 as it is shown in Table 2.

Metal oxide	2016	2017	2018	2019	2020
Lanthanum	1856	2021	2185	18877	1810
Cerium	1565	1856	2146	1899	1815
Terbium	405	430	454	504	510
Dysprosium	192	185	177	235	240
Europium	68	60	51	35	30
Neodymium	39 327	44 566	49 804	44 578	14 700
Praseodymium	47 988	55 737	63 486	54 017	52 200

Table 2. Prices of rare earth metal oxides in US $/ ton during the years 2016-2020 [33].

I.5. Metals removal technologies

The recovery of heavy metals is an important concern that requires appropriate attention and this has led to the advancement of techniques and processes for the recovery of the metallic ions from various sources. Water pollution from the addition of metals from industrial activities is increasing greatly and also becoming a global concern because mining, mineral processing and metallurgical operations are generating effluents containing REE metals [34]. Thus, how to effectively and deeply remove undesirable metals from water systems is still a very important but still challenging task for environmental engineers. This issue has been addressed by the development of innovative methods for sequestering metal ions. Nowadays, several methods have been proposed for efficient metal removal from waters, including but not limited to chemical precipitation, ion exchange, membrane filtration, electrochemical technologies and adsorbents [35].

I.5.1. Chemical precipitation

Precipitation is regarded as an easy and effective method of recovering metals. In industry, chemical precipitation is by far the most widely used process to remove metals from wastewaters [36], using hydroxide [37], carbonate, or sulphide treatment [38] or some combinations of these treatments [39]. Precipitation is relatively simple, inexpensive, and effective method for removing REE metals from aqueous solutions. It involves the addition of chemicals such as lime, or iron salts followed by pH adjustment to form insoluble precipitates. The forming precipitates can be separated from the water by sedimentation or filtration. The treated water is then decanted and discharged or reused as needed. But its disadvantages, such as the large amount of chemical reagents required, ineffectiveness at low metal concentrations, and sludge generation, make it less appealing [40].

I.5.2. Ion exchange

Ion-exchange technology have been widely used to remove heavy metals from wastewater due to their many advantages, such as high treatment capacity, high removal efficiency and fast kinetics [41]. This method was used to obtain small quantities of high purity REE product from electronics or analytical applications [42]. A variety of materials: synthetic or natural can be used in ion-exchange technology. Organic materials, specifically polymeric materials have more development and studies due to their greater versatility. These materials are more commonly known as ion exchange resins. Among the materials used in ion-exchange processes, synthetic resins are commonly preferred as they are effective to nearly remove the heavy metals from dilute solutions since the extractant is bound to a solid phase, simplifying the separation process [43]. Though this makes it suitable for separations of mixtures with complex matrices and also environmentally safe but they can exhibit poor metal ion selectivity and kinetics [44].

I.5.3. Electrochemical technologies

Electrochemical or Electrocoagulation (EC) is a promising electrochemical treatment technique that does not involve the addition of chemicals or regeneration [45]. EC involves the electrochemical production of destabilization agents, which bring about charge neutralization for pollutant removal and offer significant potential for removing soluble

ionic species from solution, particularly heavy metals in water or wastewater treatment. EC operating conditions are highly dependent on the chemistry of the aqueous medium, especially conductivity and pH. Other important characteristics such as particle size, type of electrodes (a variety of electrodes can be used for the treatment of wastewater, and they include iron or steel, zinc, aluminum, magnesium or combination of them) [46], retention time between plates, plate spacing and chemical constituent concentrations dictate the operating parameters of the process [47]. Electrochemical wastewater technologies involve relatively large capital investment and the expensive electricity supply, so they haven't been widely applied.

I.5.4. Adsorbents

Adsorption is an alternative treatment technique that has been used to remove elements or toxic metals from wastewaters even at low concentrations [48][49]. Adsorption process is now recognized as one of the most efficient, promising and widely used to treat industrial waste effluents, offering significant advantages like low-cost, availability, profitability, ease of operation and efficiency [50]. In addition, because adsorption is sometimes reversible, adsorbents can be regenerated by suitable desorption process. Several sorption mechanisms such as electrostatic interaction, chelation, and complexation could be involved in the adsorption process. In fact, adsorption can deal with a wide range of target pollutants using mass transfer process where a substance is transferred from the liquid phase to the surface of a solid. The performance of these adsorbents largely depends on their physical and chemical properties, which results in the transfer of metals from the aqueous phase to the solid phase [51]. A variety of materials, ranging in complexity, have been tested for REEs.

Mechanical properties such as strength, resistance and kinetic properties are fundamental properties for any adsorbents, that it must be capable of transferring adsorbing molecules rapidly to the adsorption sites. Numerous adsorbent materials and their adsorption capacities are listed latter, such as but not limited to polymer adsorbents, nanofiber adsorbents and magnetic nanoparticle adsorbents.

I.5.4.1 Polymer adsorbents

Polymer adsorbents is one of the intriguing group of materials for heavy metal extraction is chelate-forming polymers and substrates containing a variety of functional groups including carboxylic acid [52] amide [53], amine [54], hydroxamic acids [55], succinic acid [56], acrylic acid [57], etc. Several polymer-supported ligands used in REEs separations include: EDTA [58] and DTPA [59]. Polymeric supports have been developed for the complexation of various metals and have received attention by their application for metal recovery from dilute solutions. The use of chelating polymers has enabled the development of ion-selective adsorbents with improved selectivity for the removal and concentration of metal ions. For example, the use of adsorbent chelating polymers appears to be the most promising method for uranium recovery from seawater. They have several advantages in terms of simplicity of operation, operating cost, environmental risk, and uptake capacity [18].

Due to their excellent mechanical properties and/or special functions, a variety of new fiber materials have been developed and have found industrial applications.

The Japanese Atomic Energy Agency (JAEA) teams worked on polymeric fiber adsorbents which contained polyethylene or polypropylene as a trunk polymer and amidoximated polyacrylonitrile (PAN) copolymerized with hydrophilic groups (e.g., poly(methacrylic acid)) as a graft chain. The incorporation of hydrophilic groups is crucial to allow seawater to access the amidoxime (AO) (-C(=NOH)NH_2) group on the graft chain [60].

According to literature, synthetic polymers have received the most interest for the recovery of metals from seawater such as uranium [61]. Many essential functional groups are known for their chelating properties can be easily added on polymer chains to harvest metal from aqueous media like amidoxime functional groups [62]. Robust and ductile polymers can be chosen as a substrate for the adsorbent and various shapes of polymeric adsorbents can be fabricated in large quantities.

In our lab, several studies have focused on the radio-decontamination from seawater using an innovative chelating polymer material, water soluble, based on dipicolinic acid [2]. Poly(4-vinyldipicolinic acid) (PVDPA) was obtained using Supplemental Activation

Reducing Agent Atom Transfer Radical Polymerization (SARA ATRP). The proposed strategy is described in Scheme 1.

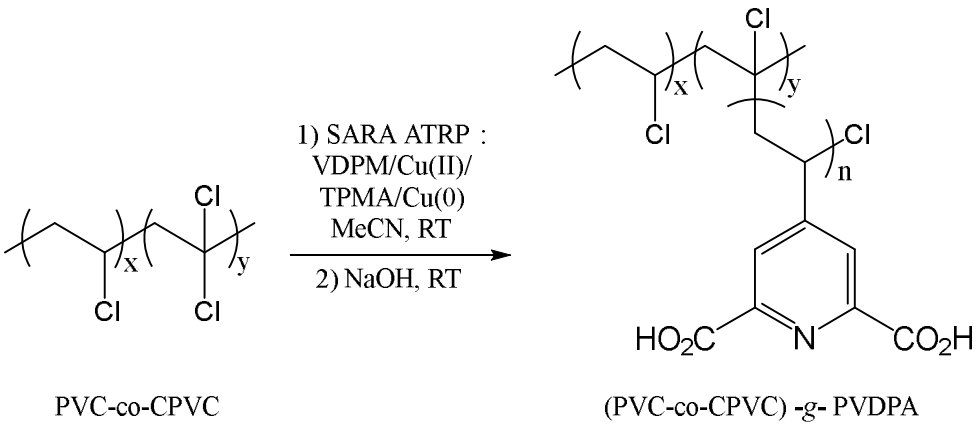

PVC-co-CPVC (PVC-co-CPVC) -*g*- PVDPA

Scheme 1. Synthesis of (PVC-co-CPVC)-g-PVDPA adsorbents.

These new materials were tested and proved their high efficiency in trapping uranium and many lanthanides in water. PVDPA showed a uranium uptake capacity of 597 mg/g in simulated seawater conditions, even at high ionic strength and in the presence of the challenging vanadium species, that tend to limit the performance of other existing materials.

I.5.4.2 Nanofiber adsorbents

Polymer nanofibers are an exciting novel class of material with diameters below 100 nm which are generally classified as nanofiber [63]. Nanofibers have distinct properties such as, the larger surface areas per unit mass, high porosity, layer thinness, high permeability, low basis weight, cost effectiveness and superior directional strength. These properties make them a promising material for a wide range of applications, from medical to consumer products, industrial to high-tech [64]. Nanofiber adsorbents have high adsorption capacity. Besides, the operation is simple, and the adsorption process rapid. So there is a growing and emergent interest in the application of these nanomaterials as adsorbents [65].

The use of polymeric nanofibers for heavy metal adsorption has increased in recent years [66].

I.5.4.3 Magnetic nanoparticle adsorbent

Functionalized magnetic nanoparticles are excellent candidates for the removal of aqueous metal ions, such as Cd^{2+}, Pb^{2+}, Co^{2+} and Ni^{2+}. These adsorbents can easily be retrieved from solution with a magnet. After the adsorbed ions are stripped, the nanoparticles can be reused, making this a promising sustainable green technology [67]. Chelating agents such as ethylene diamine tetraacetic acid (EDTA) [68][69], and ethylene glycol-bis(2-aminoethylether)-*N*,*N*,*N'*,*N'*-tetraacetic acid (EGTA) [70] coated on magnetic (Fe_3O_4) and nonmagnetic (TiO_2 and SiO_2) nanoparticles form very strong chelates with metal ions.

I.5.5. Membrane filtration

Membrane filtration technologies using various types of membranes hold great promise for heavy metal removal due to their high efficiency, ease of operation, and ability to save space. The membrane processes used to remove metals from the wastewater are ultrafiltration, reverse osmosis, nanofiltration and electrodialysis:

Micellar Enhanced Ultrafiltration (MEUF)

Ultrafiltration (UF) has a high removal efficiency owing to the effective trapping of solutes by micelles [71]. It is a membrane technique for removing dissolved and colloidal material. Since UF membrane pore sizes are larger than dissolved metal ions in the form of hydrated ions or low molecular weight complexes, these ions would easily pass through UF membranes. But, traditional ultrafiltration are usually limited to the separation of molecules with high molecular weights and are not sufficient to retain all the contaminants. In order to remove metallic ions, reverse osmosis (RO) or nanofiltration can be used due to the size of the ions in aqueous solutions. However, the usual permeate fluxes of RO membranes are limited and require high transmembrane pressure, which makes the process expensive [72]. Micellar Enhanced Ultrafiltration (MEUF) based on the addition of surfactants to wastewater. This method combines the high selectivity of RO and the high flux of UF [73].

When the concentration of surfactants in aqueous solutions is beyond the critical micelle concentration (CMC), the surfactant molecules will aggregate into micelles that can bind metal ions to form large metal-surfactant structures been proven to be an alternative process that can be used for heavy metals removal. One of the disadvantages of this method is the monomeric surfactants permeating through the membrane cause the secondary pollution in aquatic environment [74].This method involve the trapping of ion metal on the surface of the oppositely charged micelles by electrostatic interaction. Sampera et al. investigated the removal of Cd^{2+}, Cu^{2+}, Ni^{2+}, Pb^{2+} and Zn^{2+} species from aqueous dilute solutions using MEUF process by anionic surfactants: SDS and linear alkylbenzene sulfonate (LAS) in a lab-scale membrane system as illustrated in Figure 5 [75].

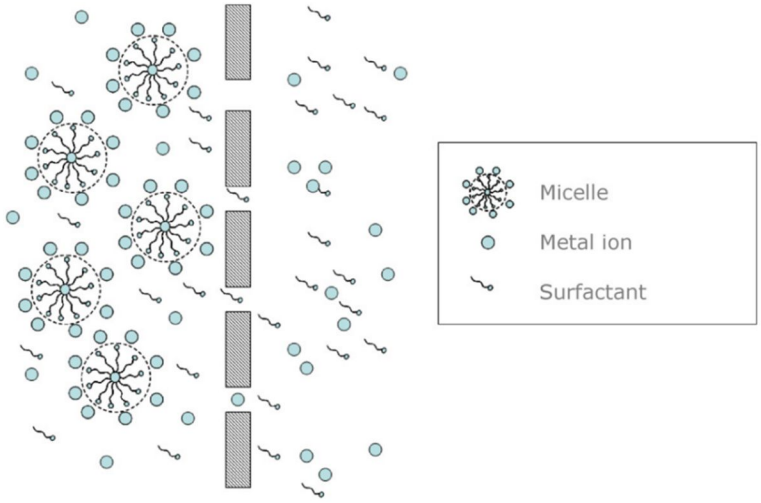

Figure 5. Scheme illustrating micellar-enhanced ultrafiltration for the removal of metal ions [75].

I.6 New strategies

In order to overcome the problem associated with the monomeric surfactants permeating through the membrane in MEUF method as mentioned before, and the advantage of polymeric adsorbents, a new system has been proposed to be an effective separation technique to remove metal ions from aqueous environments.

In the present work, polymeric nanoparticles functionalized with chelating agents, are employed for metals harvesting from the aqueous media. Because of their strong metal

chelating properties, the poly(4-vinyldipicolinic acid) (PVDPA) residues impart an excellent performance to the engineered nanoparticles, in the capture of lanthanide ions in aqueous solution. This approach offers the following advantages:

1. PVDPA is water soluble, which make it a good candidat for hydrophilic block in an amphiphilic block copolymer.
2. The adsorption capacities of these nanoparticles in large volume of contaminated water will be due to their small diameter (less than 120 nm) and high surface area.
3. Since dialysis membrane pore sizes are smaller than nanoparticles diameter, these nanoparticles can not pass through the membrane before and after complexation.

In this study, we will focus on the preparation of core-shell nanoparticles capable of chelating heavy metals, in which the core will be composed of polystyrene (PS), and the shell will be coated of PVDPA as shown in Scheme 2.

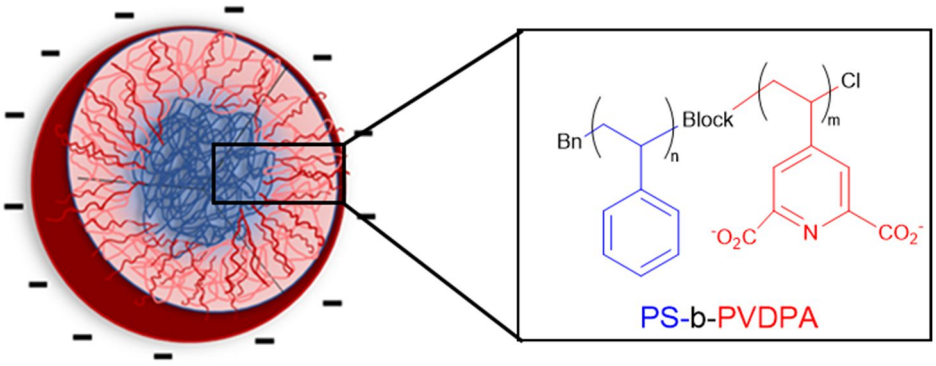

Scheme 2. Core-shell nanoparticles targeted.

On the other hand, another polymeric system (star polymer) will be prepared in this PhD project. Scheme 3 shows the synthetic route of this system. The use of star polymers offer several advantages such as their high solubility compared to the linear polymer. In other word, these polymers are more soluble than linear polymers because their high critical overlapping concentration (c*) [76]. Following this logic, it is easy to imagine that higher molar masses could be obtained, and therefore more captured metals. Here, hexafunctional star polymers have been proposed, where calixarene derivatives have been used as initiator

as showed in Scheme 3 and Atom Transfer Radical Polymerization (ATRP) as polymerization method. The synthesis and characterization of hexafunctional calixarene initiators and their use in the ATRP of 4-vinyl dimethyl dipicolinate (VDPM) will be discussed in details throughout this manuscript.

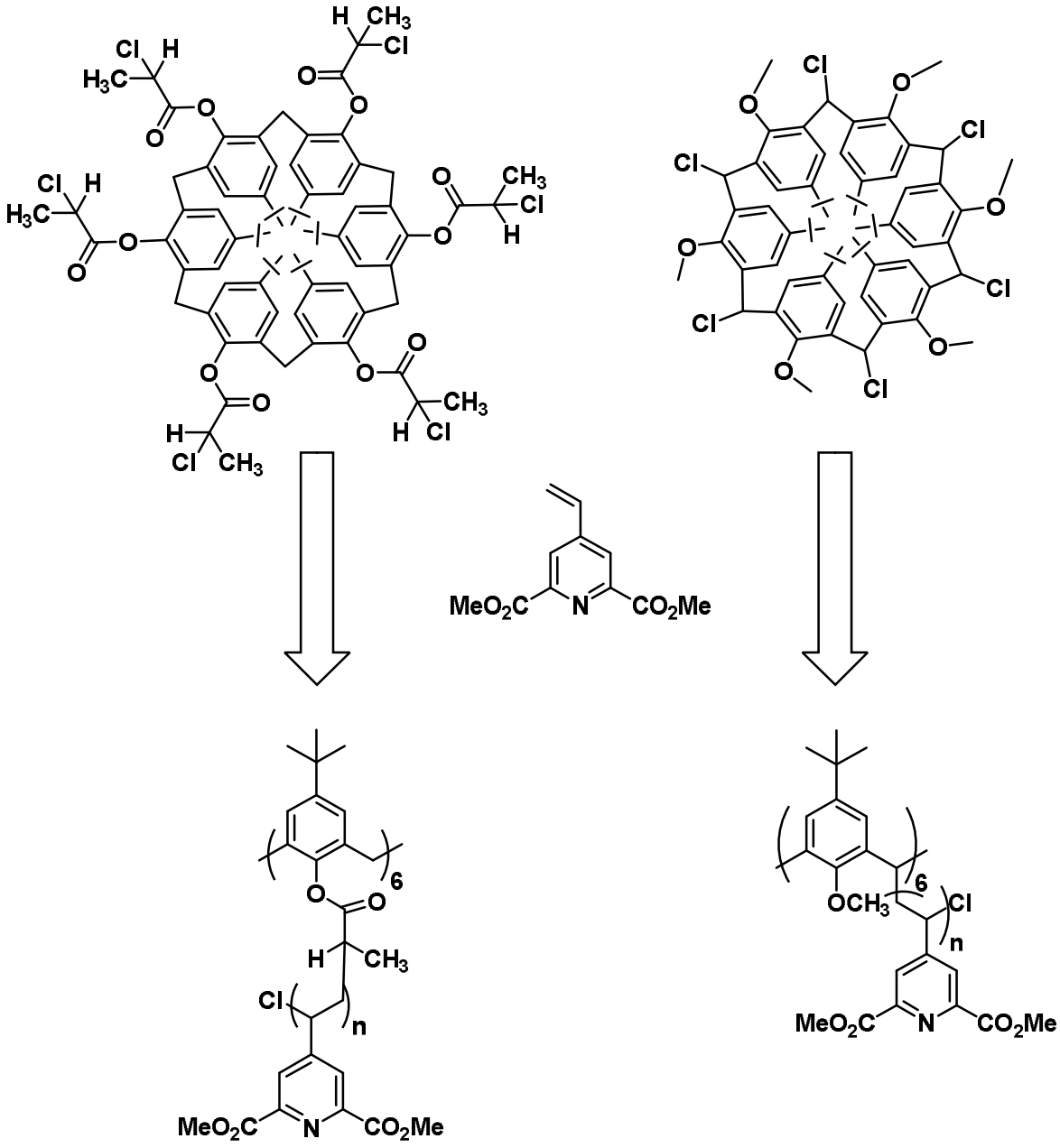

Scheme 3. Synthesis of new materials based on PVDPM using calixarene derivatives.

II.1. Controlled Radical Polymerization

Conventional radical polymerization (CRP) is one of the most popular methods to synthesize commodity polymers, more than 100 million tons of polymers produced annually using CRP, with thousands of different compositions [77]. However, the architectural control in these polymers is very limited because of the short lifetime of radical propagation which would eventually undergo termination processes such as statistical termination, disproportionation or chain transfers. For such reasons, the control of molecular architecture in a CRP had been considered an urge in polymer chemistry in the past. During the last two decades, the advent of reversible-deactivation radical polymerization (RDRP) has paved the way for a variety of advanced materials with precisely controlled molar mass, dispersity and it opened new avenues to a wide variety of advanced materials with precisely controlled molecular architecture [78][79][80]. So, the RDRP can be achieved by adding reagents that help minimize the event of termination through reversible deactivation and extension of propagating radical's lifetime. The addition of such reagents may alter the coupling reaction of propagating radicals by either reversible termination or reversible transfer.

All of the RDRP methods are based on establishing a dynamic equilibrium between a limited amount of growing free radicals and a large majority of dormant species. Within CRP, there are three main polymerization processes including Reversible Addition Fragmentation chain Transfer processes (RAFT) [83], Nitroxide Mediated Polymerization (NMP) [81] and Atom Transfer Radical Polymerization (ATRP) [82]. Though each of these three has certain advantages and limitations which will be discussed later, with their different mechanisms.

II.1.1. Reversible Addition Fragmentation chain Transfer processes (RAFT)

Among the three most well-established RDRP techniques, RAFT polymerization is the sole based on the degenerative Chain Transfer Agent (CTA) process and chain equilibration to control the polymerization. Chain transfer in RAFT polymerization involves addition and fragmentation steps as shown Scheme 4, the process is applicable to a wide range of monomers (most monomers polymerizable by free radical methods) and reaction conditions [83]. A thiocarbonylthio compound is the most common and versatile CTA in RAFT polymerization.

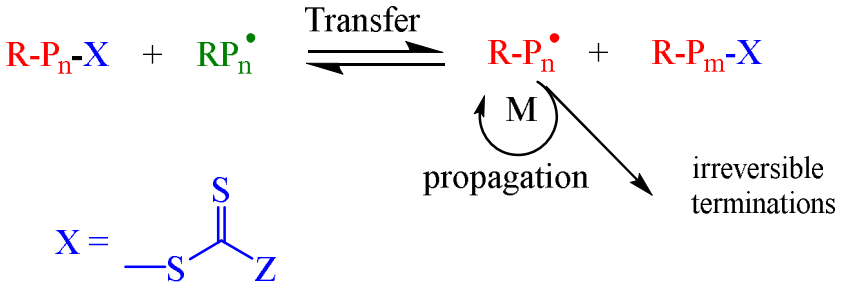

Scheme 4. RAFT polymerization mechanism.

II.1.2. Nitroxide Mediated Polymerization (NMP)

NMP polymerization involves the thermal decomposition of an alkoxyamine to form reactive radical and nitroxide stable radical or by mixing a free radical initiator with a nitroxide radical, which is stable at room temperature [84]. However, The higher reaction temperatures can be harmful to a wide array of substrates and, high temperature makes NMP energy consuming. Scheme 5 presents the mechanism of NMP.

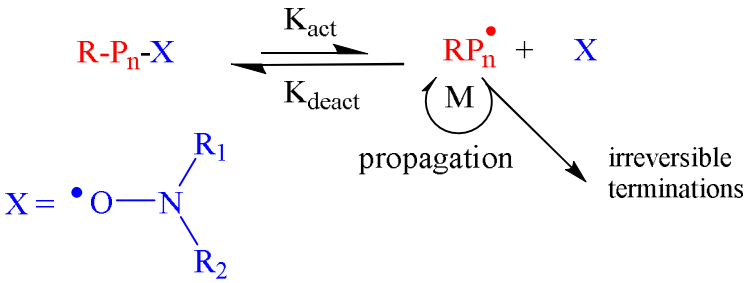

Scheme 5. NMP polymerization mechanism.

II.1.3. Atom Transfer Radical Polymerization (ATRP)

Atom Transfer Radical Polymerization is one of the most widely used RDRP methods [85]. ATRP is a catalytic process and can be mediated by numerous redox-active transition metal complexes (Cu has been the most often used transition metal) [86], Metal-ligand complex in the low oxidation state (Mt^m /ligand), known as the activator, beside an organic halide species (R-X), known as the ATRP initiator. The driving force in ATRP control is the equilibrium between propagating radicals and dormant species. Indeed, the dormant species (P_n-X) reacts with metal complex at lower oxidation state (Mt^m/L) to form propagating radicals ($P_n^\bullet$) and metal complex of higher oxidation state (X-Mt^{m+1}/L) called deactivator. The activity of the activator complex must be high enough to create homolytic dissociation of the C-X bond in the alkyl halide initiator. The radical center can then undergo radical addition across double bonds of monomers, affording polymerization, This is called activation process, which is characterized by activation constant K_{act}. Similarly, the deactivator rapidly transfers the halogen back to the propagating radicals to reform the dormant alkyl halides this is called the deactivation process characterized by deactivation constant K_{deact}. Polymer chains grow eventually by the addition of the intermediate radicals to monomers like in conventional radical polymerization, with the rate constant of propagation k_p. Termination reactions k_t can also occur mainly through radical coupling and disproportionation; however, in a well-controlled ATRP, termination is limited to no more than a few percent of the polymer chains. Scheme 6.

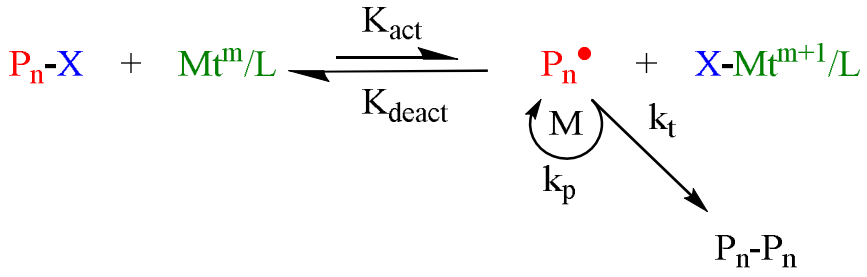

Scheme 6. ATRP Polymerization mechanism.

The polymerization rate of ATRP depends on the rate constant of propagation and on the concentrations of monomer and growing radicals. The radical concentration depends on

the equilibrium constant and the concentration of dormant species, activators, and deactivators, as shown in following equation [87]:

$$Rp = Kp\,[M][Pn^{\bullet}] = Kp.Keq.\frac{[M][Pn-X][Mt^{m}L]}{[X-Mt^{m+1}L]}$$

where [M] is the monomer concentration, [$P_n^{\bullet}$] the propagating chain radical concentration, [P_n-X] the dormant chains concentration and $k_{eq} = K_{act}/K_{deact}$.

One limitation of 'classical' ATRP was the relatively large amount of catalyst used typically of the order of 0.1–1 mol%, relative to the monomer thus the final products often contained a significant amount of residual metal [88].

Unlike ATRP, Organometallic Mediated Radical Polymerization (OMRP) is based on the fast and reversible homolytic cleavage of a metal-carbon bond in the metal complex. In such polymerization, the monomer type [89][90], metal/ligand combination [91], and initiator may dramatically affect the mechanism of polymerization in OMRP.

As seen before, The control in ATRP largely depends on the appropriate equilibrium between the activation process (generation of radicals, K_{act}) and the deactivation process (formation of alkyl halides, K_{deact}). The rate constants and their ratio ($K_{ATRP} = K_{act}/K_{deact}$) determines the concentration of radicals and, consequently, the rates of polymerization and termination as well as dispersities. The values of K_{ATRP}, k_{act} and k_{deact} depend on the catalyst, initiator and monomer structure, as well as on the type of solvent and the reaction conditions. The influences of these parameters have been well explained in literature in term of ATRP equilibrium constant. In order to have a successful ATRP, the following subsections summarize overall the influences of various factors have to be finely tuned.

II.1.3.1. The initiator

In ATRP, alkyl halides (RX) are typically used as initiators [92]. But, several multifunctional initiators have been also successfully used in ATRP [76]. The initiator structures have shown a critical role in the control of ATRP [93]. Hence, to obtain well-defined polymers with narrow molecular weight distributions, the halide group, X, must migrate between the growing chain and the transition metal complex rapidly and

selectively. A selection of initiators is shown in Figure 6 and placed as a function of activation rate constants in a certain ATRP system.

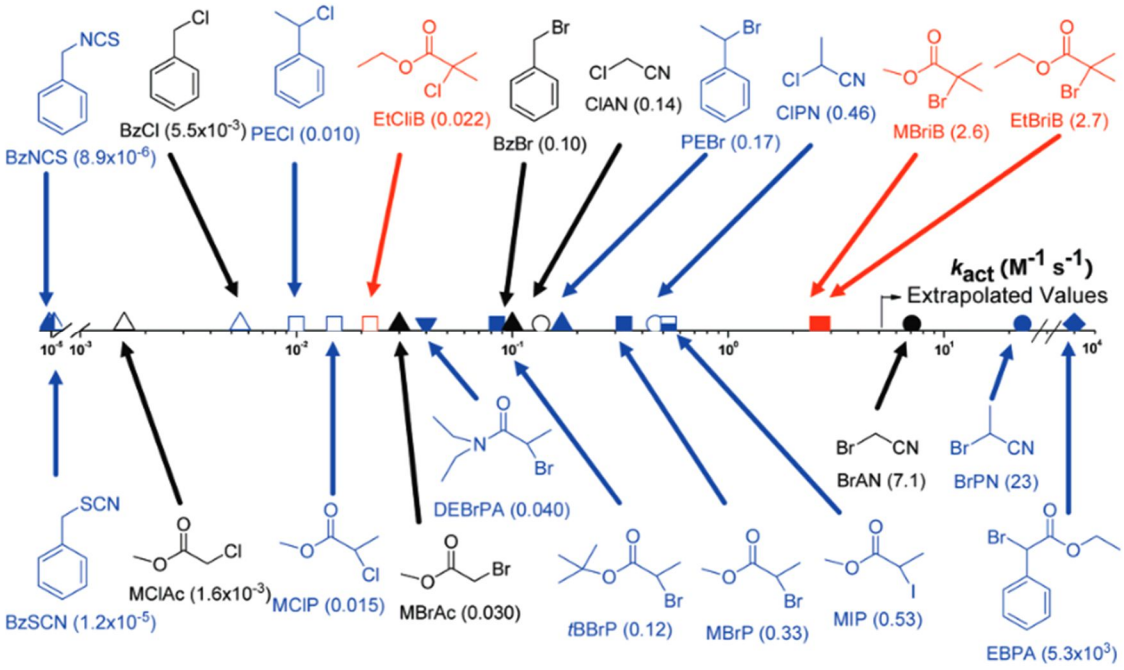

Figure 6. Effect of various initiator structures with Cu^{I} X/ PMDETA (X : Br or Cl) in MeCN at 35°C on the values of K_{ATRP} [93].

As seen in Figure 6 the effect of the initiators structures shows moderate to enormous change in activation rate constants. Three factors can have an impact on the efficiency of initiator: the nature of leaving atom/group, the substitution degree of initiator, and the activity of alkyl group. The activity of the leaving atom/group for the initiators decreases in the order of I > Br > Cl ≫ SCN ≈ NCS. The stabilization of (pseudo) radicals: phenyl ester > cyanide > ester > benzyl > amide. The k_{act} for primary, secondary, and tertiary alkyl halides follows the order of 1° < 2° < 3°.

II.1.3.2. Influence of the catalyst (metal/ ligand)

A number of metal complexes like ruthenium [94], copper [95], iron [96] and nickel [97] are known to be effective ATRP catalysts. Similarly, ligands can tune the electronic, steric and solubility of ATRP catalysts. Therefore, the use of ligands, as well as the selection of metal complexes, may have a significant impact on the kinetics of ATRP polymerization

as seen in Figure 7. In general, the activity of copper complex in classic ATRP follows the order of tetradentate (cyclic-bridged) > tetradentate (branched) > tetradentate (cylic) > tridentate > tetradentate (linear) > bidentate [98]. These complexes are the key to a successful ATRP since they influence the equilibrium between dormant and active species. All are able to accept a halide ligand, have low affinity for alkyl radicals and contain a metal with low Lewis acidity.

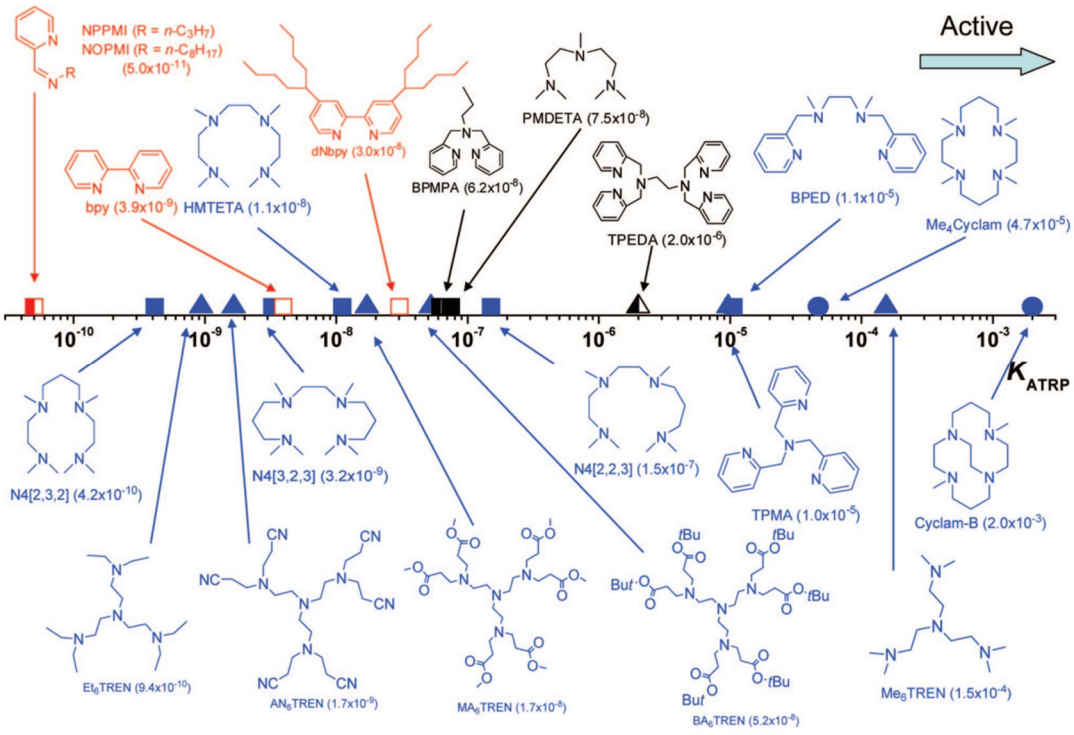

Figure 7. ATRP equilibrium constants K_{ATRP} for various N-based ligands with the initiator eBiB in the presence of CuBr in MeCN at 22 °C [98].

II.1.3.3. The monomer

Monomers like styrene [99][100], (meth)acrylates [101][102], (meth)acrylamides, and acrylonitrile [103] have been successfully polymerized with ATRP, each monomer has its own set of values for K_{ATRP}, K_{act}, K_{deact} and intrinsic radical propagation rate using the same conditions.

II.1.3.4. The solvent

Various solvents have been used for different monomers, including organic solvents such as benzene, toluene, anisole, diphenyl ether, ethyl acetate, acetone, dimethyl formamide, ethylene carbonate, alcohols [104]. Despite the fact that radical polymerization is less solvent selective than ionic polymerization, the kinetics of ATRP are still affected by the solvent choice because solvent polarity can significantly influence the polymerization equilibrium and rate constant [105].

II.1.3.5. Temperature

Elevated temperatures are usually beneficial in ATRP because 1) the increase of temperature increase the rate of polymerization due to the increase of both the radical propagation rate constant (k_p) and the atom transfer equilibrium constant (k_t). 2) As a result of the higher activation energy for the radical propagation than for the radical termination, higher k_p/k_t ratios and better control may be observed at higher temperatures. 3) the solubility of the catalyst increases [106]. However, chain transfer and other side reactions become more pronounced [107].

II.1.3.6. ATRP applications

Since 1995, ATRP was developed, the interset for creating functional materials with complex architectures (stars, cycles, brushes, regular networks) and composition (block, gradient, periodic copolymers) gradually increased [100]. Since then, it can be applied widely because it is compatible with a variety of functional monomers and reaction conditions and gives polymers with high chain-end functionality variety of monomers under mild conditions [108][109]. Polymers prepared by ATRP have been commercially produced in the United States, Japan, and Europe since 2002 [110].

Polymer topology

Figure 8 illustrates some examples of polymers with controlled topology prepared by ATRP. ATRP is very well suited for the preparation of (co)polymers with controlled topologies, including star- and comb-like polymers as well as branched, hyperbranched,

dendritic, network, and cyclic type structures [111]. The use of either a monofunctional, difunctional initiator leads to formation of linear polymers, growing in one or two directions, respectively. The resulting mono- and difunctional macroinitiators can be used as precursors for AB diblock and ABA triblock copolymers, respectively. With difunctional initiators, chains can grow concurrently in two directions, and it is easier to reach higher MW. Multifunctional initiators attached to a central core can yield star or graft polymers by the core-first approach [112].

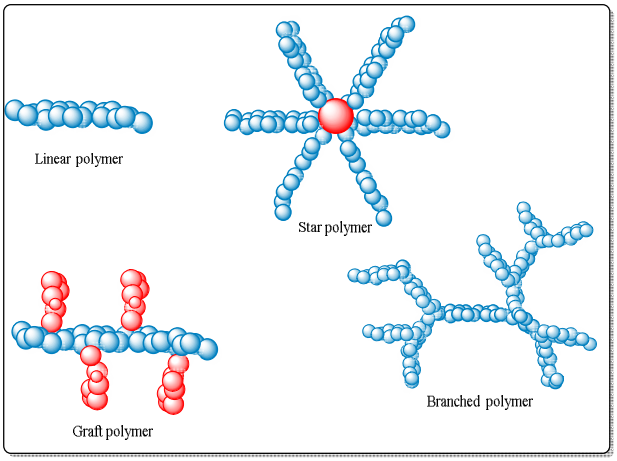

Figure 8. Different polymer topologies achieved by ATRP.

Polymer Composition

The composition of a material is an important parameter that influences its macroscopic properties [113]. Several compositions can be obtained by ATRP such as block, gradient, and periodic/alternating. Scheme 7 presents some examples of copolymers with controlled chain composition.

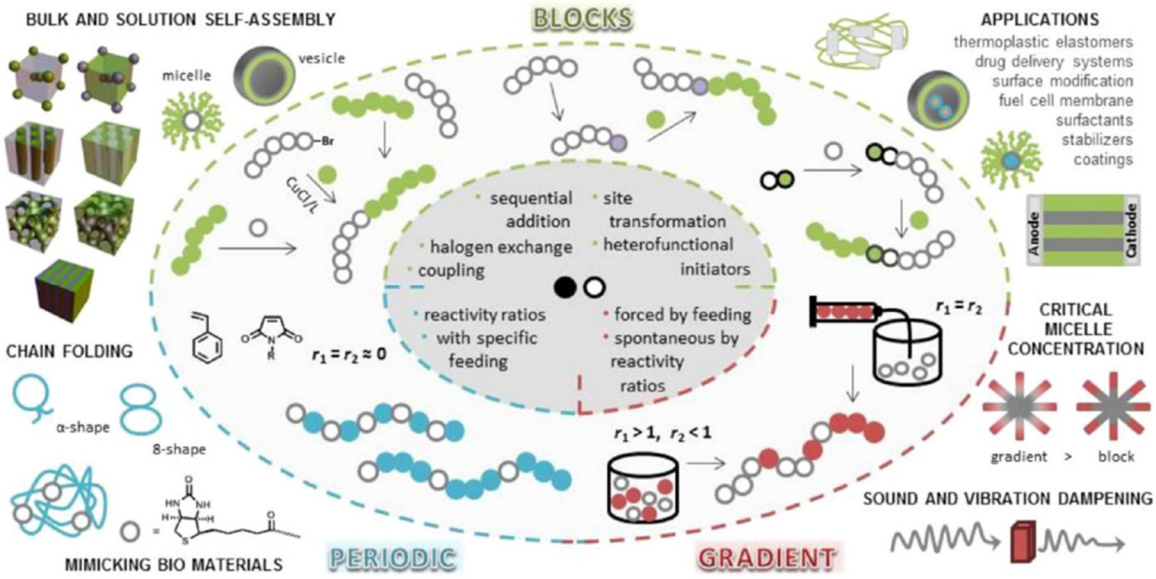

Scheme 7. Synthetic routes for block, gradient, and periodic copolymers and their applications [78].

Block copolymers: Block copolymers have received special attention because they spontaneously self-assemble in hydrophobic or hydrophilic environments. For instance, several macroinitiators with halogen end functionality were prepared by step-growth polymerization, coordination, anionic or cationic vinyl polymerization, ring opening polymerization (cationic, anionic, metathesis), or even conventional radical polymerization or two different RDRP techniques [114][115]. Their applications range from thermoplastic elastomers to drug delivery systems, coatings, sealants, templates or membranes found in such products as foam, adhesive tape and asphalt additives [116].

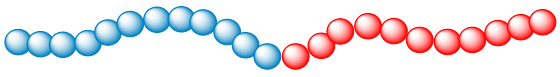

Block copolymer

Gradient copolymers: ATRP is a useful tool for getting gradient copolymers [117] by spontaneous copolymerization, based on different reactivity ratios of comonomers, or through continuous controlled feeding of one monomer. Gradient copolymers are well suited for a variety of applications, including cosmetic additives [118] compatibilizers of

immiscible polymer blends [119][120]. They show very broad glass transition temperatures and can be used as sound or vibration dampening materials [121].

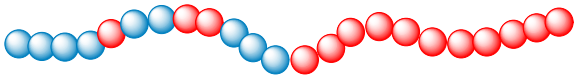

Gradient copolymer

Alternating copolymers: Periodic copolymers employ copolymerization of a strong electron-accepting monomer (for example, maleic anhydride or *N*-substituted maleimides) and an electron-donating comonomer (for example, styrene) [122], This behavior is a consequence of the highly pronounced copolymerization tendency of donor/acceptor comonomer pairs combined with a living chain-growth mechanism [123].

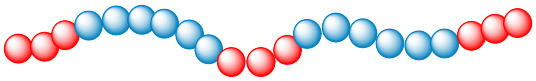

Alternating copolymer

II.1.3.7. Supplemental activator and reducing agent (SARA-ATRP)

Regardless of its enormous versatility, ATRP has several drawbacks including 1) its oxygen sensitivity necessitating the use of hard degassing techniques such as freeze-pump-thaw cycles, and the non-stable Cu^{1} must be purified before each reaction to eliminate the oxidized fraction 2) the requirement of high catalyst concentration. These drawbacks limit its widespread industrial utilization.

To reduce the residual transition metal in the final product, various techniques have been developed using ppm amounts of Cu in the presence of a reducing agent. A suitable balance between cost and product performance is required for the commercial application of any synthetic methodology. ATRP methods that were recently developed, involve the direct (re)generation of Cu(I) *in situ* using chemical reductants method (Activator Regenerated by Electron Transfer (ARGET) ATRP) [124], or the employment of Cu(II) halide and solid Cu(0) such as Single Electron Transfer Living Radical Polymerization (SET-LRP) [125],

and (Supplemental Activator and Reducing Agent Atom Transfer Radical Polymerization (SARA-ATRP))

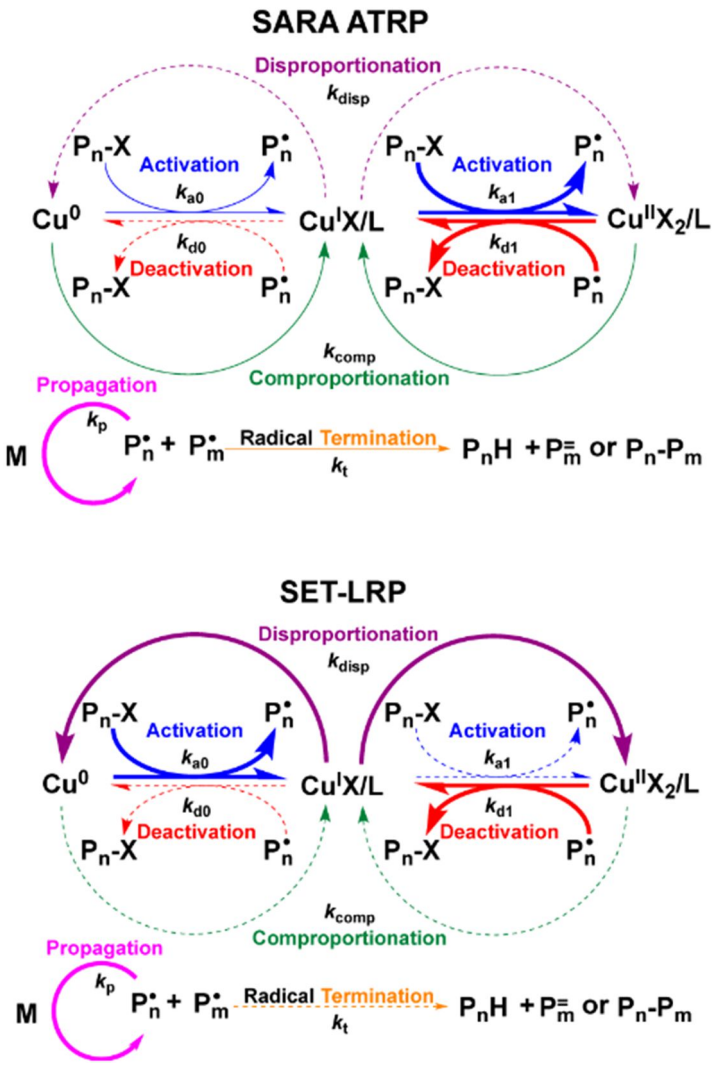

Scheme 8. SARA-ATRP (top) and SET-LRP (bottom) mechanism [126].

Scheme 8 shows the mechanism of SARA ATRP and SET-LRP. Firstly, one proposed mechanism, called supplemental activator and reducing agent (SARA-ATRP), has Cu(I)/Cu(II) reactions as the major activation/deactivation reactions, with Cu(0) acting as a supplemental activator of alkyl halides and a reducing agent for Cu(II) and limited disproportionation of Cu(I) [127]. Secondary, the other model, called single electron transfer living radical polymerization (SET-LRP), has Cu(0) as the major activator of alkyl halides, Cu(II) as the major deactivator, and Cu(I) not participating in activation reactions but instead undergoing very rapid disproportionation to Cu(0) and Cu(I) [128][129].

Furthermore, SET-LRP and SARA ATRP are debating on the equilibrium of disproportionation and comproportionation where SET-LRP suggests the instantaneous disproportionation of Cu(I) is the dominant event while SARA ATRP assumes the comproportionation of Cu(0) and Cu(II) to generate the activator Cu(I) to be the main process. Additionally, the two proposed mechanisms also have different point of view on the effect of solvent [130]. Regardless of that debate, The SARA-ATRP method was successfully used for controlled polymerization of a wide range of monomers like methyl methacrylate (MMA) [131], styrene (Sty) [132], and vinyl chloride (VC) [133]. It is a very useful method to prepare polymers with distinct architectures like well-defined block copolymer [134].

Conclusion

In conclusion, this chapter presents an overview on different aspects of the research, it includes major knowledge about sources, distribution, toxicological and economical effects of heavy metals. In addition, we have presented a brief summary of all the achievements to date of different prospects for heavy metals removal technologies and the advancement and revolution of these techniques. The use of polymer like poly(4-vinyldipicolinic acid) (PVDPA) is an outstanding approach to obtain highly innovative chelating materials. Variable modifications to this type of material, including diblock copolymers, star polymer, have been synthesized and discussed thereafter to improve the capacity of complexation with heavy metals (lanthanides and actinides). Classical ATRP and SARA-ATRP, will be used to synthesize innovative chelating materials in the following chapters.

References

[1] M. Q. Yang, N. Zhang, M. Pagliaro, and Y. J. Xu, "Artificial photosynthesis over graphene-semiconductor composites. Are we getting better?," *Chemical Society Reviews*, vol. 43, no. 24. Royal Society of Chemistry, pp. 8240–8254, Dec. 21, 2014. doi: 10.1039/c4cs00213j.

[2] M. Maaz *et al.*, "New insights on Uranium recovery from seawater and aqueous media," *Applied Materials Today*, vol. 18, Mar. 2020, doi: 10.1016/j.apmt.2019.100461.

[3] G. T. Seaborg, "Overview of the Actinide and Lanthanide (the f) Elements," 1993.

[4] S. kobayashi, "Lanthanides: Chemistry and Use in Organic Synthesis," 1999.

[5] G. Charalampides, K. I. Vatalis, B. Apostoplos, and B. Ploutarch-Nikolas, "Rare Earth Elements: Industrial Applications and Economic Dependency of Europe," *Procedia Economics and Finance*, vol. 24, pp. 126–135, 2015, doi: 10.1016/s2212-5671(15)00630-9.

[6] S. F. Wolf, "Trace Analysis of Actinides in Geological, Environmental, and Biological Matrices," in *The Chemistry of the Actinide and Transactinide Elements*, Springer Netherlands, 2007, pp. 3273–3338. doi: 10.1007/1-4020-3598-5_30.

[7] R. G. Pearson and D. H. Busch, "Hard and Soft Acids and Bases," 1963.

[8] D. D. Schnaars *et al.*, "Differences in actinide metal-ligand orbital interactions: Comparison of U(IV) and Pu(IV) β-ketoiminate N,O donor complexes," *Chemical Communications*, vol. 47, no. 27, pp. 7647–7649, 2011, doi: 10.1039/c1cc12409a.

[9] J. C. Berthet *et al.*, "The affinity and selectivity of terdentate nitrogen ligands towards trivalent lanthanide and uranium ions viewed from the crystal structures of the 1:3 complexes," *Journal of the Chemical Society, Dalton Transactions*, no. 16, pp. 3265–3272, 2002, doi: 10.1039/b203725d.

[10] Z. Wang *et al.*, "Selective extraction of americium(III) over europium(III) ions in nitric acid solution by NTAamide(C8) using a novel water-soluble bisdiglycolamide as a masking agent," *Separation and Purification Technology*, vol. 181, pp. 148–158, 2017, doi: 10.1016/j.seppur.2017.02.043.

[11] A. Kovács, C. Apostolidis, and O. Walter, "Comparative study of complexes of rare earths and actinides with 2,6-bis(1,2,4-triazin-3-yl)pyridine," *Inorganics (Basel)*, vol. 7, no. 3, 2019, doi: 10.3390/INORGANICS7030026.

[12] "Energy, Electricity and Nuclear Power Estimates for the Period up to 2050," *IAEA-VIENNA,* , 2021.

[13] D. S. Sholl and R. P. Lively, "Seven chemical separations to change the world," *Nature*, vol. 532, pp. 435–437, 2016.

[14] Z. M. Migaszewski and A. Gałuszka, "The characteristics, occurrence, and geochemical behavior of rare earth elements in the environment: A review," *Critical Reviews in*

Environmental Science and Technology, vol. 45, no. 5. Taylor and Francis Inc., pp. 429–471, Mar. 04, 2015. doi: 10.1080/10643389.2013.866622.

[15] M. I. Leybourne and K. H. Johannesson, "Rare earth elements (REE) and yttrium in stream waters, stream sediments, and Fe-Mn oxyhydroxides: Fractionation, speciation, and controls over REE + Y patterns in the surface environment," *Geochimica et Cosmochimica Acta*, vol. 72, no. 24, pp. 5962–5983, Dec. 2008, doi: 10.1016/j.gca.2008.09.022.

[16] K. Sultan and N. A. Shazili, "Rare earth elements in tropical surface water, soil and sediments of the Terengganu River Basin, Malaysia," *Journal of Rare Earths*, vol. 27, no. 6, pp. 1072–1078, 2009, doi: 10.1016/S1002-0721(08)60391-9.

[17] R. V. ; K. J. ; M. R. W. ; S. R. Davies, "EXTRACTION OF URANIUM FROM SEA WATER," *Nature*, vol. 203, pp. 1110–1115, 1964.

[18] J. Kim *et al.*, "Recovery of Uranium from Seawater: A Review of Current Status and Future Research Needs," *Separation Science and Technology (Philadelphia)*, vol. 48, no. 3. pp. 367–387, Jan. 2013. doi: 10.1080/01496395.2012.712599.

[19] S. Piarulli *et al.*, "Sources, distribution and effects of rare earth elements in the marine environment: Current knowledge and research gaps," *Environmental Pollution*, vol. 291. Elsevier Ltd, Dec. 15, 2021. doi: 10.1016/j.envpol.2021.118230.

[20] T. Liang, K. Li, and L. Wang, "State of rare earth elements in different environmental components in mining areas of China," *Environmental Monitoring and Assessment*, vol. 186, no. 3, pp. 1499–1513, 2014, doi: 10.1007/s10661-013-3469-8.

[21] T. Sasaki, Y. Takeno, T. Kobayashi, A. Kirishima, and N. Sato, "Leaching behavior of gamma-emitting fission products and Np from neutron-irradiated UO2-ZrO2 solid solutions in non-filtered surface seawater," *Journal of Nuclear Science and Technology*, vol. 53, no. 3, pp. 303–311, Mar. 2016, doi: 10.1080/00223131.2015.1055315.

[22] K. Nishihara *et al.*, "Radionuclide release to stagnant water in the Fukushima-1 nuclear power plant1," *Journal of Nuclear Science and Technology*, vol. 52, no. 3, pp. 301–307, Mar. 2015, doi: 10.1080/00223131.2014.946455.

[23] H. Geckeis, T. Ngo Manh, M. Bouby, and J. I. Kim, "Aquatic colloids relevant to radionuclide migration: Characterization by size fractionation and ICP-mass spectrometric detection," in *Colloids and Surfaces A: Physicochemical and Engineering Aspects*, Apr. 2003, vol. 217, no. 1–3, pp. 101–108. doi: 10.1016/S0927-7757(02)00564-2.

[24] W. L. Mao *et al.*, "X-ray-induced dissociation of H2O and formation of an O 2-H2 alloy at high pressure," *Science (1979)*, vol. 314, no. 5799, pp. 636–638, Oct. 2006, doi: 10.1126/science.1132884.

[25] A. P. Novikov, I. E. Vlasova, A. v. Safonov, V. M. Ermolaev, E. v. Zakharova, and S. N. Kalmykov, "Speciation of actinides in groundwater samples collected near deep

nuclear waste repositories," *Journal of Environmental Radioactivity*, vol. 192, pp. 334–341, Dec. 2018, doi: 10.1016/j.jenvrad.2018.07.007.

[26] M. J. Khan, "Contamination of agro ecosystem and human health hazards from wastewater used for irrigation. Phosphate Sorption in Calcareous Soil Series View project Compost mixed fruits and vegetable waste biochar with ACC deaminase rhizobacteria can minimize lead stress in mint plants View project," 2009. [Online]. Available: https://www.researchgate.net/publication/267327798

[27] S. H. Peng, W. X. Wang, X. Li, and Y. F. Yen, "Metal partitioning in river sediments measured by sequential extraction and biomimetic approaches," *Chemosphere*, vol. 57, no. 8, pp. 839–851, 2004, doi: 10.1016/j.chemosphere.2004.07.015.

[28] S. Kulaksiz and M. Bau, "Anthropogenic gadolinium as a microcontaminant in tap water used as drinking water in urban areas and megacities," *Applied Geochemistry*, vol. 26, no. 11, pp. 1877–1885, Nov. 2011, doi: 10.1016/j.apgeochem.2011.06.011.

[29] E. Fattal, N. Tsapis, and G. Phan, "Novel drug delivery systems for actinides (uranium and plutonium) decontamination agents," *Advanced Drug Delivery Reviews*, vol. 90. Elsevier B.V., pp. 40–54, Aug. 01, 2015. doi: 10.1016/j.addr.2015.06.009.

[30] L. Grappin *et al.*, "Treatment of actinide exposures: A review of Ca-DTPA injections inside CEA-COGEMA plants," *Radiation Protection Dosimetry*, vol. 127, no. 1–4. pp. 435–439, 2007. doi: 10.1093/rpd/ncm296.

[31] O. Pereao, C. Bode-Aluko, O. Fatoba, K. Laatikainen, and L. Petrik, "Rare earth elements removal techniques from water/wastewater: A review," *Desalination and Water Treatment*, vol. 130. Desalination Publications, pp. 71–86, Oct. 01, 2018. doi: 10.5004/dwt.2018.22844.

[32] N. Haque, A. Hughes, S. Lim, and C. Vernon, "Rare earth elements: Overview of mining, mineralogy, uses, sustainability and environmental impact," *Resources*, vol. 3, no. 4. MDPI AG, pp. 614–635, Dec. 01, 2014. doi: 10.3390/resources3040614.

[33] E. Elbashier, A. Mussa, M. A. Hafiz, and A. H. Hawari, "Recovery of rare earth elements from waste streams using membrane processes: An overview," *Hydrometallurgy*, vol. 204. Elsevier B.V., Sep. 01, 2021. doi: 10.1016/j.hydromet.2021.105706.

[34] M. Hua, S. Zhang, B. Pan, W. Zhang, L. Lv, and Q. Zhang, "Heavy metal removal from water/wastewater by nanosized metal oxides: A review," *Journal of Hazardous Materials*, vol. 211–212. pp. 317–331, Apr. 15, 2012. doi: 10.1016/j.jhazmat.2011.10.016.

[35] F. Fu and Q. Wang, "Removal of heavy metal ions from wastewaters: A review," *Journal of Environmental Management*, vol. 92, no. 3. pp. 407–418, Mar. 2011. doi: 10.1016/j.jenvman.2010.11.011.

[36] Y. Ku and I.-L. Jung, “PHOTOCATALYTIC REDUCTION OF Cr(VI) IN AQUEOUS SOLUTIONS BY UV IRRADIATION WITH THE PRESENCE OF TITANIUM DIOXIDE,” 2001. [Online]. Available: www.elsevier.com/locate/watres

[37] J. L. Huisman, G. Schouten, and C. Schultz, “Biologically produced sulphide for purification of process streams, effluent treatment and recovery of metals in the metal and mining industry,” *Hydrometallurgy*, vol. 83, no. 1–4, pp. 106–113, Sep. 2006, doi: 10.1016/j.hydromet.2006.03.017.

[38] A. Özverdi and M. Erdem, “Cu2+, Cd2+ and Pb2+ adsorption from aqueous solutions by pyrite and synthetic iron sulphide,” *Journal of Hazardous Materials*, vol. 137, no. 1, pp. 626–632, Sep. 2006, doi: 10.1016/j.jhazmat.2006.02.051.

[39] M. J. González-Muñoz, M. A. Rodríguez, S. Luque, and J. R. Álvarez, “Recovery of heavy metals from metal industry waste waters by chemical precipitation and nanofiltration,” *Desalination*, vol. 200, no. 1–3, pp. 742–744, Nov. 2006, doi: 10.1016/j.desal.2006.03.498.

[40] N. van Nguyen, A. Iizuka, E. Shibata, and T. Nakamura, “Study of adsorption behavior of a new synthesized resin containing glycol amic acid group for separation of scandium from aqueous solutions,” *Hydrometallurgy*, vol. 165, pp. 51–56, Oct. 2016, doi: 10.1016/j.hydromet.2015.11.016.

[41] S. Y. Kang, J. U. Lee, S. H. Moon, and K. W. Kim, “Competitive adsorption characteristics of Co2+, Ni2+, and Cr3+ by IRN-77 cation exchange resin in synthesized wastewater,” *Chemosphere*, vol. 56, no. 2, pp. 141–147, 2004, doi: 10.1016/j.chemosphere.2004.02.004.

[42] F. Xie, T. A. Zhang, D. Dreisinger, and F. Doyle, “A critical review on solvent extraction of rare earths from aqueous solutions,” *Minerals Engineering*, vol. 56. Elsevier Ltd, pp. 10–28, 2014. doi: 10.1016/j.mineng.2013.10.021.

[43] B. Alyüz and S. Veli, “Kinetics and equilibrium studies for the removal of nickel and zinc from aqueous solutions by ion exchange resins,” *Journal of Hazardous Materials*, vol. 167, no. 1–3, pp. 482–488, Aug. 2009, doi: 10.1016/j.jhazmat.2009.01.006.

[44] A. N. Pustam and S. D. Alexandratos, “Engineering selectivity into polymer-supported reagents for transition metal ion complex formation,” *Reactive and Functional Polymers*, vol. 70, no. 8, pp. 545–554, Aug. 2010, doi: 10.1016/j.reactfunctpolym.2010.05.002.

[45] J. R. Parga *et al.*, “Arsenic removal via electrocoagulation from heavy metal contaminated groundwater in la Comarca Lagunera México,” *Journal of Hazardous Materials*, vol. 124, no. 1–3, pp. 247–254, Sep. 2005, doi: 10.1016/j.jhazmat.2005.05.017.

[46] X. Chen, G. Chen, and P. Lock Yue, “Investigation on the electrolysis voltage of electrocoagulation,” 2002. [Online]. Available: www.elsevier.com/locate/ces

[47] T. Ölmez, "The optimization of Cr(VI) reduction and removal by electrocoagulation using response surface methodology," *Journal of Hazardous Materials*, vol. 162, no. 2–3, pp. 1371–1378, Mar. 2009, doi: 10.1016/j.jhazmat.2008.06.017.

[48] C. A. Bode-Aluko, O. Pereao, G. Ndayambaje, and L. Petrik, "Adsorption of Toxic Metals on Modified Polyacrylonitrile Nanofibres: A Review," *Water, Air, and Soil Pollution*, vol. 228, no. 1, Jan. 2017, doi: 10.1007/s11270-016-3222-3.

[49] P. K. Neghlani, M. Rafizadeh, and F. A. Taromi, "Preparation of aminated-polyacrylonitrile nanofiber membranes for the adsorption of metal ions: Comparison with microfibers," *Journal of Hazardous Materials*, vol. 186, no. 1, pp. 182–189, Feb. 2011, doi: 10.1016/j.jhazmat.2010.10.121.

[50] A. Demirbas, "Heavy metal adsorption onto agro-based waste materials: A review," *Journal of Hazardous Materials*, vol. 157, no. 2–3. pp. 220–229, Sep. 15, 2008. doi: 10.1016/j.jhazmat.2008.01.024.

[51] K. Y. Foo and B. H. Hameed, "An overview of landfill leachate treatment via activated carbon adsorption process," *Journal of Hazardous Materials*, vol. 171, no. 1–3. pp. 54–60, Nov. 15, 2009. doi: 10.1016/j.jhazmat.2009.06.038.

[52] A. A. Tolba *et al.*, "Synthesis and characterization of poly(carboxymethyl)-cellulose for enhanced La(III) sorption," *Carbohydrate Polymers*, vol. 157, pp. 1809–1820, Feb. 2017, doi: 10.1016/j.carbpol.2016.11.064.

[53] F. M. de Melo, S. da N. Almeida, N. S. Uezu, C. A. O. Ramirez, A. D. dos Santos, and H. E. Toma, "Extraction of Dysprosium Ions with DTPA Functionalized Superparamagnetic Nanoparticles Probed by Energy Dispersive X-ray Fluorescence and TEM/High-Angle Annular Dark Field Imaging," *Journal of Nanoscience and Nanotechnology*, vol. 18, no. 6, pp. 4155–4159, Dec. 2017, doi: 10.1166/jnn.2018.15245.

[54] E. Polido Legaria, M. Samouhos, V. G. Kessler, and G. A. Seisenbaeva, "Toward Molecular Recognition of REEs: Comparative Analysis of Hybrid Nanoadsorbents with the Different Complexonate Ligands EDTA, DTPA, and TTHA," *Inorganic Chemistry*, vol. 56, no. 22, pp. 13938–13948, Nov. 2017, doi: 10.1021/acs.inorgchem.7b02056.

[55] F. A. Alakhras, K. A. Dari, and M. S. Mubarak, "Synthesis and chelating properties of some poly(amidoxime-hydroxamic acid) resins toward some trivalent lanthanide metal ions," *Journal of Applied Polymer Science*, vol. 97, no. 2, pp. 691–696, Jul. 2005, doi: 10.1002/app.21825.

[56] C. S. K. Raju and M. S. Subramanian, "A novel solid phase extraction method for separation of actinides and lanthanides from high acidic streams," *Separation and Purification Technology*, vol. 55, no. 1, pp. 16–22, May 2007, doi: 10.1016/j.seppur.2006.10.013.

[57] Y. Zhu, Y. Zheng, and A. Wang, "A simple approach to fabricate granular adsorbent for adsorption of rare elements," *International Journal of Biological Macromolecules*, vol. 72, pp. 410–420, Jan. 2015, doi: 10.1016/j.ijbiomac.2014.08.039.

[58] D. Dupont, W. Brullot, M. Bloemen, T. Verbiest, and K. Binnemans, "Selective uptake of rare earths from aqueous solutions by EDTA-functionalized magnetic and nonmagnetic nanoparticles," *ACS Applied Materials and Interfaces*, vol. 6, no. 7, pp. 4980–4988, Apr. 2014, doi: 10.1021/am406027y.

[59] R. Rahal, F. Annani, S. Pellet-Rostaing, G. Arrachart, and S. Daniele, "Surface modification of titanium oxide nanoparticles with chelating molecules: New recognition devices for controlling the selectivity towards lanthanides ionic separation," *Separation and Purification Technology*, vol. 147, pp. 220–226, Jun. 2015, doi: 10.1016/j.seppur.2015.04.038.

[60] T. Kawai *et al.*, "Comparison of amidoxime adsorbents prepared by cografting methacrylic acid and 2-hydroxyethyl methacrylate with acrylonitrile onto polyethylene," *Industrial and Engineering Chemistry Research*, vol. 39, no. 8, pp. 2910–2915, 2000, doi: 10.1021/ie990474a.

[61] T. Saito *et al.*, "Uranium recovery from seawater: Development of fiber adsorbents prepared via atom-transfer radical polymerization," *Journal of Materials Chemistry A*, vol. 2, no. 35, pp. 14674–14681, Sep. 2014, doi: 10.1039/c4ta03276d.

[62] A. Zhang, T. Asakura, and G. Uchiyama, "The adsorption mechanism of uranium(VI) from seawater on a macroporous fibrous polymeric adsorbent containing amidoxime chelating functional group," *Reactive and Functional Polymers*, vol. 57, no. 1, pp. 67–76, Nov. 2003, doi: 10.1016/j.reactfunctpolym.2003.07.005.

[63] O. K. Pereao, C. Bode-Aluko, G. Ndayambaje, O. Fatoba, and L. F. Petrik, "Electrospinning: Polymer Nanofibre Adsorbent Applications for Metal Ion Removal," *Journal of Polymers and the Environment*, vol. 25, no. 4. Springer New York LLC, pp. 1175–1189, Dec. 01, 2017. doi: 10.1007/s10924-016-0896-y.

[64] J. Fang, H. T. Niu, T. Lin, and X. G. Wang, "Applications of electrospun nanofibers," *Chinese Science Bulletin*, vol. 53, no. 15. pp. 2265–2286, Aug. 2008. doi: 10.1007/s11434-008-0319-0.

[65] A. Rahmani, H. Z. Mousavi, and M. Fazli, "Effect of nanostructure alumina on adsorption of heavy metals," *Desalination*, vol. 253, no. 1–3, pp. 94–100, Apr. 2010, doi: 10.1016/j.desal.2009.11.027.

[66] C. S. Ki, E. H. Gang, I. C. Um, and Y. H. Park, "Nanofibrous membrane of wool keratose/silk fibroin blend for heavy metal ion adsorption," *Journal of Membrane Science*, vol. 302, no. 1–2, pp. 20–26, Sep. 2007, doi: 10.1016/j.memsci.2007.06.003.

[67] F. Zhao, E. Repo, M. Sillanpää, Y. Meng, D. Yin, and W. Z. Tang, "Green synthesis of magnetic EDTA- And/or DTPA-cross-linked chitosan adsorbents for highly efficient

removal of metals," *Industrial and Engineering Chemistry Research*, vol. 54, no. 4, pp. 1271–1281, Feb. 2015, doi: 10.1021/ie503874x.

[68] E. Repo, J. K. Warchoł, A. Bhatnagar, and M. Sillanpää, "Heavy metals adsorption by novel EDTA-modified chitosan-silica hybrid materials," *Journal of Colloid and Interface Science*, vol. 358, no. 1, pp. 261–267, Jun. 2011, doi: 10.1016/j.jcis.2011.02.059.

[69] E. Repo, J. K. Warchol, T. A. Kurniawan, and M. E. T. Sillanpää, "Adsorption of Co(II) and Ni(II) by EDTA- and/or DTPA-modified chitosan: Kinetic and equilibrium modeling," *Chemical Engineering Journal*, vol. 161, no. 1–2, pp. 73–82, 2010, doi: 10.1016/j.cej.2010.04.030.

[70] F. Zhao, E. Repo, D. Yin, and M. E. T. Sillanpää, "Adsorption of Cd(II) and Pb(II) by a novel EGTA-modified chitosan material: Kinetics and isotherms," *Journal of Colloid and Interface Science*, vol. 409, pp. 174–182, Nov. 2013, doi: 10.1016/j.jcis.2013.07.062.

[71] R. S. Juang, Y. Y. Xu, and C. L. Chen, "Separation and removal of metal ions from dilute solutions using micellar-enhanced ultrafiltration," *Journal of Membrane Science*, vol. 218, no. 1–2, pp. 257–267, Jul. 2003, doi: 10.1016/S0376-7388(03)00183-2.

[72] F. Heu, J. Lahnsteiner, H. Frischherz, and G. Baumgartner, "Experience with full-scale electrodialysis for nitrate and hardness removal," 1998.

[73] K. Back, H.-H. Leeb, and J.-W. Yang, "DESALINATION Micellar-enhanced ultrafiltration for simultaneous removal of ferricyanide and nitrate," 2003. [Online]. Available: www.elsevier.com/locate/desal

[74] J. Lee, J. S. Yang, H. J. Kim, K. Baek, and J. W. Yang, "Simultaneous removal of organic and inorganic contaminants by micellar enhanced ultrafiltration with mixed surfactant," *Desalination*, vol. 184, no. 1–3, pp. 395–407, Nov. 2005, doi: 10.1016/j.desal.2005.03.050.

[75] E. Samper, M. Rodríguez, M. A. de la Rubia, and D. Prats, "Removal of metal ions at low concentration by micellar-enhanced ultrafiltration (MEUF) using sodium dodecyl sulfate (SDS) and linear alkylbenzene sulfonate (LAS)," *Separation and Purification Technology*, vol. 65, no. 3, pp. 337–342, Mar. 2009, doi: 10.1016/j.seppur.2008.11.013.

[76] S. Angot, K. S. Murthy, D. Taton, and Y. Gnanou, "Atom transfer radical polymerization of styrene using a novel octafunctional initiator: Synthesis of well-defined polystyrene stars," *Macromolecules*, vol. 31, no. 21, pp. 7218–7225, Oct. 1998, doi: 10.1021/ma980712y.

[77] K. Matyjaszewski, "Atom Transfer Radical Polymerization (ATRP): Current status and future perspectives," *Macromolecules*, vol. 45, no. 10, pp. 4015–4039, May 2012, doi: 10.1021/ma3001719.

[78] K. Matyjaszewski and N. v. Tsarevsky, “Macromolecular engineering by atom transfer radical polymerization,” *Journal of the American Chemical Society*, vol. 136, no. 18. American Chemical Society, pp. 6513–6533, May 07, 2014. doi: 10.1021/ja408069v.

[79] K. Matyjaszewski and N. v. Tsarevsky, “Nanostructured functional materials prepared by atom transfer radical polymerization,” *Nature Chemistry*, vol. 1, no. 4, pp. 276–288, Jul. 2009, doi: 10.1038/nchem.257.

[80] W. A. Braunecker and K. Matyjaszewski, “Controlled/living radical polymerization: Features, developments, and perspectives,” *Progress in Polymer Science (Oxford)*, vol. 32, no. 1. pp. 93–146, Jan. 2007. doi: 10.1016/j.progpolymsci.2006.11.002.

[81] C. J. Hawker, A. W. Bosman, and E. Harth, “New polymer synthesis by nitroxide mediated living radical polymerizations,” *Chemical Reviews*, vol. 101, no. 12. pp. 3661–3688, Dec. 2001. doi: 10.1021/cr990119u.

[82] K. Matyjaszewski and J. Xia, “Atom transfer radical polymerization,” *Chemical Reviews*, vol. 101, no. 9, pp. 2921–2990, Sep. 2001, doi: 10.1021/cr940534g.

[83] Y. Zhao and S. Perrier, “Synthesis of well-defined conjugated copolymers by RAFT polymerization using cysteine and glutathione-based chain transfer agents,” *Chemical Communications*, no. 41, pp. 4294–4296, 2007, doi: 10.1039/b708293b.

[84] C. J. Hawker, A. W. Bosman, and E. Harth, “New polymer synthesis by nitroxide mediated living radical polymerizations,” *Chemical Reviews*, vol. 101, no. 12. pp. 3661–3688, Dec. 2001. doi: 10.1021/cr990119u.

[85] N. v. Tsarevsky and K. Matyjaszewski, “"Green:atom transfer radical polymerization: From process design to preparation of well-defined environmentally friendly polymeric materials,” *Chemical Reviews*, vol. 107, no. 6. pp. 2270–2299, Jun. 2007. doi: 10.1021/cr050947p.

[86] F. di Lena and K. Matyjaszewski, “Transition metal catalysts for controlled radical polymerization,” *Progress in Polymer Science (Oxford)*, vol. 35, no. 8. Elsevier Ltd, pp. 959–1021, 2010. doi: 10.1016/j.progpolymsci.2010.05.001.

[87] T. E. Patten and K. Matyjaszewski, “Copper(I)-catalyzed atom transfer radical polymerization,” *Accounts of Chemical Research*, vol. 32, no. 10, pp. 895–903, 1999, doi: 10.1021/ar9501434.

[88] Y. Shen, H. Tang, and S. Ding, “Catalyst separation in atom transfer radical polymerization,” *Progress in Polymer Science (Oxford)*, vol. 29, no. 10. pp. 1053–1078, Oct. 2004. doi: 10.1016/j.progpolymsci.2004.08.002.

[89] C. H. Peng, J. Scricco, S. Li, M. Fryd, and B. B. Wayland, “Organo-cobalt mediated living radical polymerization of vinyl acetate,” *Macromolecules*, vol. 41, no. 7, pp. 2368–2373, Apr. 2008, doi: 10.1021/ma702500b.

[90] B. B. Wayland, C. H. Peng, X. Fu, Z. Lu, and M. Fryd, “Degenerative transfer and reversible termination mechanisms for living radical polymerizations mediated by

cobalt porphyrins," *Macromolecules*, vol. 39, no. 24, pp. 8219–8222, Nov. 2006, doi: 10.1021/ma061643n.

[91] B. B. Wayland, G. Poszmik, S. L. Mukerjee, M. Fryd, D. H. Polym Bull, and D. H. J Macromol Sci, "Living Radical Polymerization of Acrylates by Organocobalt Porphyrin Complexes (12) (a) Moad," 1994. [Online]. Available: https://pubs.acs.org/sharingguidelines

[92] A. K. Nanda and K. Matyjaszewski, "Effect of [PMDETA]/[Cu(I)] ratio, monomer, solvent, counterion, ligand, and alkyl bromide on the activation rate constants in atom transfer radical polymerization," *Macromolecules*, vol. 36, no. 5, pp. 1487–1493, Mar. 2003, doi: 10.1021/ma0340107.

[93] W. Tang and K. Matyjaszewski, "Effects of initiator structure on activation rate constants in ATRP," *Macromolecules*, vol. 40, no. 6, pp. 1858–1863, Mar. 2007, doi: 10.1021/ma062897b.

[94] M. Kato, M. Kamigaito, M. Sawamoto, and T. Higashimura3, "Polymerization of Methyl Methacrylate with the Carbon Tetrachloride/Dichlorotris-(triphenylphosphine)ruthenium(II)/ Methylaluminum Bis(2,6-di-ferf-butylphenoxide) Initiating System: Possibility of Living Radical Polymerization1 Scheme 1. Proposed Pathway of the Polymerization of MMA with CCIVRuChíPPhalVMeAKODBPlü," 1995. [Online]. Available: https://pubs.acs.org/sharingguidelines

[95] T. Grimaud and K. Matyjaszewski, "Controlled/"Living" Radical Polymerization of Methyl Methacrylate by Atom Transfer Radical Polymerization," 1997.

[96] T. Ando, M. Kamigaito, and M. Sawamoto, "Iron(II) Chloride Complex for Living Radical Polymerization of Methyl Methacrylate 1," 1997.

[97] C. Granel, P. Dubois, R. Jé rô me, and P. Teyssié, "Controlled Radical Polymerization of Methacrylic Monomers in the Presence of a Bis(ortho-chelated) Arylnickel(II) Complex and Different Activated Alkyl Halides," 1996. [Online]. Available: https://pubs.acs.org/sharingguidelines

[98] W. Tang, Y. Kwak, W. Braunecker, N. v. Tsarevsky, M. L. Coote, and K. Matyjaszewski, "Understanding atom transfer radical polymerization: Effect of ligand and initiator structures on the equilibrium constants," *J Am Chem Soc*, vol. 130, no. 32, pp. 10702–10713, Aug. 2008, doi: 10.1021/ja802290a.

[99] J. Qiu and K. Matyjaszewski, "Polymerization of Substituted Styrenes by Atom Transfer Radical Polymerization," 1997.

[100] J.-S. Wang and K. Matyjaszewski, "Control1ed"Living" Radical Polymerization. Atom Transfer Radical Polymerization in the Presence of Transition-Metal Complexes," 1995.

[101] M. P. Kurlykin, A. E. Bursian, M. M. Dudkina, and A. v. Ten'kovtsev, "Synthesis of Star-Shaped Polymers Based on 2-ALKYL-2-Oxazoline with a Calix[8]Arene Central

Core and the Study of Their Heat-Sensitive Properties," *Fibre Chemistry*, vol. 47, no. 4, pp. 291–297, Nov. 2015, doi: 10.1007/s10692-016-9681-x.

[102] A. E. Acar, M. B. Yağci, and L. J. Mathias, "Adventitious effect of air in atom transfer radical polymerization: air-induced (reverse) atom transfer radical polymerization of methacrylates in the absence of an added initiator," *Macromolecules*, vol. 33, no. 21, pp. 7700–7706, Oct. 2000, doi: 10.1021/ma000623x.

[103] K. Matyjaszewski, "CONCEPTS," 1999.

[104] W. A. Braunecker, N. v. Tsarevsky, A. Gennaro, and K. Matyjaszewski, "Thermodynamic components of the atom transfer radical polymerization equilibrium: Quantifying solvent effects," *Macromolecules*, vol. 42, no. 17, pp. 6348–6360, Sep. 2009, doi: 10.1021/ma901094s.

[105] N. Bortolamei, A. A. Isse, A. J. D. Magenau, A. Gennaro, and K. Matyjaszewski, "Controlled aqueous atom transfer radical polymerization with electrochemical generation of the active catalyst," *Angewandte Chemie - International Edition*, vol. 50, no. 48, pp. 11391–11394, Nov. 2011, doi: 10.1002/anie.201105317.

[106] F. Seeliger and K. Matyjaszewski, "Temperature effect on activation rate constants in ATRP: New mechanistic insights into the activation process," *Macromolecules*, vol. 42, no. 16, pp. 6050–6055, Aug. 2009, doi: 10.1021/ma9010507.

[107] K. Matyjaszewski, K. Davis, T. E. Patten, and M. Wei, "Observation and Analysis of a Slow Termination Process in the Atom Transfer Radical Polymerization of Styrene," 1997.

[108] S. Averick *et al.*, "ATRP under biologically relevant conditions: Grafting from a protein," *ACS Macro Letters*, vol. 1, no. 1, pp. 6–10, Jan. 2012, doi: 10.1021/mz200020c.

[109] V. Coessens, T. Pintauer, and K. Matyjaszewski, "Functional polymers by atom transfer radical polymerization."

[110] K. Matyjaszewski and J. Spanswick, "Controlled/living radical polymerization," *Materials Today*, vol. 8, no. 3, pp. 26–33, 2005, doi: 10.1016/S1369-7021(05)00745-5.

[111] E. G. Koulouri, J. K. Kallitsis, and G. Hadziioannou, "Terminal anhydride functionalized polystyrene by atom transfer radical polymerization used for the compatibilization of nylon 6/PS blends," *Macromolecules*, vol. 32, no. 19, pp. 6242–6248, Sep. 1999, doi: 10.1021/ma990087c.

[112] H. Gao and K. Matyjaszewski, "Synthesis of star polymers by a new 'core-first' method: Sequential polymerization of cross-linker and monomer," *Macromolecules*, vol. 41, no. 4, pp. 1118–1125, Feb. 2008, doi: 10.1021/ma702560f.

[113] N. Badi, D. Chan-Seng, and J. F. Lutz, "Microstructure control: An underestimated parameter in recent polymer design," *Macromolecular Chemistry and Physics*, vol. 214, no. 2, pp. 135–142, Jan. 2013, doi: 10.1002/macp.201200475.

[114] Y. Kwak, R. Nicolaÿ, and K. Matyjaszewski, "Synergistic interaction between ATRP and RAFT: Taking the best of each world," *Australian Journal of Chemistry*, vol. 62, no. 11, pp. 1384–1401, 2009, doi: 10.1071/CH09230.

[115] S. Coca and K. Matyjaszewski, "Block Copolymers by Transformation of 'Living' Carbocationic into 'Living' Radical Polymerization," 1997. [Online]. Available: https://pubs.acs.org/sharingguidelines

[116] F. S. Bates and G. H. Fredrickson, "Block copolymers-designer soft materials," *Physics Today*, vol. 52, no. 2, pp. 32–38, 1999, doi: 10.1063/1.882522.

[117] K. Matyjaszewski, M. J. Ziegler, S. v Arehart, D. Greszta, and T. Pakula, "Gradient copolymers by atom transfer radical copolymerization," 2000.

[118] "WO2006003317A1".

[119] J. Kim, M. K. Gray, H. Zhou, S. B. T. Nguyen, and J. M. Torkelson, "Polymer blend compatibilization by gradient copolymer addition dining melt processing: Stabilization of dispersed phase to static coarsening," *Macromolecules*, vol. 38, no. 4, pp. 1037–1040, Feb. 2005, doi: 10.1021/ma047549t.

[120] J. Kim, H. Zhou, S. B. T. Nguyen, and J. M. Torkelson, "Synthesis and application of styrene/4-hydroxystyrene gradient copolymers made by controlled radical polymerization: Compatibilization of immiscible polymer blends via hydrogen-bonding effects," *Polymer (Guildf)*, vol. 47, no. 16, pp. 5799–5809, Jul. 2006, doi: 10.1016/j.polymer.2006.06.030.

[121] J. Kim, M. M. Mok, R. W. Sandoval, D. J. Woo, and J. M. Torkelson, "Uniquely broad glass transition temperatures of gradient copolymers relative to random and block copolymers containing repulsive comonomers," *Macromolecules*, vol. 39, no. 18, pp. 6152–6160, Sep. 2006, doi: 10.1021/ma061241f.

[122] M. Zamfir and J. F. Lutz, "Ultra-precise insertion of functional monomers in chain-growth polymerizations," *Nature Communications*, vol. 3, 2012, doi: 10.1038/ncomms2151.

[123] J. F. Lutz, B. V. K. J. Schmidt, and S. Pfeifer, "Tailored polymer microstructures prepared by atom transfer radical copolymerization of styrene and N-substituted maleimides," *Macromolecular Rapid Communications*, vol. 32, no. 2, pp. 127–135, Jan. 2011, doi: 10.1002/marc.201000664.

[124] W. Jakubowski and K. Matyjaszewski, "Activators regenerated by electron transfer for atom-transfer radical polymerization of (meth)acrylates and related block copolymers," *Angewandte Chemie - International Edition*, vol. 45, no. 27, pp. 4482–4486, Jul. 2006, doi: 10.1002/anie.200600272.

[125] A. Anastasaki *et al.*, "Cu(0)-Mediated Living Radical Polymerization: A Versatile Tool for Materials Synthesis," *Chemical Reviews*, vol. 116, no. 3. American Chemical Society, pp. 835–877, Feb. 10, 2016. doi: 10.1021/acs.chemrev.5b00191.

[126] D. Konkolewicz *et al.*, "Aqueous RDRP in the presence of Cu0: The exceptional activity of CuI confirms the SARA ATRP mechanism," *Macromolecules*, vol. 47, no. 2, pp. 560–570, Jan. 2014, doi: 10.1021/ma4022983.

[127] D. Konkolewicz *et al.*, "Reversible-deactivation radical polymerization in the presence of metallic copper. A critical assessment of the SARA ATRP and SET-LRP mechanisms," *Macromolecules*, vol. 46, no. 22. pp. 8749–8772, Nov. 26, 2013. doi: 10.1021/ma401243k.

[128] V. Percec *et al.*, "Ultrafast synthesis of ultrahigh molar mass polymers by metal-catalyzed living radical polymerization of acrylates, methacrylates, and vinyl chloride mediated by SET at 25 °C," *J Am Chem Soc*, vol. 128, no. 43, pp. 14156–14165, Nov. 2006, doi: 10.1021/ja065484z.

[129] B. M. Rosen and V. Percec, "Single-electron transfer and single-electron transfer degenerative chain transfer living radical polymerization," *Chemical Reviews*, vol. 109, no. 11, pp. 5069–5119, Nov. 2009, doi: 10.1021/cr900024j.

[130] G. Lligadas, B. M. Rosen, M. J. Monteiro, and V. Percec, "Solvent choice differentiates SET-LRP and Cu-mediated radical polymerization with non-first-order kinetics," *Macromolecules*, vol. 41, no. 22, pp. 8360–8364, Nov. 2008, doi: 10.1021/ma801774d.

[131] G. R. Jones *et al.*, "Cu(0)-RDRP of methacrylates in DMSO: Importance of the initiator," *Polymer Chemistry*, vol. 9, no. 18, pp. 2382–2388, May 2018, doi: 10.1039/c7py01196b.

[132] R. Whitfield, A. Anastasaki, G. R. Jones, and D. M. Haddleton, "Cu(0)-RDRP of styrene: Balancing initiator efficiency and dispersity," *Polymer Chemistry*, vol. 9, no. 34, pp. 4395–4403, Sep. 2018, doi: 10.1039/c8py00814k.

[133] J. P. Mendes *et al.*, "Ambient temperature SARA ATRP for meth(acrylates), styrene, and vinyl chloride using sulfolane/1-butyl-3-methylimidazolium hexafluorophosphate-based mixtures," *Journal of Polymer Science, Part A: Polymer Chemistry*, vol. 55, no. 8, pp. 1322–1328, Apr. 2017, doi: 10.1002/pola.28499.

[134] M. Kopeć *et al.*, "Polyacrylonitrile-b-poly(butyl acrylate) Block Copolymers as Precursors to Mesoporous Nitrogen-Doped Carbons: Synthesis and Nanostructure," *Macromolecules*, vol. 50, no. 7, pp. 2759–2767, Apr. 2017, doi: 10.1021/acs.macromol.6b02678.

Chapter II. Core-shell nanoparticles

Part I. Synthesis and characterization of polystyrene-b-poly(vinyldipicolinic acid) pH-responsive core-shell nanoparticles.

Abdel Wahab Mouhamad[a,b], Tamara Elzein[a,*], Nadine Barroca-Aubry[b], Eric Simoni[b], Nael Berri[a,b], Philippe Roger[b,*]

[a] Lebanese Atomic Energy Commission, National Council for Scientific Research (CNRS-L), Beirut, Lebanon

[b] Institut de Chimie Moléculaire et des Matériaux d'Orsay (ICMMO), UMR 8182, Université Paris-Saclay, 91405, Orsay, France

Graphical abstract

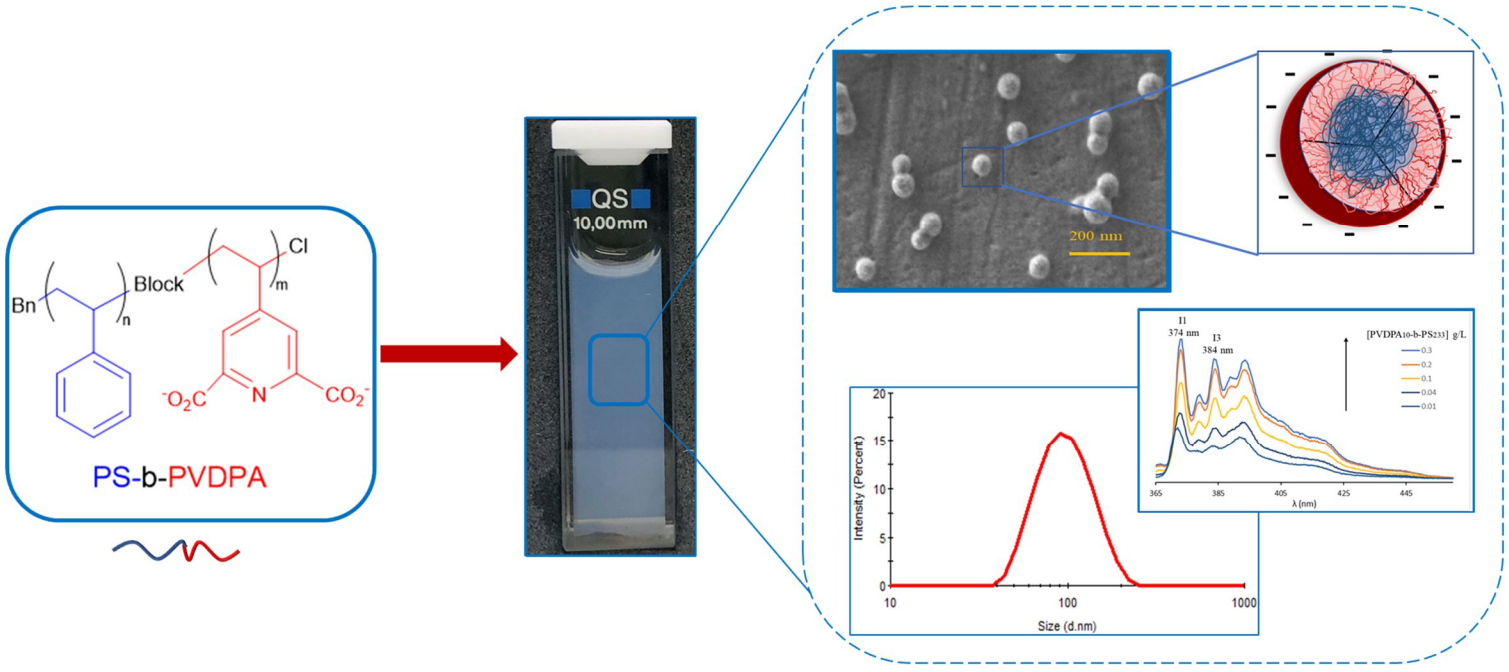

Abstract

In this paper, the self-assembly of a new series of amphiphilic polystyrene-b-poly(4-vinyldipicolinic acid) PS-b-PVDPA diblock copolymers in aqueous solution is reported. These well-defined diblock copolymers were synthesized by Supplemental Activation Reducing Agent-Atom Transfer Radical Polymerization (SARA-ATRP). Latex nanoparticles of PS-b-PVDPA were prepared by solvent displacement methods. The synthesized nanoparticles were found to have a core, shell-like structure composed of a PS core and PVDPA shell. DLS was used to determine nanoparticle size, with SEM and TEM used to determine and confirm both size and spherical shape. All three methods found the size for these nanoparticles to be less than 120 nm. Using fluorimetry and DLS methods, Critical Micelle Concentration (CMC) for each type of nanoparticle was determined to be within the range of 33-69 mg/L. Our findings indicate that their high stability and their resistance to many external stimuli (temperature and pH) make nanoparticles excellent candidates for use in medical, pharmaceutical, and environmental fields.

Keywords: Amphiphilic diblock copolymer, self-assembly, anionic nanoparticles, CMC, pH responsive.

Introduction

Special attention has been dedicated to amphiphilic block copolymers, which undergo spontaneous self-assembly in hydrophobic or hydrophilic environments, and form supramolecular structures with a high degree of ordering of copolymer chains [1][2]. The use of block copolymer colloidal systems has been reported in a wide field of applications, such as smart gels [3] controlled drug delivery systems [4][5] and carriers of biological markers dyes [6].

The most important and effective synthetic strategies for the preparation of amphiphilic block copolymers involve various controlled radical polymerization methods such as Reversible Addition Fragmentation Chain Transfer (RAFT) [7], Iodine Transfer Polymerization (ITP) [8] and Atom Transfer Radical Polymerization (ATRP) [9]. The use

of these efficient controlled/living radical polymerizations for the synthesis of well-defined copolymers, with different architecture resulted in a controlled molar mass of the blocks.

Atom Transfer Radical Polymerization (ATRP) is one of the most studied methods due to its robustness, versatility, monomer tolerance and mild reactions conditions [10]. This process is usually catalyzed by copper complexes, with amine ligands (L), in the Cu^{I} oxidation state. An equilibrium is established between active radicals and dormant species through a reversible redox reaction between Cu^{I}/L species and an organic halide (R−X). Important research efforts have been devoted to the reduction of the amount of metal complexes required to perform ATRP reactions. On this matter, different ATRP variations have been developed, lowering the required amount of catalyst to ppm levels to afford fast and controlled polymerizations. In our work, we focused on the supplemental activator and reducing agent SARA-ATRP [11]. The SARA-ATRP method was successfully used for controlled polymerization of a wide range of monomers like methyl methacrylate (MMA) [12], styrene (Sty) [13], and vinyl chloride (VC) [14]. This method allows preparation polymers with distinct architectures like well-defined block copolymer [15].

The literature abounds with studies using amphiphilic block copolymers of different compositions and various methods of preparation that produce nanoparticles (NPs) referred to as micelles, nanospheres, core-shell nanoparticles, micelle-like nanoparticles, crew cut micelles, nanocapsules and polymersomes [16].

A practical method developed to prepare nanoparticles is nanoprecipitation. For instance, when water is slowly added to an organic polymer solution, larger spherical particles and vesicle structures are frequently obtained. When the opposite occurs and an organic polymer solution is slowly added to water, spherical particles with small hydrodynamic radii often result [17].

Herein, we report the synthesis of a new diblock copolymer polystyrene-b-poly(4-vinyl dimethyl dipicolinate) PS-b-PVDPM by varying the ratio between blocks domain size and the preparation of nanoparticles behavior. Previously reported works has been shown that poly(vinyldipicolinic acid) PVDPA homopolymer is an excellent chelating material for lanthanides and actinides and in particular has an excellent ability for uranium harvesting from seawater [18]. Hence, nanoparticles with PVDPA chains have a negatively chelating

charged hydrophilic shell may be used for many applications i.e., luminescent nanoparticles with lanthanides-containing [19].

The self-assembly of PS-b-PVDPM copolymers in water performed by dialysis was studied to find the Critical Micelle Concentration (CMC) and to establish the structures formed by the copolymer above the CMC. Fluorescence spectroscopy and Dynamic Light Scattering (DLS) were used for such purpose. Fluorescence spectroscopy has been used to determine the CMC of diblock copolymer micelles. The pyrene molecule is frequently used as fluorescent probe in spectrofluorometry since its fluorescence intensity peaks at λ_{max} = 373 and 384 nm, denoted I_1 and I_3 respectively, are sensitive to the local environment [20]. Using the characteristic dependence of the fluorescence vibrational fine structure of pyrene, the so-called pyrene 1:3 ratio method has widely been used to determine the CMC [21]. By contrast, DLS is a relatively new technique for this purpose [22]. At very low concentrations, when the copolymer chains are isolated, the intensity of light scattered is weak. Above a certain concentration, when the CMC is reached in solution, the intensity of scattered light increases dramatically due to the formation of micelles.

The effect of degree of polymerization (DP) of both PS and PVDPA blocks on hydrodynamic diameter and pH-responsive behavior had been explored for the nanoparticles systems. DLS was used to study the colloidal stability of these diblock copolymer nanoparticles at different pH values and temperature while their charged characters were determined by zeta potential studies. Scanning Electron Microscope SEM and Transmission Electron Microscopy (TEM) were used to determine the morphologies of copolymer nanoparticles. CMC values were determined by using DLS and pyrene 1:3 ratio method.

Materials and methods

Materials.

Styrene (Sty, Sigma Aldrich, ≥ 99%) was passed through silica gel to remove the inhibitor, copper (II) chloride ($CuCl_2$, 98%), Benzyl chloride (BnCl, >98%), Tris(2-pyridylmethyl)amine (TPMA, TCI, >98%) were used without further purification. Tetrahydrofuran (THF, pure), sulfolane (Alfa Aesar, 99% pure), were obtained from Alfa-

Aesar and Copper (0) wire (d = 1.0 mm, density ≈ 7.02 g/m^2, 99.9% Alfa-Aesar) was activated by a quick wash in HCl (1 M)/ MeOH (1/1) then dried.

Methods.

Size-Exclusion Chromatography (SEC): Size Exclusion Chromatography (SEC) analysis of polymers was carried out at 35 °C using THF as eluent. Typically, the polymer solution was prepared at 4 mg.mL^{-1} and then filtered through 0.45 µm PTFE filter to remove insoluble residues. The separation system includes one guard column (Malvern TGuard) and two separation columns: 1) Viscotek LC3000L (300 x 8.0 mm) and 2) ViscoGELTM GMHH r-H (300 x 7.8 mm). The intensity was recorded using a refractive index (RI) detector (Walter 410) and a multi-angle light scattering (MALS) detector (Viscotek SEC-MALS 20). A refractive index increment (dn/dc) of 0.185 mL.g^{-1} was determined experimentally and used for the determination of absolute molecular weight using OmniSec™ 5.12.467 software distributed by Malvern Panalytical.

Nuclear magnetic resonance (NMR): All ^{1}H NMR spectra were recorded in $CDCl_3$ using Bruker Avance 360 MHz at 25 °C. DOSY ^{1}H spectra were recorded in $CDCl_3$ on a Bruker Avance 400 MHz at 25 °C.

Dynamic Light Scattering (DLS): DLS was performed on a Malvern Zetasizer nano ZS instrument equipped with a He-Ne laser beam at a wavelength (λ = 632 nm) and scattering angle of 173°. The critical micelle concentration (CMC) for each micelle system was determined by first examining the micelle sample at a concentration of 0.1 mg/mL and manually setting the attenuator so that the count rate ranged around 400-900 KCPS. Then, the sample was serially diluted, and each sample was measured with this fixed attenuator. The count rate was plotted as a function of concentration, with the CMC corresponding to the intersection of the upper and lower linear trend lines.

Fluorescence measurements: Fluorescence measurements were performed in a fluoro-Max-4 spectrofluorometer, fluorescence emission spectra of several diblock copolymer solutions containing 2 µM of pyrene were excited at 334 nm and its emission was recorded at 374 and 384 nm, which correspond to the first and third vibrational peaks, respectively and with use of excitation slit of 5.

Thermogravimetric Analysis (TGA): Thermal stability of the polymers were performed under argon at a flow rate of 20 mL.min^{-1} and a temperature ramp of 10 °C.min^{-1} up to 900 °C using a TA Instruments SDT Q600 apparatus.

Experimental.

Diblock copolymers Poly(4-vinyl dimethyl dipicolinate)-block-Polystyrene (PVDPM-b-PS) have been prepared by two methods:

Synthesis of the hydrophobic block homopolymer PS-Cl

The macro-initiator polystyrene (PS-Cl) was prepared by using SARA-ATRP polymerization. A solution of $CuCl_2$ (2.3 mg), TPMA (50 mg) and 10 mL styrene was prepared (Sty/ $CuCl_2$/ TPMA = 100 / 0.02 / 0.2). Then, 6 mL of this solution was placed in a 10 mL tube with 5 cm copper wire and 30 µL of BnCl initiator (DP = 200). The tube was closed and placed in a preheated oil bath at 60°C.

The appearance of dark green color is obvious, and the mixture becomes progressively more viscous. The monomer conversion was determined by ^{1}H NMR in $CDCl_3$ and the molecular weight parameters were determined by SEC analysis. The reaction solution was then diluted with DCM and the polymer was precipitated in excess methanol, filtrated, and dried under vacuum.

$\bar{M}_n$ = 11 100 g/mol, $\bar{M}_w$ / $\bar{M}_n$ = 1.07. ^{1}H NMR (360 MHz, $CDCl_3$): δ (ppm) = 1.15-2.37 (m, CH_2 and CH of PS,), 4.50 (m, 1H, CHCl), 6.28 -7.27 (m, 5H, aromatic).

Synthesis of amphiphilic diblock copolymer PS-b-PVDPM

The diblock copolymer PS-b-PVDPM chains were built from the PS-Cl as the macro-initiator described above substrate by SARA-ATRP polymerization. According to our previous work [18], VDPM was synthesized with the following modification, the $PdCl_2(PPh_3)_2$ catalyst was used instead of $Pd(OAc)_2$ for the Suzuki coupling reaction in order to increase the yield and reduce the time of reaction. VDPM (82.3 mg, 0.375 mmol), TPMA (0.87 mg, 0.003 mmol), $CuCl_2$ (0.02 mg, 0.00015 mmol), and the copper wire at 1 cm/mL were placed in a 10 mL tube equipped with magnetic bar with 0.8 mL DMSO, with prior degassing. 88.8 mg of crude PS-Cl dissolved in 0.8 mL dioxane was added. The tube

was closed and placed in a preheated oil bath at 60 °C for 2 h (S / VDPM / BnCl / CuCl2 / TPMA = 400 / 10 / 1 / 0.02 / 0.4). Monomer conversion was determined using ^{1}H NMR in $CDCl_3$. The afforded product was purified by diluted with DCM and precipitation in MeOH.

^{1}H NMR (360 MHz, $CDCl_3$): δ (ppm) = 1.20-2.08 (m, CH_2 and CH of PS), 3.80-4.05 (m, 6H, $COOCH_3$), 6.28-7.19 (m, 5H, aromatic).

Synthesis of amphiphilic diblock copolymer PVDPM-b-PS

VDPM monomer (110.6 mg), TPMA (5.8 mg), $CuCl_2$ (0.135 mg), DMSO (0.3 mL) and Cu^0 (1cm) were placed in a 10 mL tube. 5.8 µL of the BnCl initiator was added and the tube was closed and placed in a preheated oil bath at 60 °C. After 30 minutes, NMR showed no traces of unreacted VDPM. 2.3 mL of styrene were injected with 0.5 mL sulfolane. One hour after styrene injection, a small aliquot was sampled, and a precipitation test was done. the sample precipitated in THF, meaning that the PVDPM block is still predominant, or maybe the styrene didn't even polymerize. After 2 hours, an aliquot was completely soluble in THF, meaning that polystyrene was successfully being built on the PVDPM block. Another 0.5 mL of sulfolane was added and the reaction kinetics monitored by NMR. At each point, an aliquot was precipitated in MeOH, filtrated and dried under vacuum.

^{1}H NMR (360 MHz, $CDCl_3$): δ (ppm) = 1.23-2.31 (m, CH_2 and CH of PS), 3.83-4.04 (m, 6H, $COOCH_3$), 6.26-7.22 (m, 5H, aromatic).

Nanoparticles preparation

The nanoparticles were prepared by self-assembly using a solvent displacement method with a THF/ACN-water system. In a typical procedure, the copolymer (5mg) was dissolved in 1 mL of THF and 0.5 mL of ACN. The polymer-solvents were added dropwise into 10 mL of deionized basic water (pH ~ 9) with stirring, and the mixture was continually stirred overnight to form micelles. The suspension was stirred under reduced pressure and dialyzed against water for 1 day to remove organic solvents.

Results and discussion

1. Block copolymer synthesis

Herein, two strategies were used to synthesize the PVDPM-b-PS, such diblock copolymers can be derived by sequential Supplemental Activation Reducing Agent-Atom Transfer Radical Polymerization (SARA-ATRP). Scheme 9 including a) the first strategy of copolymerization (one pot reaction), b) synthesis of the polystyrene block, c) polymerization of PVDPM initiated by the PS macro-initiator and d) hydrolysis of copolymer.

The first strategy is through the polymerization of the first block of VDPM with a fixed DP = 10 using BnCl as initiator. The NMR showed a total conversion of VDPM (Equation , see supporting information (SI)) then, the second styrene monomer can be added. Styrene conversion of $PVDPM_{10}$-b-PS was monitored by NMR (Equation 2, SI). Variable polystyrene block lengths were obtained depending on reaction time (Figure SI 1, SI). Three copolymers with DP of PS equal to 184, 233 and 260 were used in this study. In this way, the DP of the first block turns out to be limited, no synthesis modification made it possible to increase the DP above 10. The second strategy consisted in the preparation of the first block of polystyrene with Cl chain end and DP = 112 leading to a first sequence as a macro-initiator of PVDPM. Its molar mass calculated from ^{1}H NMR and measured by SEC are very close (c.a. 11100 g/mol). The signal of the macroinitiator's Cl end group is clearly visible in NMR spectra at 4.5 ppm (Figure SI 2, SI). However, the successful copolymerization using PS-Cl as macroinitiator was observed by appearing of broad peak of PVDPM at 3.9 ppm (Figure SI 3, SI). Two copolymers with DP of PVDPM equal to 30, 50 were obtained. Thanks to these strategies, 2 blocks with control length could be afforded.

Information about PVDPM-b-PS used in this study are presented in Table 3.

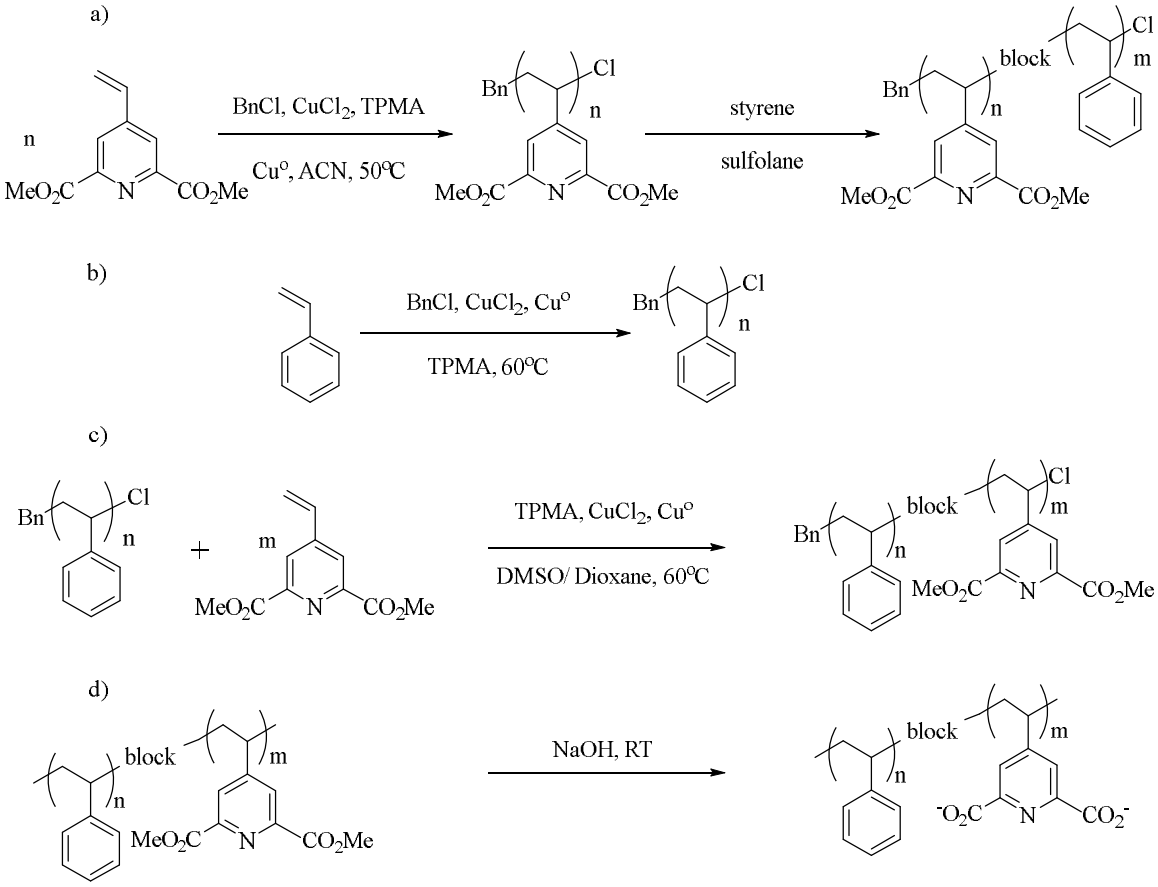

Scheme 9. Synthetic routes of a) PVDPM-b-PS following two steps one pot reaction b) homopolystyrene (macro-initiator), c) amphiphilic diblock copolymer (PS-b-PVDPM) and d) hydrolysis reaction of copolymer.

2. Diffusion data

To further demonstrate that polystyrene blocks are covalently joined with the PVDPM blocks, ^{1}H-DOSY experiments were performed. Briefly, this method allows us to assign a diffusion coefficient to every peak in an ^{1}H-NMR spectrum. If two peaks are assigned to similar diffusion coefficients, it can be inferred they come from the same molecule. In ^{1}H-DOSY plot in Figure 9a, the homopolystyrene (PS_{112}) signal at around 2 and 6.5 ppm have a diffusion coefficient close to 3.18×10^{-10} m^2 s^{-1}. However, the signals of the diblock copolymer (PS_{112}-b-$PVDPM_{50}$) in Figure 9b, have higher diffusion coefficient of 1.23×10^{-9} m^2 s^{-1} than the signals of the PS_{112}. Consequently, this demonstrates that the architecture of the products is indeed that of a diblock copolymer.

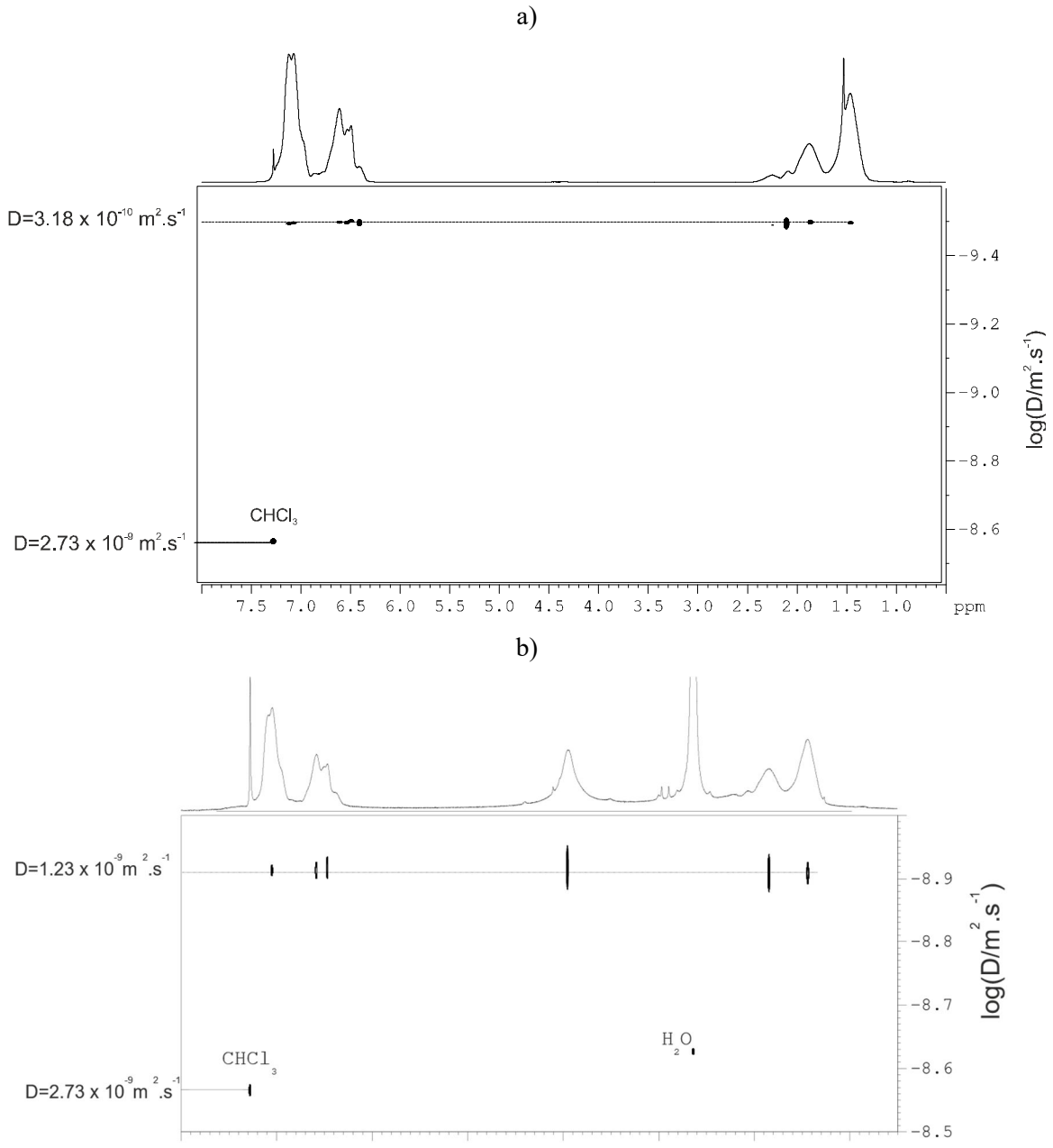

Figure 9. DOSY ^{1}H spectrum ($CDCl_3$, 400 MHz, 298 K) of the sample of a) the homopolystyrene (PS_{112}) b) the target polymerized diblock copolymer (PS_{112}-b-$PVDPM_{50}$)

Diblock copolymer	Time (hours)	NMR conversion (%)	MM_{NMR} (g/mol)
$PVDPM_{10}$-b-PS_{184}	18	46[a]	21 500
$PVDPM_{10}$-b-PS_{233}	22	58[a]	26 600
$PVDPM_{10}$-b-PS_{260}	29	65[a]	29 400
PS_{112}-b-$PVDPM_{30}$	3	30[b]	18 400
PS_{112}-b-$PVDPM_{50}$	5	50[b]	22 900

Table 3. Time of reaction, a) % of conversion of styrene (targeted DP = 400), b) % of conversion of VDPM (targeted DP = 100) and molar masses obtained by NMR.

3. Thermal characterization of polymers

Thermal stabilities of polymer ($PVDPM_{10}$), copolymer (PS_{112}-b- $PVDPM_{30}$ and PS_{112}-b-$PVDPM_{50}$) and polystyrene (PS_{112}) were established by TGA under argon atmosphere as shown in Figure 10. PVDPM and PS_{112} have only one step degradation, however, PS_{112}-b-$PVDPM_{30}$ and PS_{112}-b- $PVDPM_{50}$ undergo a two-step degradation. Early decrease in weight % below 100 °C is due to the loss of residuel solvents. In fact, as observed in the insert figure, the $PVDPM_{10}$ (~ 323 °C) homopolymer has much lower thermal stability than PS_{112} polystyrene (~ 410 °C). PS_{112}-b- $PVDPM_{30}$ have a two temperature of degradation (Td), the first Td_1 is arround 349 °C, which corresponds to the loss of the pendant group $PVDPM_{30}$ (~ 23% of weight loss). For PS_{112}-b- $PVDPM_{50}$ ~ 28% of weight was lost in the first time. The second temperature (Td_2) occurs between 340 °C and 830 °C, and it can be attributed to the degradation of polystyrene backbone (around 65% of weight loss). In addition, the derivative thermogravimetric (DTG) data along with the decomposition temperature (Td) in each degradation steps are shown in (Figure SI 4 SI).

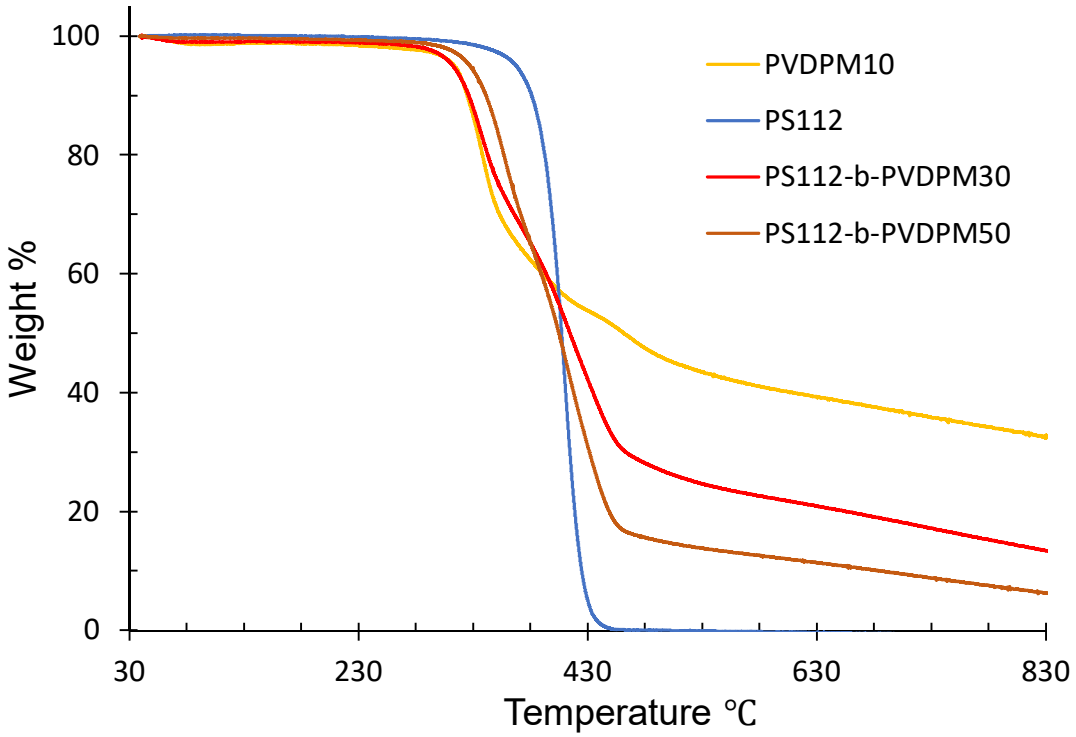

Figure 10. TGA traces of VDPM, PVDPM, PS, $PVDPM_{30}$-b-PS_{112} and $PVDPM_{50}$-b-PS_{112} with heating rate 10 °C min^{-1} from 30 °C min^{-1} to 830 °C min^{-1}

4. Nanoparticles preparation and morphology

Nanoprecipitation is based on the reduction of the quantity of the solvent in which the main composition of NPs is dissolved. At first, DLS studies of the block copolymer in organic solvent (THF/ACN) and nanoparticles in basic water were performed, suggesting particle sizes around 10 nm and 90 nm for diblock copolymer in organic solvent and nanoparticles formed in water respectively (Figure 11). Basic water (pH ~ 9) was used to transform ester to carboxylate functions as shown in Scheme 9. An explanation for the observed behavior might be the self-assembly demand of the blocks copolymer.

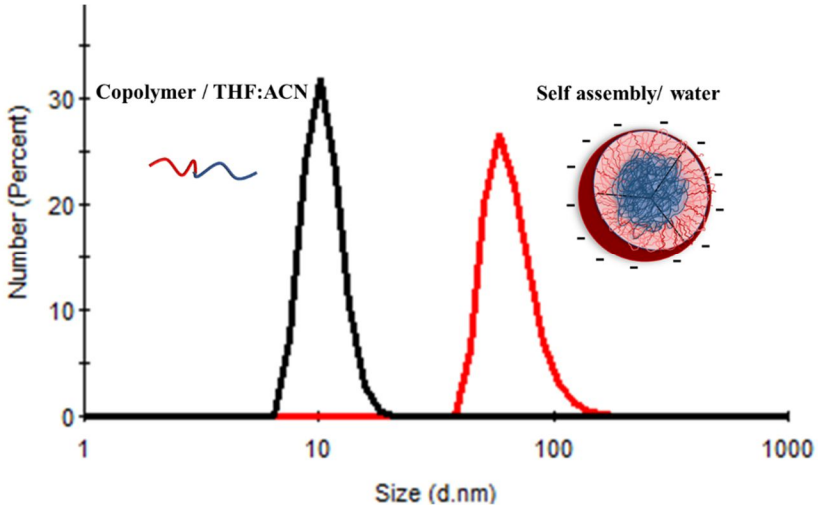

Figure 11. Hydrodynamic diameter distributions of $PVDPM_{10}$-b-PS_{184} obtained in THF/ ACN (black line) and in water (red line).

Using two different solvent displacement approaches, nanoparticles were prepared from $PVDPM_{10}$-b-PS_{260} (NP_3) either by the slow addition of water (pH ~ 9) to an organic polymer solution or vice versa. As seen in Figure 12A, a broad distribution of spherical particle sizes, and the overall diameters are consistent with DLS data (D_h = 248 nm, PDI = 0.1)(Figure SI 5, SI) obtained by the slow addition of water to an organic polymer solution. However, the nanoparticles prepared by the slow addition of organic polymer solution to water tend to be more uniform and smaller in size (Figure 12B) with a D_h of 120 nm and PDI of 0.01 (Figure SI 5, SI).

Based on of these observations, nanoparticles preparation, for all the synthesized copolymer, was done using the order of adding organic to water.

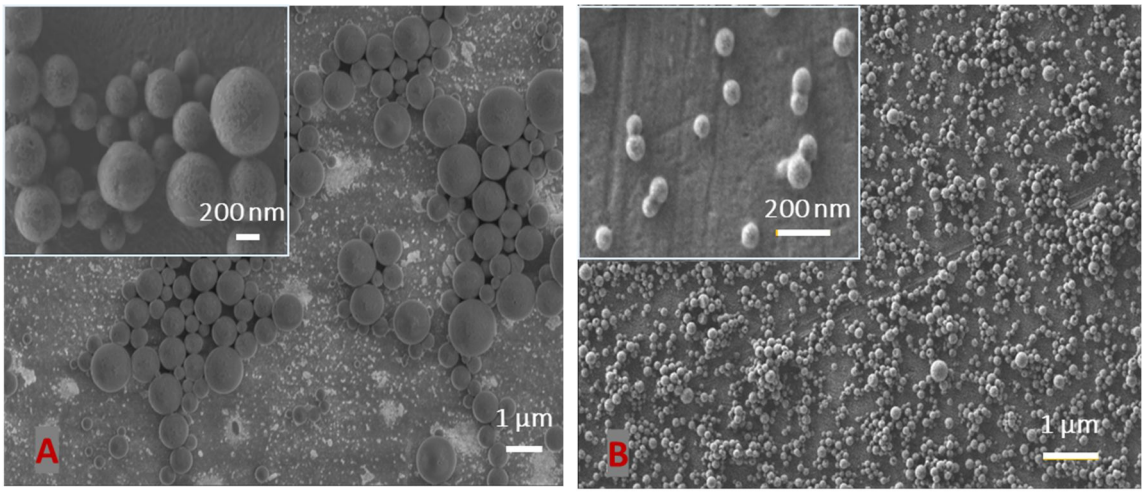

Figure 12. SEM photographs of the self-assembled nanoparticles from $PVDPM_{10}$-b-PS_{260} in aqueous solution: A) the addition of water to organic solution and B) the addition of organic solution to water.

The solution assemblies were characterized by dynamic light scattering (DLS) to determine the hydrodynamic diameter (Dh), zeta potential (ζ) and polydispersity (PDI). The morphology of the nanoparticles was further investigated by SEM and TEM which allow for direct visualization of the nanostructures formed. The detailed results are shown in . Table 4. The resulting nanoparticles had sizes between 75 and 120 nm depending on the copolymer composition. Table 4. self-assembled nanoparticles from the PVDPA-b-PS or PS-b-PVDPA copolymers in aqueous solution at 20 °C, pH ~ 5.5.

Entry	Copolymer	D_h (nm)[a]	ζ (mV)[b]	PDI[c]	CMC[d] (mg/L)	CMC[e] (mg/L)
NP_1	$PVDPA_{10}$-b-PS_{184}	86.3 ± 2.2	-26.9	0.136	63	69
NP_2	$PVDPA_{10}$-b-PS_{233}	96.3 ± 0.6	-27.2	0.044	59	56
NP_3	$PVDPA_{10}$-b-PS_{260}	120.0 ± 0.4	-27.5	0.014	50	43
NP_4	PS_{112}-b-$PVDPA_{30}$	75.1 ± 0.6	-37.3	0.144	40	47
NP_5	PS_{112}-b-$PVDPA_{50}$	87.2 ± 1.3	-37.9	0.072	33	35

[a] D_h average diameter of nanoparticles [b] ζ zeta potential were determined by the DLS technique. [c] PDI denotes the polydispersity of nanoparticles in aqueous solution. [d] CMC data obtained from fluorescence measurements (pyrene 1:3 ratio) and [e] CMC data obtained from DLS measurement.

Both the morphology and the average size of the self-assembled nanoparticles were investigated by SEM, TEM and DLS techniques. For the PVDPA-b-PS copolymers, when the weight fraction of hydrophobic (PS) block was 90 wt % within NP_1 sample, spherical nanoparticles were produced with an average diameter of 86.3 ± 2.2 nm. However, when the weight fraction of PS increased to 92 wt % for $PVDPA_{10}$-b-PS_{233} and 96 wt% for $PVDPA_{10}$-b-PS_{260} samples, an average diameter of 96.3 ± 0.6 and 120 ± 0.4 was obtained, respectively. On the other hand, for the same hydrophobic head (DP = 112), when the weight fraction of PVDPA was 36 wt % within NP_4, an average diameter of 75.1 ± 0.6 was achieved. As for the NP_5 having a weight fraction of 49 wt % PVDPA the average diameter increased to 87.2 ± 1.3. All the nanoparticle suspensions had a narrow size distribution (PDI ≤ 0.14) with zeta potential (≥ -26.9 mV) indicating strong electrostatic repulsions due to carboxylate anions and therefore high colloidal stability. As a note, the average size of these nanoparticles remained basically unchanged at least within 40 days at 20 °C (Figure SI 6a, SI). Moreover, these nanoparticles showed a notable stability even at high temperature (20-60°C) (Figure SI 6b, SI), suggesting a very good stability, providing them suitable for many applications.

Visualization of core-shell nanoparticles was done using the TEM. Microphotographs (Figure SI 7, SI) revealed spherical particles with diameter corresponding to those obtained from DLS measurements. In TEM, the diameters of the aggregates were about 105 nm for NP_3, and 60 nm for NP_4. All diameters given are an average of values taken for about 20 species.

5. CMC determination

The formation of nanoparticles of diblock copolymers was revealed using two methods. The Critical Micelle Concentration (CMC) of the block copolymer was detected by fluorescence spectroscopy using pyrene as a fluorescence probe [21]. Figure 13a shows the typical spectrum of pyrene fluorescence excited at 334 nm. The intensity of these spectra increases with increasing polymer concentration, which is one of their most notable characteristics only small changes appeared in the intensity ratio of the first and third vibrational bands, I_1/I_3. In the absence of nanopartices (below CMC), pyrene senses the polar environment of methanol so the fluorescence intensity of I_1/I_3 pyrene ratio is high. Above the CMC nanoparticles are formed, owing to the high hydrophobicity of pyrene, pyrene molecules are solubilized in the nanoparticles core. Because this is a non-polar solvent, the environment sensed by pyrene is less polar, and thus the I_1/I_3 pyrene ratio decreases. Figure 13b shows the plot of I_1/I_3 pyrene ratio versus the copolymer concentration for NP_2. Those of the other nanoparticles are reported on Figure SI 8. CMC is taken as intersection of the tangent to the curve at the inflection with the horizontal tangent through the points at low polymer concentration [23]. CMC were found using the DLS method [22] with a fixed attenuator, an increase in count rate accompanied the transition from single dissolved chains to self-assembled micelles as the polymer concentration was increased. From Figure 13c, it is observed that CMC can be obtained from the intersection of the straight lines for NP_2. Table 4 it seems obvious that CMCs founded values obtained by pyrene 1:3 ratio method is very close to those obtained by DLS method for each copolymer solution. Values for the calculated CMCs ranged from 33 to 69 g/L. The influence of the length of the hydrophilic block is negligible compared to that of the hydrophobic block [24][25]. Astafieva et al. [26] have shown that the length of the hydrophilic block on PS-b-PANa influences micellization when the hydrophobic block of the copolymer is short, i.e., about 6-110 units. So, as we can see increasing the content of hydrophilic PVDPA units in the copolymers resulted in decreasing the copolymers'CMC, as it is indicated in . Table 4. The increasing number of PVDPA units in designed copolymers allowed us to investigate the effect of hydrophilic block length on their aggregation (NP_4 and NP_5).

The results obtained for CMC of all the samples with fixed PVDPA equal to 10 (NP_1, NP_2 and NP_3) were displayed in . Table 4 as a function of polystyrene contents. It was shown that with increasing the PS/PVDPA ratio, the CMC of the copolymers decreased. The data concluded that the CMC was decreased with the increase in polystyrene contents. This dependence is often found for amphiphilic block copolymers and was reported for several diblock copolymers [25][26].

a)

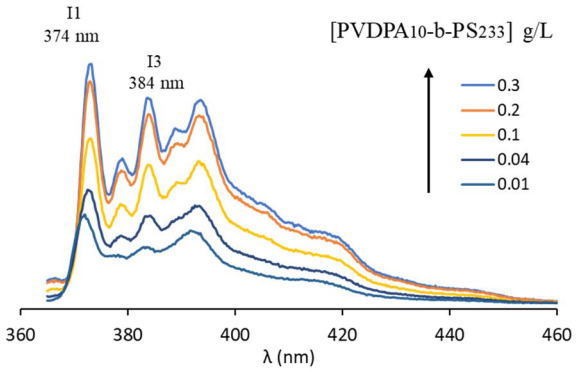

b)

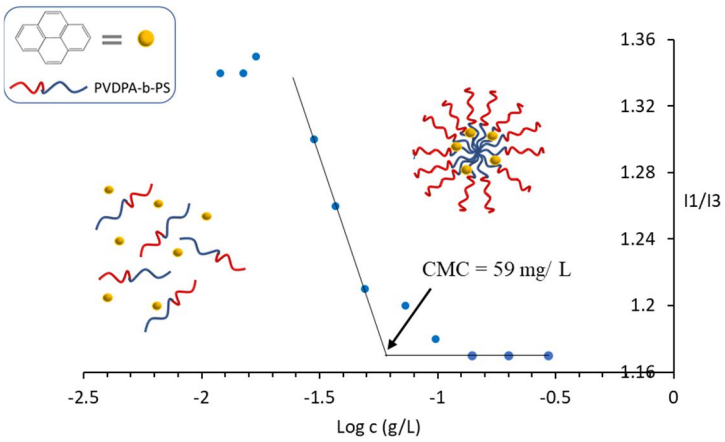

c)

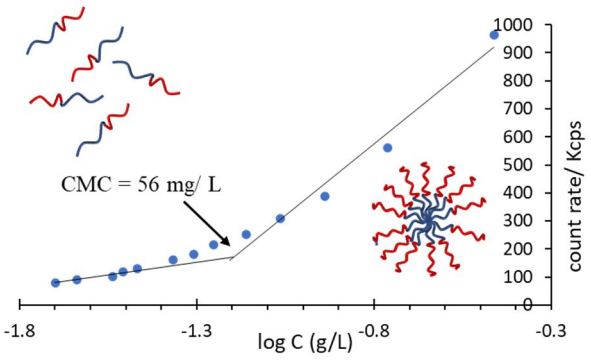

Figure 13. a) fluorescence spectra of pyrene in water in presence of increasing concentrations of diblock copolymer. The determination of the CMC for NP_2 using b) pyrene I_1/I_3 ratio method and c) the count rate obtained by DLS analysis at 20°C.

6. pH-responsive behavior of PVDPA-b-PS

DLS was used to measure the particle sizes and zeta potential of the nanoparticles at different pH values. The original solution pH value of PVDPA-b-PS latex was 5.5 after dialysis at room temperature. Scheme 10 shows an optical observation experiment determining the colloidal stability of NP_4 as a function of the pH values. It revealed that precipitation occurred for this latex nanoparticle when the pH value was < 4. The white solid is, in fact, the protonated form of carboxyl PVDPA block. DLS experiments were carried out to characterize the colloidal stabilities of NP_1 and NP_4 latex with varying solution pH values Scheme 11a. The colloidal stability of NP_4 latex was observed above pH 4 with a D_h of 74 ± 1 nm with PDI around 0.14, the particle dimension increases from 74 to 83 nm (PDI~0.23) with reducing pH values from pH 4 to pH 3.5 with appearance of a white precipitate (not detected by DLS) providing good evidence for a dispersion-to-aggregation transition. Zeta potential measurements were also correlated with the pH variation, as shown in Scheme 11a. The zeta potential of original latex was -37.3 mV indicating that colloids are highly stabilized by electrostatic repulsive force between carboxylate units of PVDPA. Once, the pH decreased, zeta potential decreased to -20.4 mV at pH 3.5. It is noteworthy to mention that, after one hour, a complete flocculation was observed. There is no doubt that the same pH-responsive behaviors of NP_1 and NP_4 latex can be attributed to the same locations of the carboxylate groups in the micellar structure. As can be seen in Scheme 11b, above pH 5.5 a slight variation on micelle diameter (D_h ~ 86 - 89 nm) and on zeta potential between -20 and -26 mV was observed. However, the fast flocculation was observed when the zeta potential value decreased to -12 mV at pH 4.

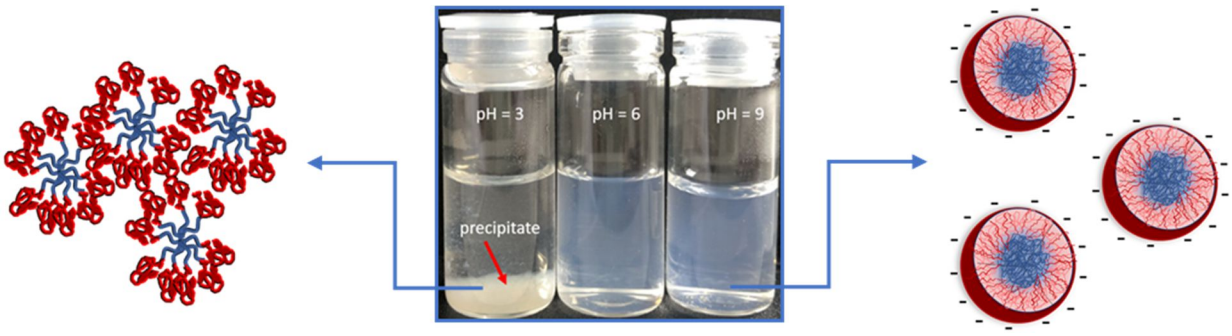

Scheme 10. Macroscopic appearances of nanosuspensions at different pH.

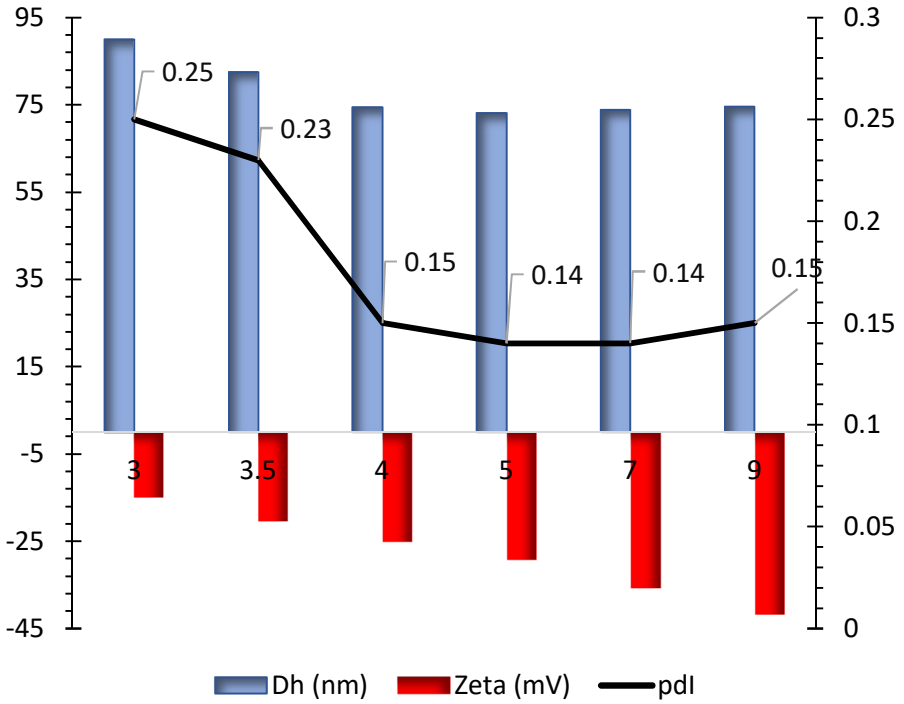

a)

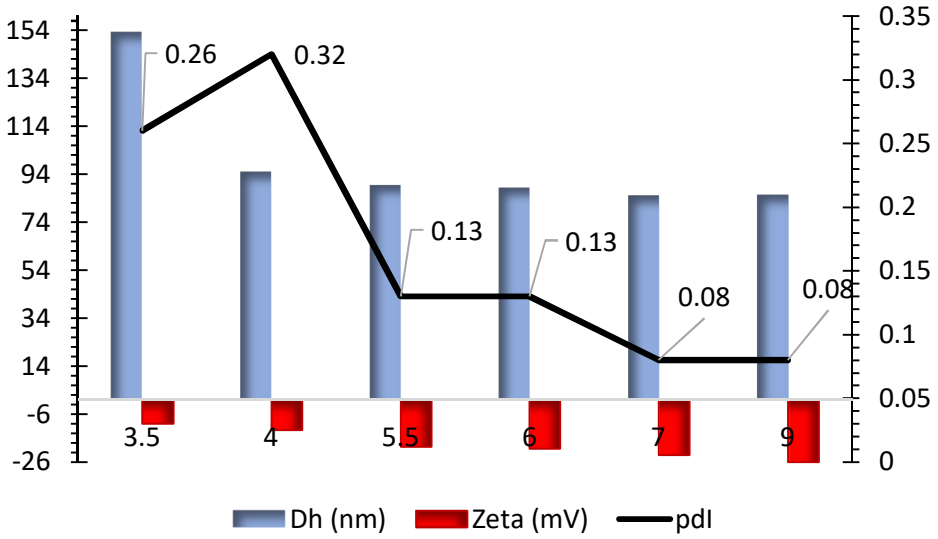

b)

Scheme 11. Variation of nanoparticles diameter (blue columns), zeta potential (red columns) and PDI (solid line) with solution pH values recorded for 0.5 g/L latex solution of a) NP_4 and b) NP_1

Conclusion

A new class of PS-b-PVDPM diblock copolymer was successfully synthesized via SARA-ATRP. Nanoprecipitation was used to prepare core-shell nanoparticles in aqueous basic solution, and both the size and morphology of nanoparticles were confirmed by DLS and SEM. The core-shell nanoparticles layers exhibited the expected structure, as detected by TEM. The CMC was measured using pyrene 1:3 ratio and DLS method. The CMC decreased with increasing the length of the PS or PVDPA blocks in the copolymer chain (range 33-69 mg/L). The latex composed of PS-b-PVDPA is highly stable as function of time and temperature. These latexes are sensitive to the pH, the deprotonation of carboxylic acid groups of PVDPA make these latexes stable at suitable pH values (pH $\geq$ 4).

Acknowledgment

The authors would like to acknowledge the Lebanese National Council for Scientific Research (CNRS-L) for funding this work. The authors are grateful to Dr. Anne Leaustic for fluorimetry experiments (ICMMO, Orsay, France), Dr François Brisset for performing SEM experiments (ICMMO, Orsay, France) and Dr. Vincent Huc for TEM experiments (ICMMO, Orsay, France).

References

1. Riess, G. Micellization of Block Copolymers. *Progress in Polymer Science (Oxford)* 2003, *28*, 1107–1170.

2. Nakashima, K.; Bahadur, P. Aggregation of Water-Soluble Block Copolymers in Aqueous Solutions: Recent Trends. *Advances in Colloid and Interface Science* 2006, *123–126*, 75–96.

3. Seo, D.G.; Kim, Y.M.; Ahn, H.; Moon, H.C. Non-Volatile, Phase-Transition Smart Gels Visually Indicating: In Situ Thermal Status for Sensing Applications. *Nanoscale* **2019**, *11*, 16733–16742, doi:10.1039/c9nr03686e.

4. Sezgin, Z.; Yüksel, N.; Baykara, T. Preparation and Characterization of Polymeric Micelles for Solubilization of Poorly Soluble Anticancer Drugs. *European Journal of Pharmaceutics and Biopharmaceutics* **2006**, *64*, 261–268, doi:10.1016/j.ejpb.2006.06.003.

5. Kushnirov Melnitzer, V.; Sosnik, A. Hybrid Titanium Oxide/Polymer Amphiphilic Nanomaterials with Controlled Size for Drug Encapsulation and Delivery. *Advanced Functional Materials* **2020**, *30*, doi:10.1002/adfm.201806146.

6. Bronstein, L.; Krämer, E.; Berton, B.; Burger, C.; Förster, S.; Antonietti, M. Successive Use of Amphiphilic Block Copolymers as Nanoreactors and Templates: Preparation of Porous Silica with Metal Nanoparticles. *Chemistry of Materials* **1999**, *11*, 1402–1405, doi:10.1021/cm980762h.

7. Montgomery, K.S.; Davidson, R.W.M.; Cao, B.; Williams, B.; Simpson, G.W.; Nilsson, S.K.; Chiefari, J.; Fuchter, M.J. Effective Macrophage Delivery Using RAFT Copolymer Derived Nanoparticles. *Polymer Chemistry* **2018**, *9*, 131–137, doi:10.1039/c7py01363a.

8. Tonnar, J.; Lacroix-Desmazes, P.; Boutevin, B. Living Radical Ab Initio Emulsion Polymerization of N-Butyl Acrylate by Reverse Iodine Transfer Polymerization. In Proceedings of the ACS Symposium Series; 2006; Vol. 944, pp. 605–619.

9. Semsarzadeh, M.A.; Amiri, S. Silicone Macroinitiator in Atom Transfer Radical Polymerization of Styrene and Vinyl Acetate: Synthesis and Characterization of Pentablock Copolymers. *Journal of Inorganic and Organometallic Polymers and Materials* **2013**, *23*, 432–438, doi:10.1007/s10904-012-9800-y.

10. Matyjaszewski, K.; Tsarevsky, N. v. Macromolecular Engineering by Atom Transfer Radical Polymerization. *J Am Chem Soc* 2014, *136*, 6513–6533.

11. Mendona, P. v.; Serra, A.C.; Coelho, J.F.J.; Popov, A. v.; Guliashvili, T. Ambient Temperature Rapid ATRP of Methyl Acrylate, Methyl Methacrylate and Styrene in Polar Solvents with Mixed Transition Metal Catalyst System. *European Polymer Journal* **2011**, *47*, 1460–1466, doi:10.1016/j.eurpolymj.2011.03.014.

12. Jones, G.R.; Whitfield, R.; Anastasaki, A.; Risangud, N.; Simula, A.; Keddie, D.J.; Haddleton, D.M. Cu(0)-RDRP of Methacrylates in DMSO: Importance of the Initiator. *Polymer Chemistry* **2018**, *9*, 2382–2388, doi:10.1039/c7py01196b.

13. Whitfield, R.; Anastasaki, A.; Jones, G.R.; Haddleton, D.M. Cu(0)-RDRP of Styrene: Balancing Initiator Efficiency and Dispersity. *Polymer Chemistry* **2018**, *9*, 4395–4403, doi:10.1039/c8py00814k.

14. Mendes, J.P.; Góis, J.R.; Costa, J.R.C.; Maximiano, P.; Serra, A.C.; Guliashvili, T.; Coelho, J.F.J. Ambient Temperature SARA ATRP for Meth(Acrylates), Styrene, and Vinyl Chloride Using Sulfolane/1-Butyl-3-Methylimidazolium Hexafluorophosphate-Based Mixtures. *Journal of Polymer Science, Part A: Polymer Chemistry* **2017**, *55*, 1322–1328, doi:10.1002/pola.28499.

15. Kopeć, M.; Yuan, R.; Gottlieb, E.; Abreu, C.M.R.; Song, Y.; Wang, Z.; Coelho, J.F.J.; Matyjaszewski, K.; Kowalewski, T. Polyacrylonitrile-b-Poly(Butyl Acrylate) Block Copolymers as Precursors to Mesoporous Nitrogen-Doped Carbons: Synthesis and Nanostructure. *Macromolecules* **2017**, *50*, 2759–2767, doi:10.1021/acs.macromol.6b02678.

16. Letchford, K.; Burt, H. A Review of the Formation and Classification of Amphiphilic Block Copolymer Nanoparticulate Structures: Micelles, Nanospheres, Nanocapsules and Polymersomes. *European Journal of Pharmaceutics and Biopharmaceutics* **2007**, *65*, 259–269.

17. Vangeyte, P.; Gautier, S.; Jérôme, R. About the Methods of Preparation of Poly(Ethylene Oxide)-b-Poly(ε- Caprolactone) Nanoparticles in Water - Analysis by Dynamic Light Scattering. *Colloids and Surfaces A: Physicochemical and Engineering Aspects* **2004**, *242*, 203–211, doi:10.1016/j.colsurfa.2004.04.070.

18. Maaz, M.; Elzein, T.; Barroca-Aubry, N.; Simoni, E.; Costa, L.; Nsouli, B.; Roger, P. New Insights on Uranium Recovery from Seawater and Aqueous Media. *Applied Materials Today* **2020**, *18*, doi:10.1016/j.apmt.2019.100461.

19. Thévenaz, D.C.; Monnier, C.A.; Balog, S.; Fiore, G.L. Luminescent Nanoparticles with Lanthanide-Containing Poly(Ethylene Glycol)-Poly(ε-Caprolactone) Block Copolymers. *Biomacromolecules* **2014**, *15*, 3994–4001, doi:10.1021/bm501058n.

20. dominguez, A.; Fernandez, A.; gonzalez, N.; Iglesias, E.; montenergro, L.J. *Determination of Critical Micelle Concentration of SomeSurfactants by Three Technique*; 1997;

21. Lord, D.R.C.; Duax, W.L.; Pressman, B.C.; Phillies, G.; Tokar, B.; Sanches, R. *EnvironmentalEffectsonVibronicBandIntensitiesinPyreneMonomerFluorescenceandTheirApplicationinStudiesofMicellarSystems With*;

22. Abd Karim, K.J.; Utama, R.H.; Lu, H.; Stenzel, M.H. Enhanced Drug Toxicity by Conjugation of Platinum Drugs to Polymers with Guanidine Containing Zwitterionic Functional Groups That Mimic Cell-Penetrating Peptides. *Polymer Chemistry* **2014**, *5*, 6600–6610, doi:10.1039/c4py00802b.

23. Aguiar, J.; Carpena, P.; Molina-Bolívar, J.A.; Carnero Ruiz, C. On the Determination of the Critical Micelle Concentration by the Pyrene 1:3 Ratio Method. *Journal of Colloid and Interface Science* **2003**, *258*, 116–122, doi:10.1016/S0021-9797(02)00082-6.

24. Zana, R.; Marques, C.; Johner, A. Dynamics of Micelles of the Triblock Copolymers Poly(Ethylene Oxide)-Poly(Propylene Oxide)-Poly(Ethylene Oxide) in Aqueous Solution. *Advances in Colloid and Interface Science* 2006, *123–126*, 345–351.

25. Astafieva, I.; Zhong, X.F.; Eisenberg, A. *Critical Micellization Phenomena in Block Polyelectrolyte Solutions*; 1993; Vol. 26;.

26. Astafieva, I.; Khougaz, K.; Eisenberg, A. *Micellization in Block Polyelectrolyte Solutions. 2. Fluorescence Study of the Critical Micelle Concentration as a Function of Soluble Block Length and Salt Concentration*; 1995; Vol. 28;.

27. Nawaz, M.; Baloch, M.K.; Price, G.J.; Ud-Din, I.; El-Mossalamy, E.S.E.B. Synthesis, Association and Surface Morphology of Poly (Ethylene Oxide)-Polystyrene Block Copolymer. *Journal of Polymer Research* **2013**, *20*, doi:10.1007/s10965-013-0180-y.

28. Pioge, S.; Fontaine, L.; Gaillard, C.; Nicol, E.; Pascual, S. Self-Assembling Properties of Well-Defmed Poly(Ethylene Oxide)-b-Poly (Ethyl Acrylate) Diblock Copolymers. *Macromolecules* **2009**, *42*, 4262–4272, doi:10.1021/ma802705b.

Supporting information

The VDPM monomer conversion was determined using Equation

$$\text{Equation 1. VDPM conversion (\%)} = \frac{A3.9{-}4.1\ ppm - 6}{A3.9{-}4.1\ ppm} \times 100$$

Where $A_{3.9\text{-}4.1ppm}$ represents the peak area in the region between 3.9 and 4.1 ppm and corresponds to the mixture of VDPM monomer and PVDPM . Vinyl's doublets at 5.66 and 6.17 ppm were used as 1 proton references for VDPM comonomer.

The styrene monomer conversion was determined using Equation .

$$\text{Equation 2. Styrene conversion (\%)} = \frac{A6.3{-}7.8ppm - 6}{A6.3{-}7.8ppm - 1} \times 100$$

Where $A_{6.3\text{-}7.8ppm}$ represents the peak area in the region between 6.3 and 7.8 ppm and corresponds to the mixture of styrene monomer and polystyrene. using the vinyl doublets at 5.33 and 5.84 ppm as references for 1 proton each.

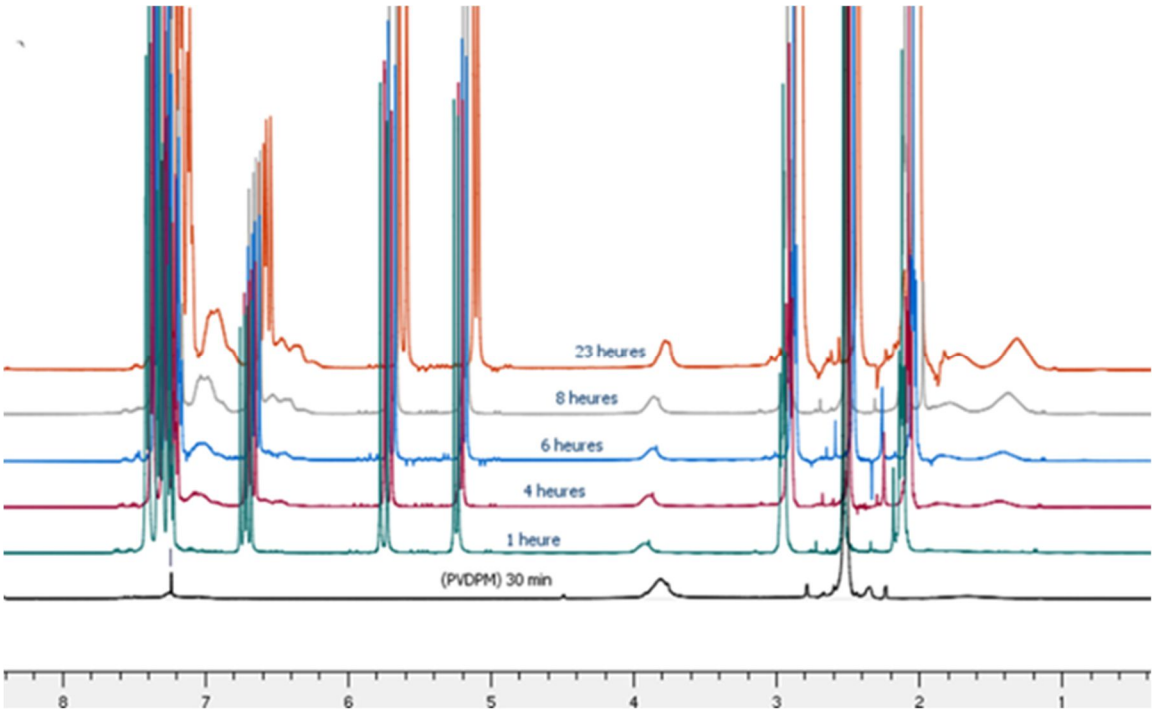

Figure SI 1. Spectra of copolymers after different reaction times

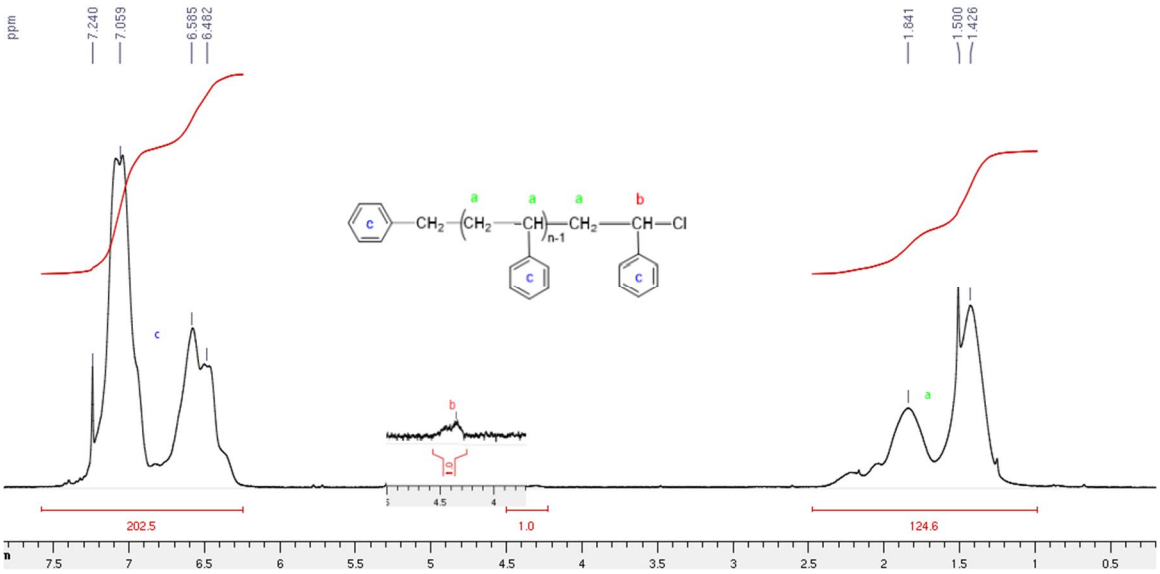

Figure SI 2. ^{1}H NMR spectrum (360 MHz, $CDCl_3$) of polystyrene PS_{112}

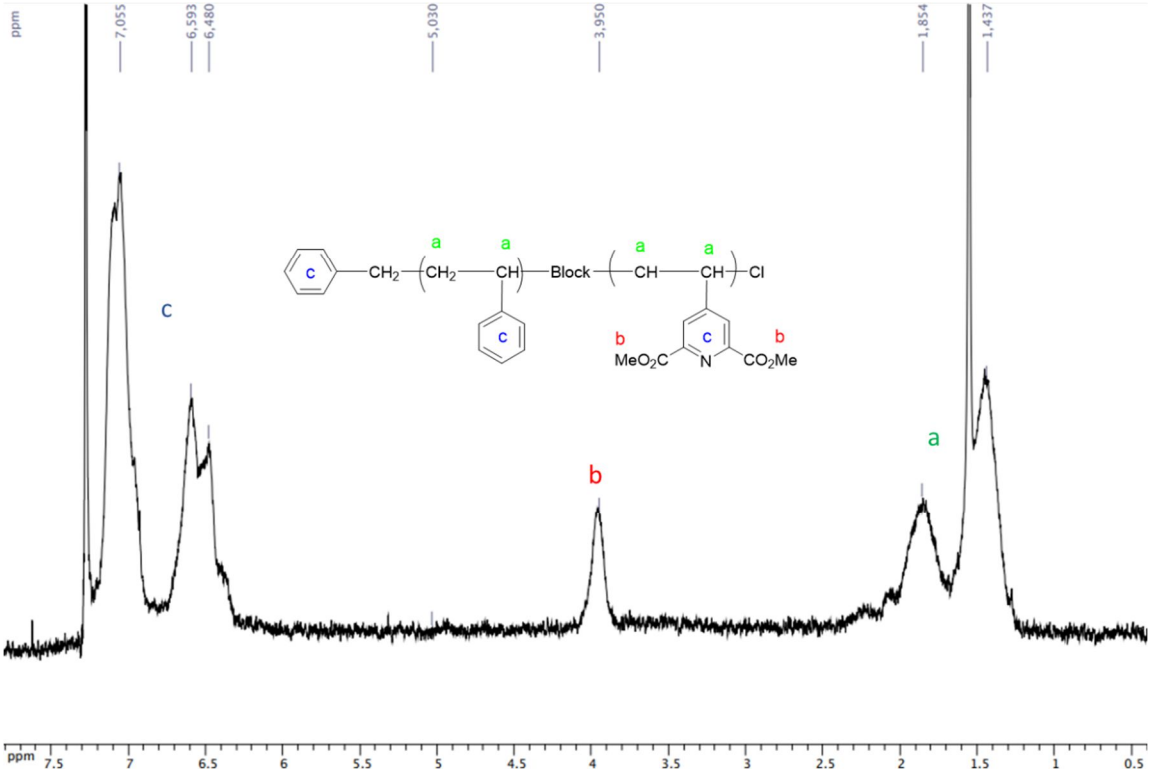

Figure SI 3. ^{1}H NMR spectrum (360 MHz, $CDCl_3$) of PS_{112}-b-$PVDPM_{50}$

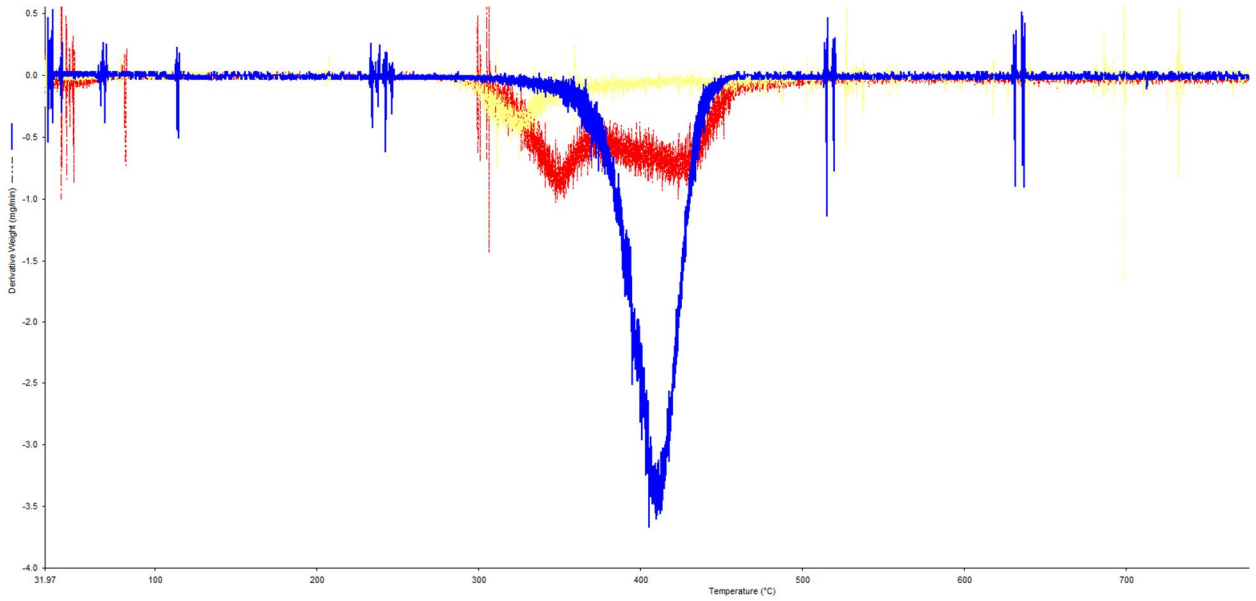

Figure SI 4. Derivative Thermogravimetric (DTG) of PVDPM10 (yellow line), PS112-b-PVDPM30 (red line), and PS112 (blue line)

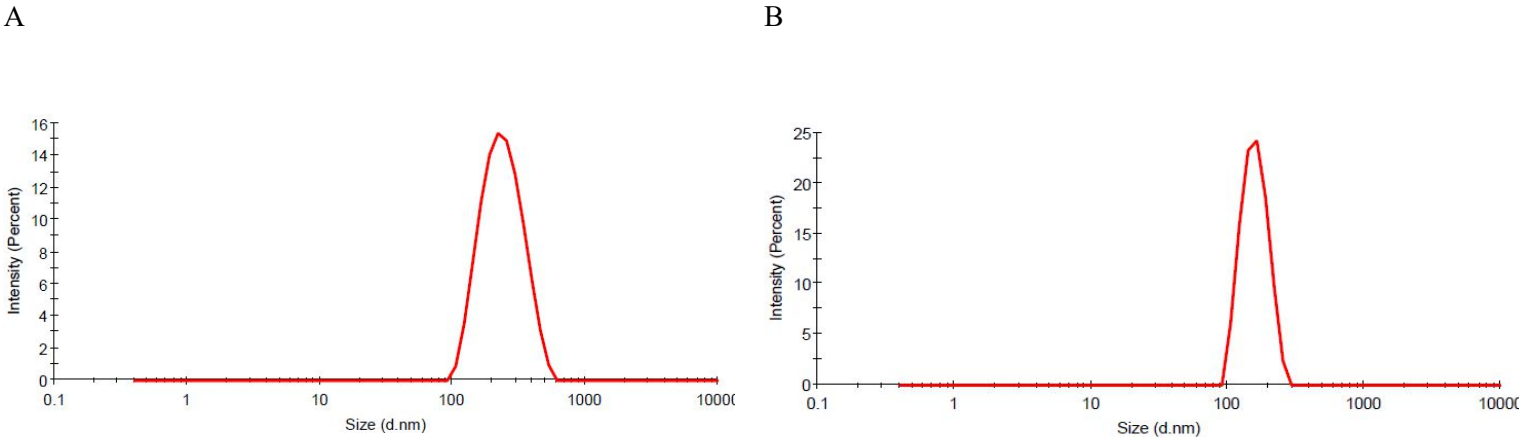

Figure SI 5. A) nanoparticles were prepared by adding water to THF/ ACN-copolymer and B) THF/ ACN-copolymer added to water using $PVDPM_{10}$-b-PS_{260}.

a)

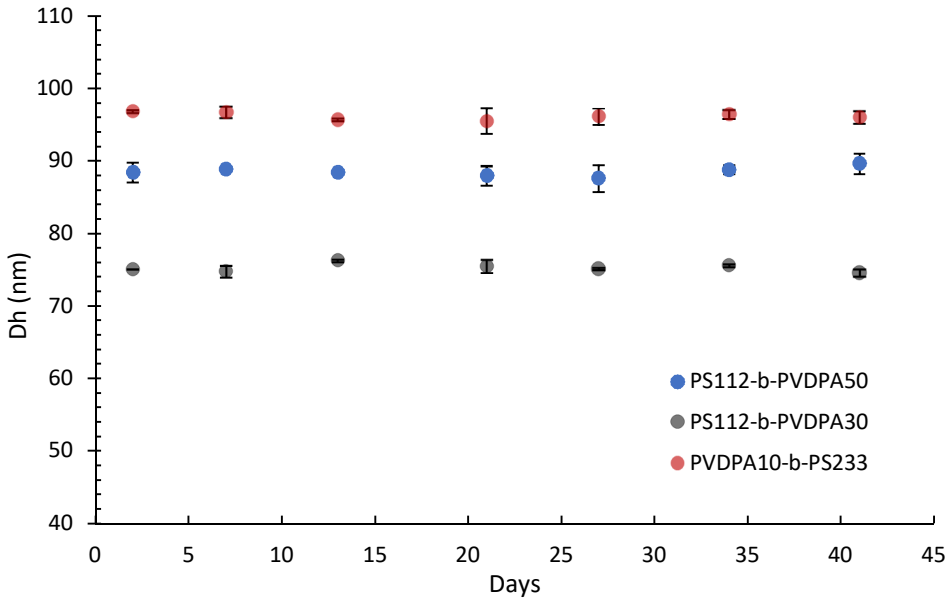

b)

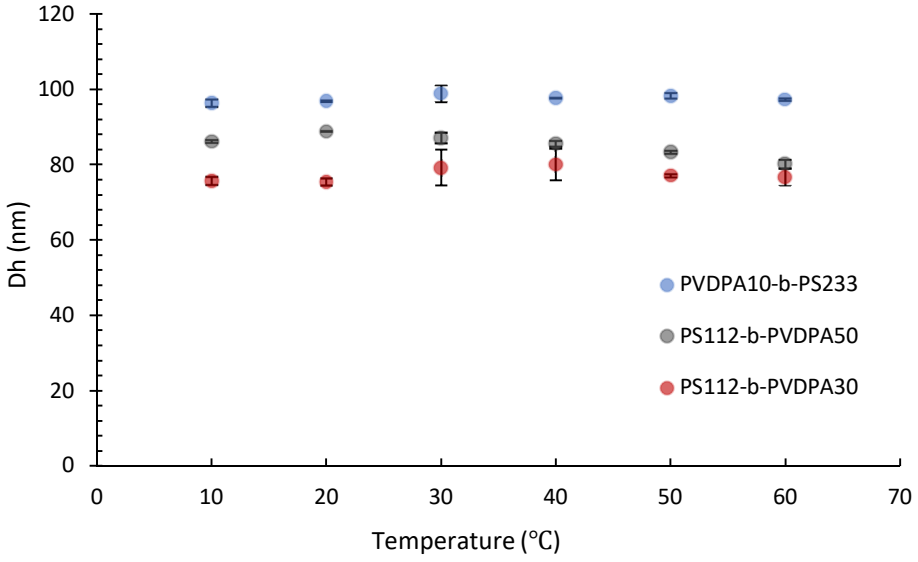

Figure SI 6. Stability of nanoparticles with a) time, b) temperature

A

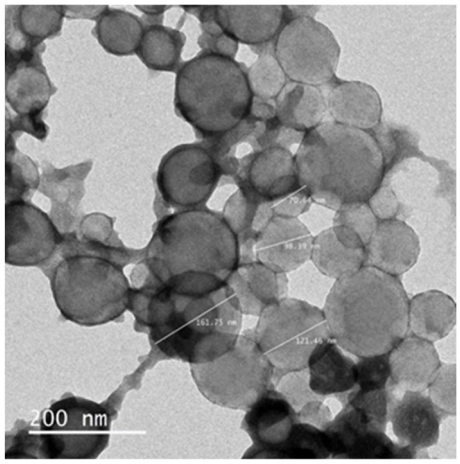

B

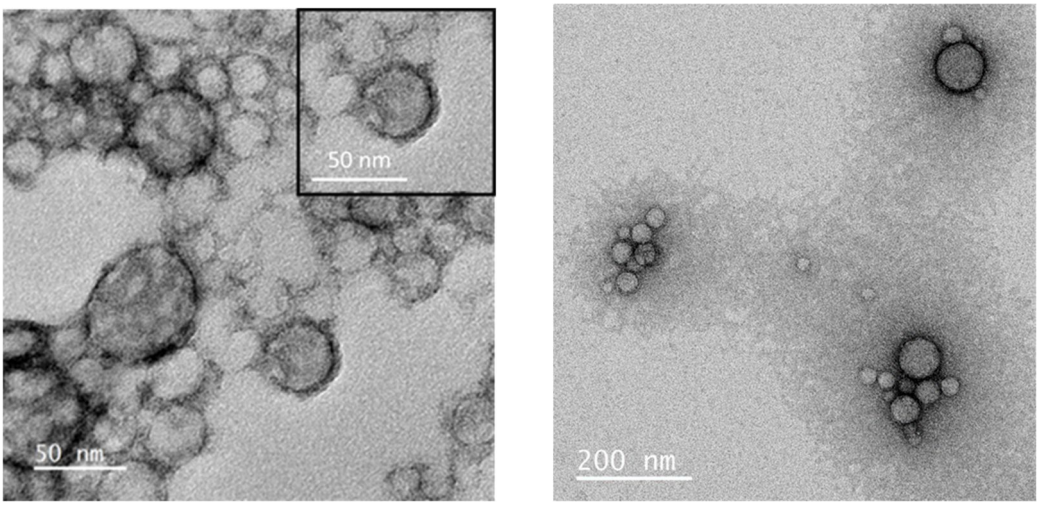

Figure SI 7. TEM photographs of the self-assembled nanoparticles A) NP_3 and B) NP_4 in aqueous solution.

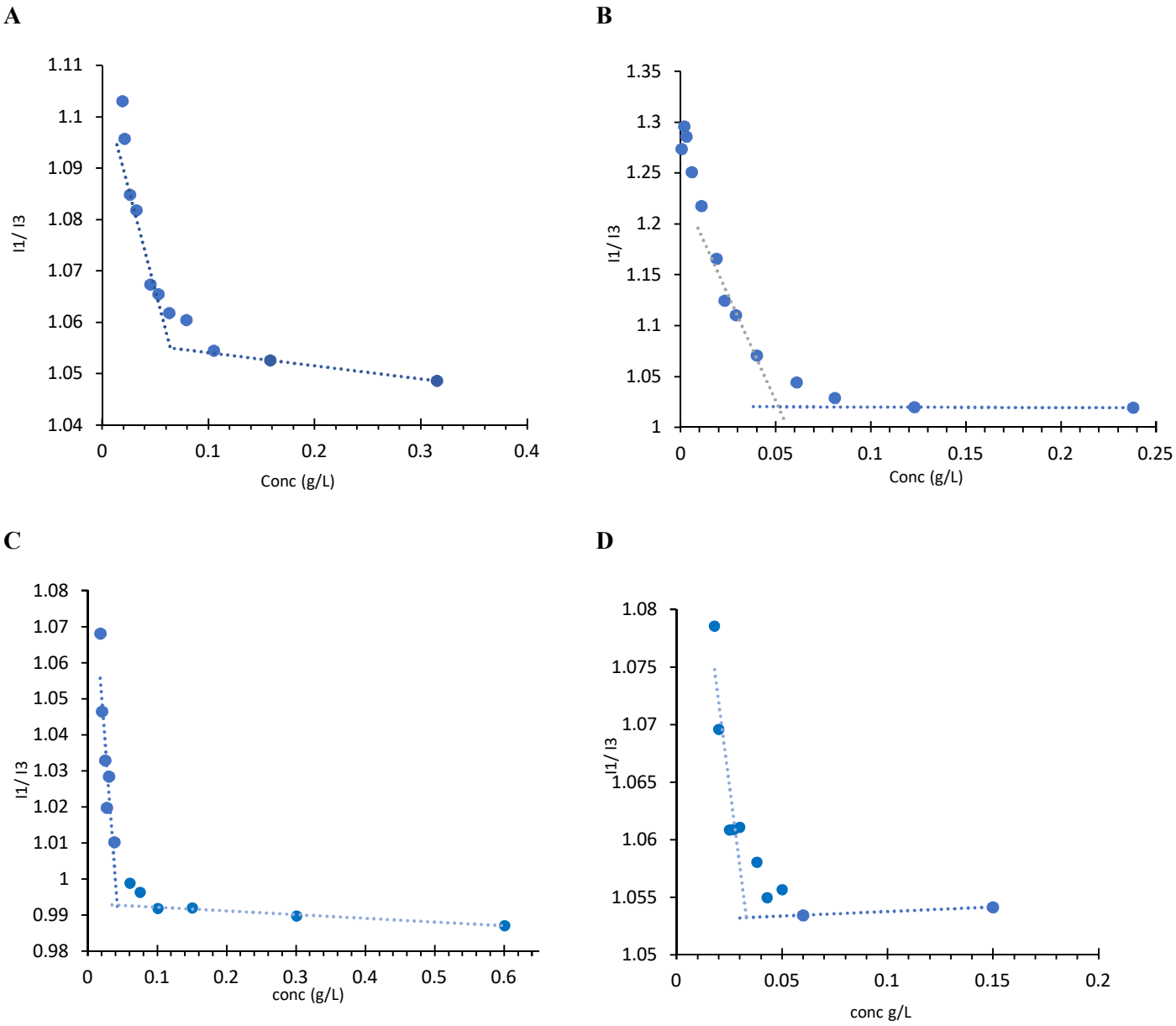

Figure SI 8. The determination of the CMC for A) NP_1 B) NP_3 C) NP_4 and D) NP_5 using) pyrene I_1/I_3 ratio method at 20°C.

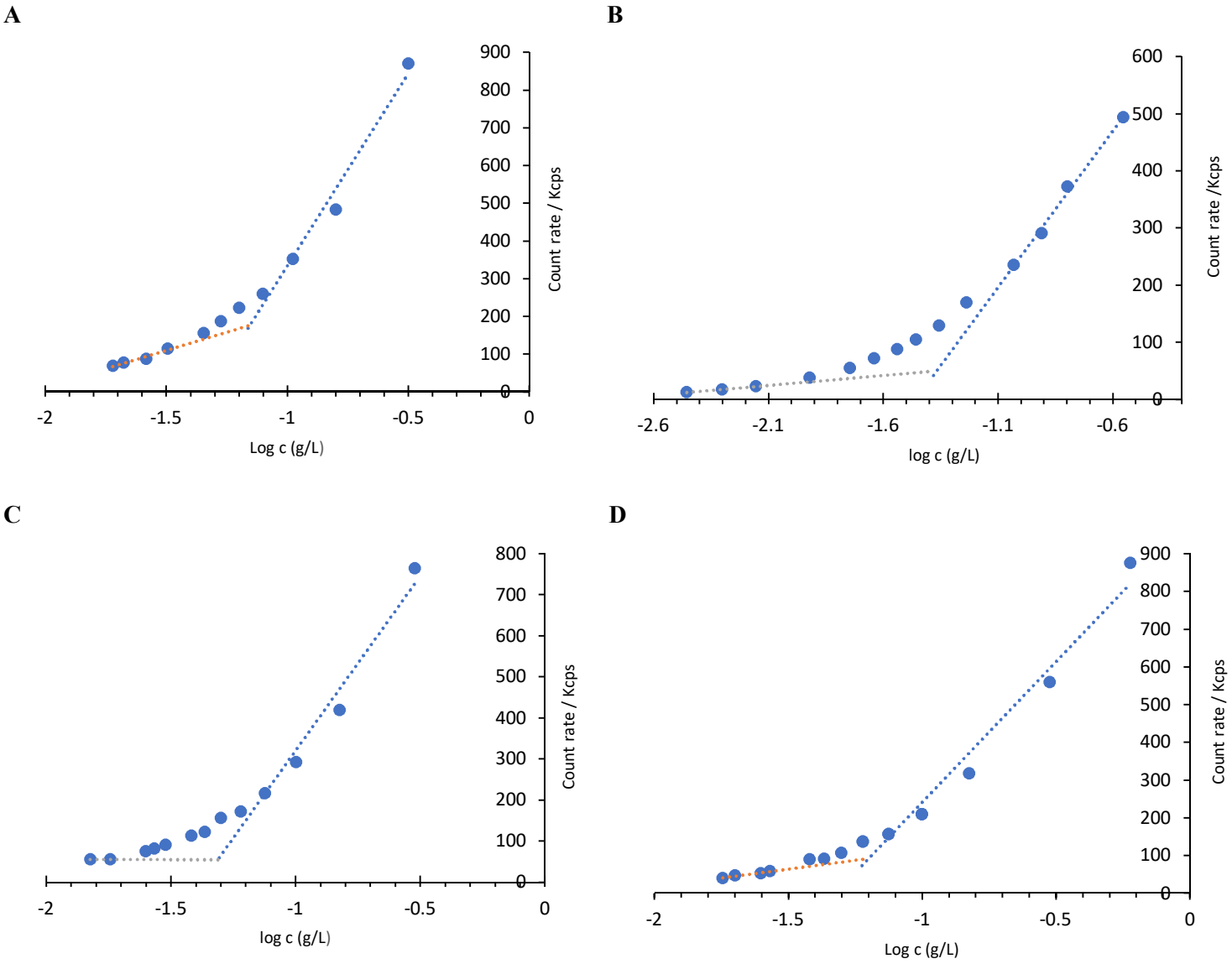

Figure SI 9. The determination of the CMC for A) NP_1 B NP_3 C) NP_4 and D) NP_5 using the count rate method obtained by DLS analysis at 20°C.

Part II. Surface active polystyrene-b-poly(4-vinyldipicolinic acid) (PS-b-PVDPA) core-shell nanoparticles for extracting lanthanides from aqueous media

Abstract

Rare-Earth Elements (REEs) have become increasingly indispensable in modern technologies; consequently, effective methods for the extraction of these elements have been developed. Polymeric materials are widely used in these applications due to intriguing functional groups, low cost, and high selectivity for target ions. In this purpose poly(4-vinyldipicolinic acid) (PVDPA), was previously synthesized, and its efficiency was revealed for trapping uranium and many lanthanides in water. In this work, we report the use of polystyrene-b-poly(4-vinyldipicolinic acid) (PS-b-PVDPA) core-shell nanoparticles which carry different chain lengths of PVPA on nanoparticles surface. They were further used in luminescent nanoparticles preparation, and REEs extraction from the aqueous environment. The complexation of nanoparticles with metal ion was investigated thermodynamically using Isothermal Titration Calorimetry (ITC), to determine ion-exchange thermodynamic parameters (ΔH, ΔS, ΔG), and binding stoichiometry (n). The calculated thermodynamic parameters indicated that complexation was spontaneous and endothermic. Luminescence spectroscopy, ATR-FTIR, UV-Vis, and Inductively Coupled Plasma−Atomic Emission Spectroscopy (ICP-AES) were used, in support of the ITC results.

Keywords: REEs extraction, core-shell nanoparticles, luminescent nanoparticles, ITC, ICP-AES.

Introduction

Rare-Earth Elements (REEs) are of considerable interest to many science areas, as well as in the medicine and consumer products such as nuclear, petroleum, electronic (e.g., mobile phones, color TV sets), military and automotive sectors [1][2]. However, industrialization has grown at a fast rate. It has thus increased the demand for exploitation of natural resources of REE at a careless speed and often has adverse effects on the environment [3]. Recovery of REEs from water has become an attractive process owing to the high costs and limited availabilities. Nowadays, several methods have been developed for efficient metal removal from waters, including but not limited to chemical precipitation [4], ion exchange [5], membrane filtration [6][7], electrochemical technologies [8] and adsorbents [9][10]. Consequently, effective, inexpensive and stable technologies for the extraction and purification of REEs are of great interest [11][12].

Polymers have great potential in metals extraction due to their intriguing group of materials and their variety of functional groups including carboxylic acid [13], acrylic acid [14] amide [15], and amine [16]. As a result, the extraction of REEs is currently based on polymers in several extraction and separation technologies such as ion-exchange resins, polymer-enhanced ultrafiltration, and absorbents.

In our lab, several studies have focused on the radio-decontamination from seawater using an innovative chelating polymer material, water soluble, based on dipicolinic acid named poly(4-vinyldipicolinic acid) (PVDPA). These new materials were tested and proved their high efficiency in trapping uranium and many lanthanides in water [17][18]. In addition, PVDPA showed a uranium uptake capacity of 597 mg/g in simulated seawater conditions, even at high ionic strength and in the presence of the challenging vanadium species, which tend to limit the performance of other existing materials. Even though this high performance for uranium scavenging, it represents some limitation for the cleaning of large volume of water.

Because of the promising PVDPA-metals binding with a high uptake capacity, we chose to systematically study its REE chelating capacity in another system. In order to overcome the limitation associated with the cleaning of large volume of water as mentioned before,

a new system has been proposed to be an effective separation technique to remove metal ions from aqueous environments.

In the present work, polymeric core-shell nanoparticles (NPs) functionalized with chelating agents can be employed for metals harvesting from the aqueous media. Because of their strong metal chelating properties, the PVDPA residues impart an excellent performance to the engineered nanoparticles, in the capture of lanthanide ions in aqueous solution.

Here, we report the direct measurement of the interaction of a series of nanoparticles with europium by Isothermal Titration Calorimetry (ITC). It is the quantitative standard method for studying the formation and dissociation of molecular complexes and the binding interactions of polymer, small proteins etc. in solution [19]. ITC is unique in its ability to provide quantitative thermodynamic information in a single experiment [20]. From the resulting data, we report, for the binding process, the equilibrium constant (K) and thermodynamics (ΔH, ΔS, ΔG), as well as the complex stoichiometry. This method has become very popular for studying heats of reactions in biology [21], however it has largely been underutilized as a tool in polymer chemistry [22]. Metal-nanoparticles complexation by ATR-FTIR, UV-Vis, fluorescence properties (TRLFS) and Inductively Coupled Plasma-Atomic Emission Spectroscopy (ICP-AES) were also investigate in support of ITC results.

Materials and methods

Materials

Milli Q water was used in the preparations of all solutions. Stock solutions of trivalent lanthanides were prepared by dissolving $Eu(NO_3)_3.5H_2O$ (99.9%, Aldrich) and $Eu(CF_3SO_3)_3$ (98%, Aldrich) in water.

Dynamic Light Scattering (DLS)

DLS was performed on a Malvern Zetasizer nano ZS instrument equipped with a He-Ne laser beam at a wavelength (λ = 632 nm) and scattering angle of 173°.

Inductively coupled plasma atomic emission spectroscopy (ICP-AES)

ICP-AES Measurements were performed using an Agilent series 720-ES with ICP Expert II, Version 2.0.5 b283 software.

I.5.4.4 Infrared

IR analyses were carried out on Bruker IFS 66 equipment with an ATR module with a diamond crystal from Pike technologies.

I.5.4.5 Isothermal titration microcalorimetry (ITC)

ITC experiments were carried out with a VP-ITC, MicrolCal®. $Eu(NO_3)_3$ solution at 1.5 mM was placed in a 295-mL continuously rotating (394 rpm) syringe. Nanoparticles suspension at 0.6 mM of copolymer was placed in the sample cell of 1.43 mL. At first 2 µL aliquot was injected, without taking into account the observed heat, to remove the effect of solute diffusion across the syringe tip during the equilibration period. Then, injections of 10 µL of the europium solution were made at intervals of 30 s. Experiments were carried out at 25 ºC.

I.5.4.6 Time-Resolved Laser-induced Fluorescence Spectroscopy (TRLFS)

TRLFS measurements were conducted at room temperature, Nd: YAG pumped optical parametric oscillator (OPO) laser is used for sample excitation at 394 nm with an energy of ~ 5 mJ/pulse and a repetition rate of 10 Hz. The emission light (at 90°) is coupled into a round to linear optical fiber bundle before being analyzed by a spectrograph SPEX 270M (Jobin-Yvon). Detection of the luminescence is performed by an intensified CCD (ICCD) detector PIMAX 4 (Princeton Instrument).

Results and discussion

1. Core-shell nanoparticles

New amphiphilic polystyrene-b-poly(4-vinyldipicolinic acid) (PS-b-PVDPA) diblock copolymers were synthesized and their self-assemblies in aqueous solution were described in detail in previous part of this chapter. The synthesized nanoparticles (NPs) had a core shell-like structure, in which the core was composed of PS, and the shell was formed of PVDPA as shown in Scheme 12. The prepared nanoparticles were stabilized in aqueous solution by electrostatic repulsive force between carboxylate units of PVDPA of diblock copolymer at pH ~ 5.5.

To evaluate the effect of polymer functionalization on heavy metals binding, a series of nanoparticles was prepared, with different length of the hydrophilic and hydrophobic block to produce a series of polymers with varied degrees of functionalization. In that way, 5 types of nanoparticles were prepared, NP_1, NP_2, NP_3, NP_4, and NP_5 using $PVDPA_{10}$-b-PS_{184}, $PVDPA_{10}$-b-PS_{260}, $PVDPA_{10}$-b-PS_{600} PS_{112}-b-$PVDPA_{30}$ and PS_{112}-b-$PVDPA_{50}$, respectively.

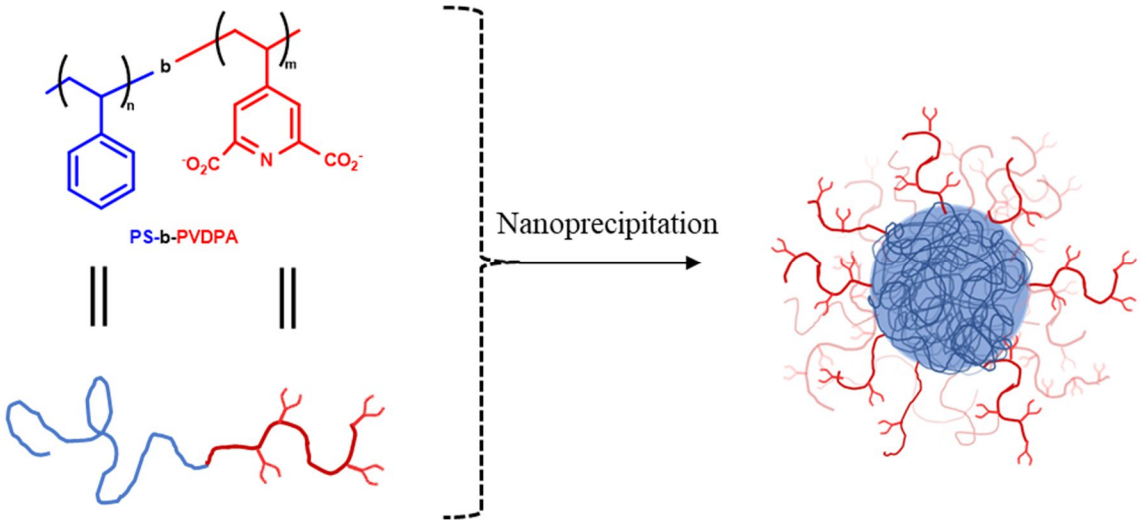

Scheme 12. Schematic representation for nanoparticles preparation of diblock copolymer; (blue) represent polystyrene block core; (red) represent PVDPA block.

On the basis of the structural features of PVDPA and the structural and thermodynamic data in the literature on the complexation of dipicolinic acid (DPA) with actinides such as Np(VI) [23], and lanthanides, it was reasonable to assume that DPA could form complexes with heavy metals in aqueous solutions. To evaluate the effect of polymer functionalization on heavy metals binding, a series of nanoparticles was prepared, with different length of the hydrophilic and hydrophobic block.

The coordination of PVDPA with lanthanide ions is determined by electrostatic interactions. Water molecules are known to be strong ligands to lanthanide ions (Ln^{3+}) and complexes prepared under anhydrous conditions often undergo partial hydrolysis even in the presence of trace amounts of water [24]. Although, multidentate ligands with one or more negatively charged oxygen donor groups, such as dipicolinic acid, have been known to form luminescent compounds with Ln^{3+} ions even in the presence of water [25].

To evaluate the ability of complexation of these nanoparticles with lanthanides, NP_4 have been place with europium (III). First, mixing nanoparticles (0.05 % w/v) (around 2 equivalents of PVDPA) with europium (III) nitrate solution (1.5 mM) (1 equivalent) at room temperature and pH ~ 5.5 were examined. When Eu (III) nitrate solution is added on nanoparticles, in within seconds, a white precipitate was observed, and under a UV lamp (254 nm) the red fluorescence is seeming in the solid precipitate as shown in Figure 14. This aggregation is probably due to the formation of complexes with the carboxylate groups of PVDPA and europium.

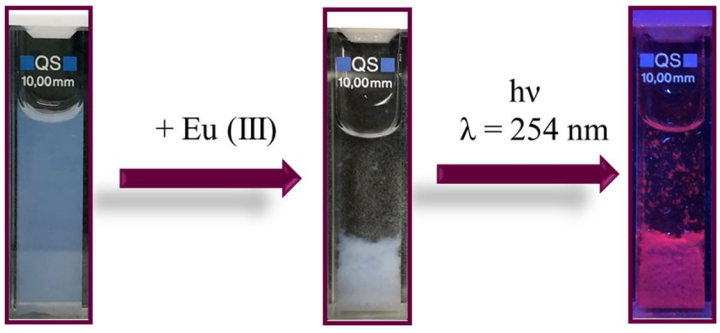

Figure 14. Images of nanoparticles NP_4 in water under visible light before adding Eu^{3+} (left), after adding Eu^{3+} (center) and UV excitation (λ = 254 nm) (right).

2. Chemical analysis by ATR-FTIR

The solid precipitate obtained due to the complexation of PVDPA shell of nanoparticles with Eu (III) can be filtrate and characterized. The carboxylate absorption bands in FT-IR spectra are modified as seen in Figure 15, which shows the ATR-IR spectra of nanoparticles before and after complexation. In the IR spectrum of nanoparticles before complexation, the peak at 1674 cm^{-1} could be attributed to C=O. The strong and broad absorption bands in the range of 3000-3600 cm^{-1} of these compounds can be assigned to the characteristic O-H stretching vibrations from the water molecules. The band at 1630 cm^{-1} could be attribute to the asymmetric stretching vibrations of carboxylate (ν_{as} COO^-), and the band at 1408 cm^{-1} could be ascribed to the symmetric stretching vibrations of carboxylate (ν_s COO^-) The difference between (ν_{as} COO^-) and (ν_s COO^-) is 222 cm^{-1} before the complexation and is comparable to that for the corresponding sodium salt of the acid as shown in the literature [26].

In the PVDPA (NPs) – Eu^{3+} complex spectrum, those bands were replaced by band at 1566 cm^{-1} (COO^- asymmetrical stretching) and 1415 cm^{-1} (COO^- symmetrical stretching) proving that PVDPA matched the Eu^{3+} through its carboxyl functions. The separation ($\Delta\nu$) between ν_{as} COO^- and ν_s COO^- can be used to explain the coordination types of carboxyl group in ligand. Therefore, the $\Delta\nu$ value of complex is 151 cm^{-1} smaller than those observed in the spectrum of the free ligand, which implies the presence of bidentate, chelating carboxylate group [27].

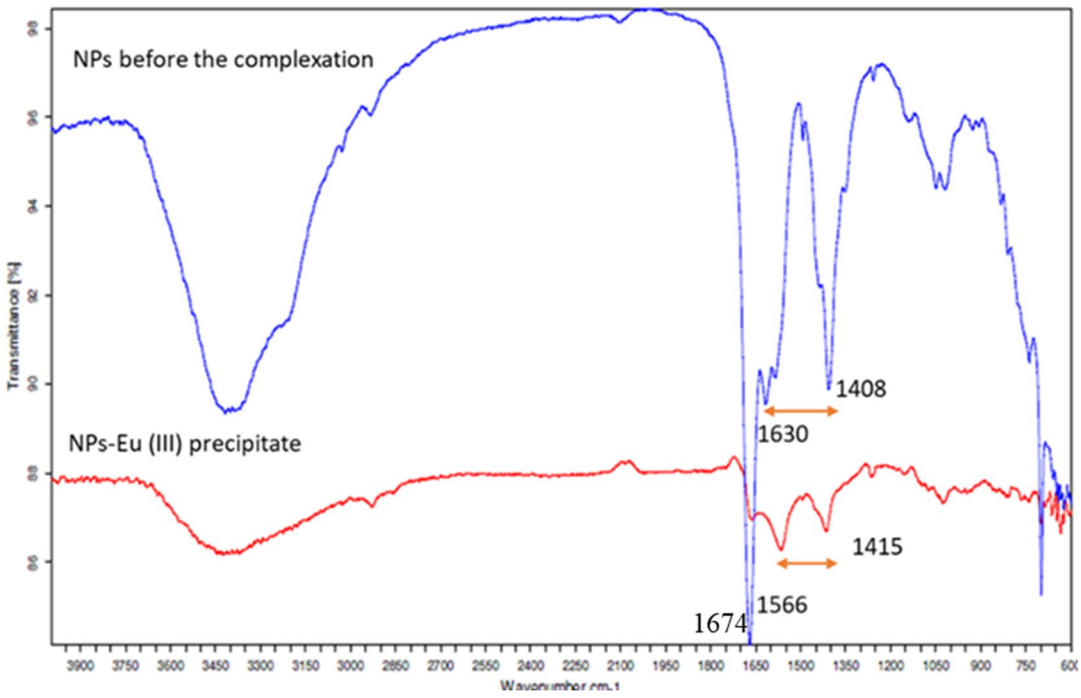

Figure 15. ATR-IR spectra of nanoparticles- Eu^{3+} complex

3. Fluorescence properties

The Eu^{3+}/ nanoparticles were further characterized by luminescence spectroscopy to help understand the coordination modes of europium complexes with nanoparticles.

Figure 16 shows the variation of the emission spectra of europium before (red spectra) and after (black spectra) adding of nanoparticles NP_4. Those for the other complexes are reported on Figure S 1 (see in the Supporting Information). The spectra contain features of electronic transition from the lowest excited state, $^5D_0$, to multiple ground states: $^7F_1$, $^7F_2$ and $^7F_4$. The luminescence spectrum is dominated by the $^5D_0 \rightarrow {}^7F_1$ transition and the $^5D_0 \rightarrow {}^7F_2$ transition is relatively weak for a free Eu^{3+} ion in aqueous solution. On the contrary, the $^5D_0 \rightarrow {}^7F_2$ transition is more intense than the $^5D_0 \rightarrow {}^7F_1$ transition in the Eu^{3+}/ PVDPA (NPs) solution. The higher intensity of the $^5D_0 \rightarrow {}^7F_2$ transition is often attributed to the low symmetry of Eu^{3+} [28]. This intensity enhancement of the $^5D_0 \rightarrow {}^7F_2$ transition is due to the formation of a Eu^{3+} complex with PVDPA in nanoparticles solution, which would destroy the symmetry of the Eu^{3+} ion.

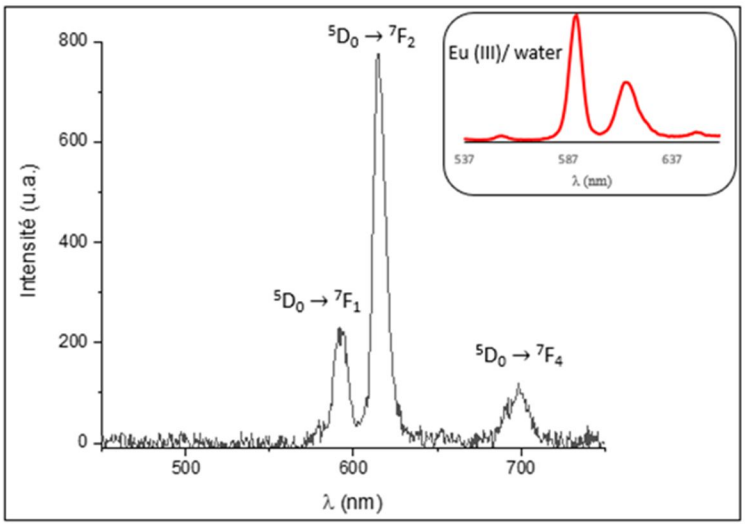

Figure 16. Luminescence emission spectra of the Eu^{3+}/ PVDPA (NP_4) systems (excitation 394 nm). The insert is the spectrum of Eu^{3+} in water as a comparison.

The Time-resolved laser-induced fluorescence spectroscopy (TRLFS) can be used as another characteristic parameter to further discuss the coordination environment of the Eu^{3+} ion. It's known that the quenching of the luminescence of Eu^{3+} in aqueous solution is due to the efficient energy transfer from the excited state $^5D_0$ of the Eu^{3+} ion to the O-H vibration of inner-sphere-coordinated water molecules. Hence, τ become longer as the PVDPA (NPs) system was increased.

The complexation is further proven by looking at the fluorescence decay of Eu^{3+}/ PVDPA (NPs), luminescence decay, recorded and fitted into an exponential function that allows the estimation of fluorescence lifetimes for different europium species as shown in Figure 17.

A)

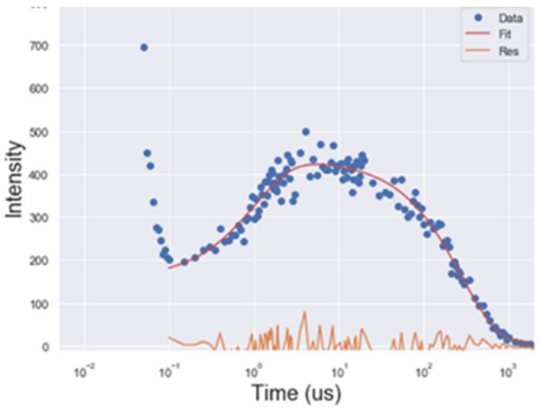

B)

	τ (µs)	n (H_2O)
$Eu(NO_3)_3$ salt	160 ± 10	6
+ NP_4	283 ± 10	3
+ NP_5	267 ± 20	3

C)

Figure 17. (A) TRLFS spectra of Eu^{3+} upon interaction with NP_5, (B) fitted lifetimes and (C) proposed PVDPA (NPs) crosslinking by Eu^{3+}.

The luminescence decays are monoexponentially functions for all the Eu^{3+} complexes. To find out the number of water molecule interacts in the first coordination sphere, hydration numbers have been determined by measuring the lifetimes in water and using this equation (n_{H2O} (±0.5) = $1.07.\tau^{-1} - 0.62$, where τ is the luminescence lifetime in millisecond) [29]. The results gathered in Figure 17 B clearly demonstrate the presence of different number of water molecule in the first coordination sphere of all of the Eu^{3+} complexes. In the case of $Eu(NO_3)_3$ the lifetime of the Eu^{3+} is in the range of 160 ± 10 µs and reflects the presence of interaction with 6 water molecules in the inner coordination sphere. At 20ºC and pH ~ 5.5, these lifetimes are longer, around 283 ± 10 µs and 267 ± 20 µs in the presence of NP_4 and NP_5 respectively. In all cases, the number of water molecule is 3 after adding NPs, meaning that PVDPA kicked out water molecule from the Eu^{3+} hydration shell, in perfect coherence with two bidentate ligand, herein the formation of the $Eu(PVDPA)_2^-$ complex. The change in fluorescence lifetimes when PVDPA (NPs) is added in excess proves the complexation between europium (III) and PVDPA. The complex structure is seemingly not straight forward and more studies would be needed to further understand the europium

coordination mode, the change in lifetimes confirms that a europium (III) atom is indeed trapped in the PVDPA matrix.

4. UV-Vis analysis

In order to determine the stoichiometry of the complexation, UV-Vis spectrophotometric titrations were investigated to get insight into the stoichiometry and the absorption of PVDPA shell of nanoparticles. Aqueous solutions 0.6 x 10^{-3} M of the latter, prepared at pH ~ 5.5, were titrated by europium solution 1.5 x 10^{-3} M up to a ratio R [Eu^{3+}]/[PVDPA] = 0.21 and 0.14 for the NP_5 and NP_4 respectively as shown in Figure 18. Unfortunately, the other three nanoparticles NP_1, NP_2 and NP_3 were not suitable for this experiment due to turbidity problem, even after dilution.

As shown in Figure 18, PVDPA has an absorption band at around 272 nm. Europium does not have absorption peaks in the available wavelength range of 230-350 nm. The PVDPA absorption spectrum went down when europium was added in increasing ratios, proving again the complexation of europium with PVDPA ligand.

Absorption analysis point to the complete disappearance of PVDPA peak, with 0.21 and 0.14 equivalent using NP_5 and NP_4 respectively.

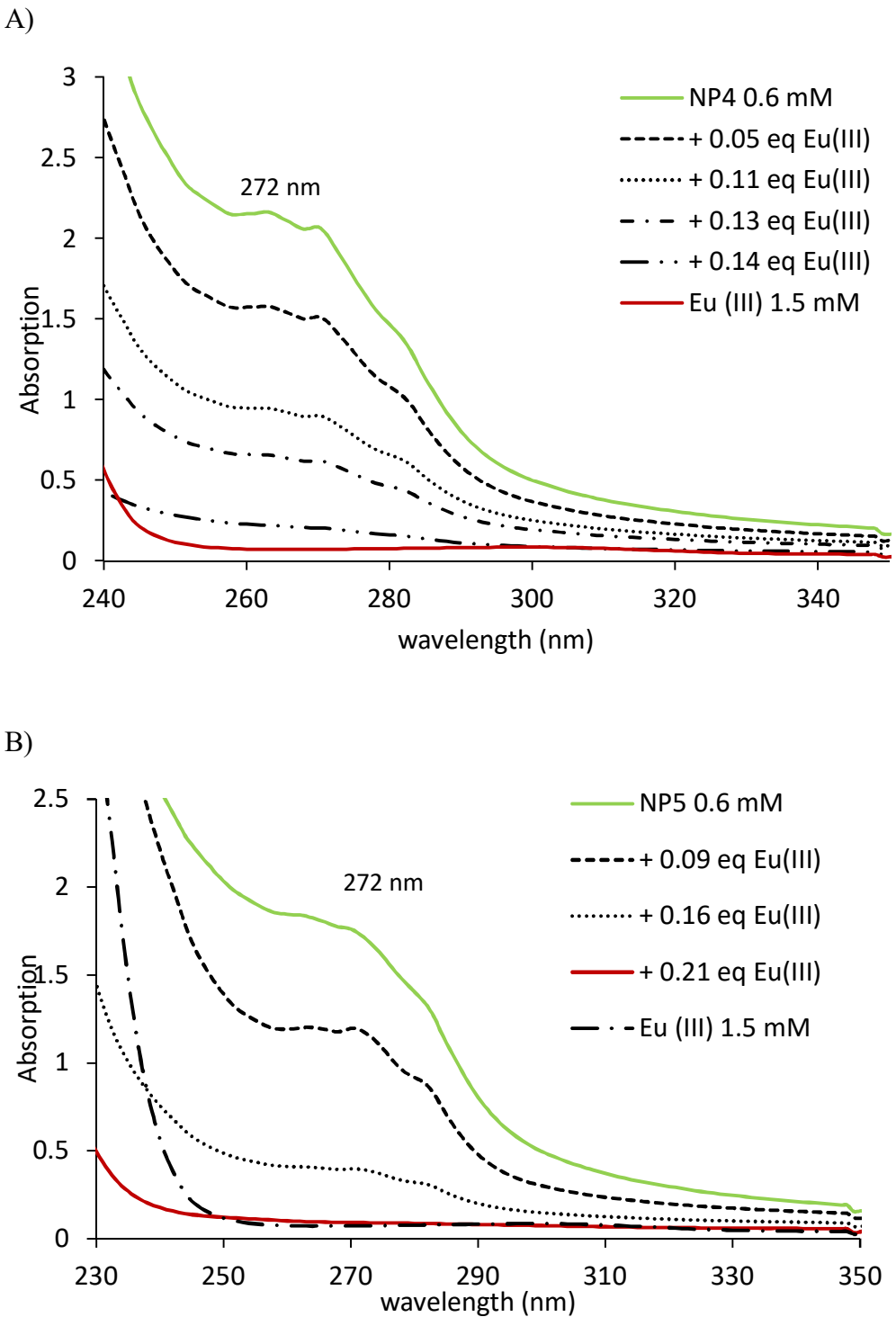

Figure 18. UV-Vis absorption spectra of A) NP_4 and B) NP_5 at pH 5.5; [PVDPA] 0.6 x 10^{-3} M, upon addition of increasing amounts of Eu^{3+}.

5. Isothermal Titration Calorimetry measurements

To better substantiate the IR, UV-Vis, and TRLFS data, Isothermal Titration Calorimetry (ITC) experiments were used to prove the binding between nanoparticles and europium. Additionally, to evaluate the effect of copolymer composition on europium complexation, a series of nanoparticles with varied length of the hydrophilic and hydrophobic block have been tested. For this purpose, interaction of 0.6 x 10^{-3} M of PVDPA from each nanoparticles dispersed in H_2O were evaluated on a 1.5 x 10^{-3} M solution of $Eu(NO_3)_3$. It worth mentioning that, no difference in heat released was found during these experiments when counter ion of metal (e.g. $Eu(CF_3SO_3)_3$) has been changed. Using ITC, we measured the thermodynamics of polymer (PVDPA)−europium binding in a pH 5.5 aqueous solution. pH 5.5 was chosen because insoluble lanthanide hydroxides form above pH 6 [30].

Figure 19 shows a typical ITC titration of Eu^{3+} into a nanoparticles NP_5 suspension at 25 ºC. ITC titrations of other nanoparticles are shown in Figure S 2 in the Supporting Information. The area upon each injection peak, equal to the total heat released for that injection, is shown by Figure 19 A. It shows that interaction of nanoparticles with europium is an endothermic reaction. From the ITC titration data, an average enthalpy (ΔH), and molar ratio (N) for each system could be estimate. As shown in Table 5, the value of molar ratio in NP_5 (N = 0.16) is higher than that of NP_4 (N = 0.13). However, when compared to the molar ratio determined for NP_1, NP_2, and NP_3 with europium, it can be observed that the molar ratio from NP_3 (N = 0.6) systems was much higher than of the one measured for NP_1 (N = 0.16) and NP_2 (N = 0.23).

The results obtained for stoichiometry of NP_4 and NP_5 with fixed polystyrene block (PS_{112}) showed that the influence of the length of the hydrophilic block is not remarkable. In contrast, the increasing number of styrene units in designed copolymers with fixing the PVDPA length allowed to increases the capacity of europium capture (NP_1, NP_2 and NP_3). Hence, the most promising results where obtained once performing these experiments of europium complexation using NP_3.

The ΔH value is slightly different for nanoparticles interaction with Eu^{3+}. On average, europium enthalpy binding to nanoparticles was ΔH = 3 480 cal/mol for these nanoparticles.

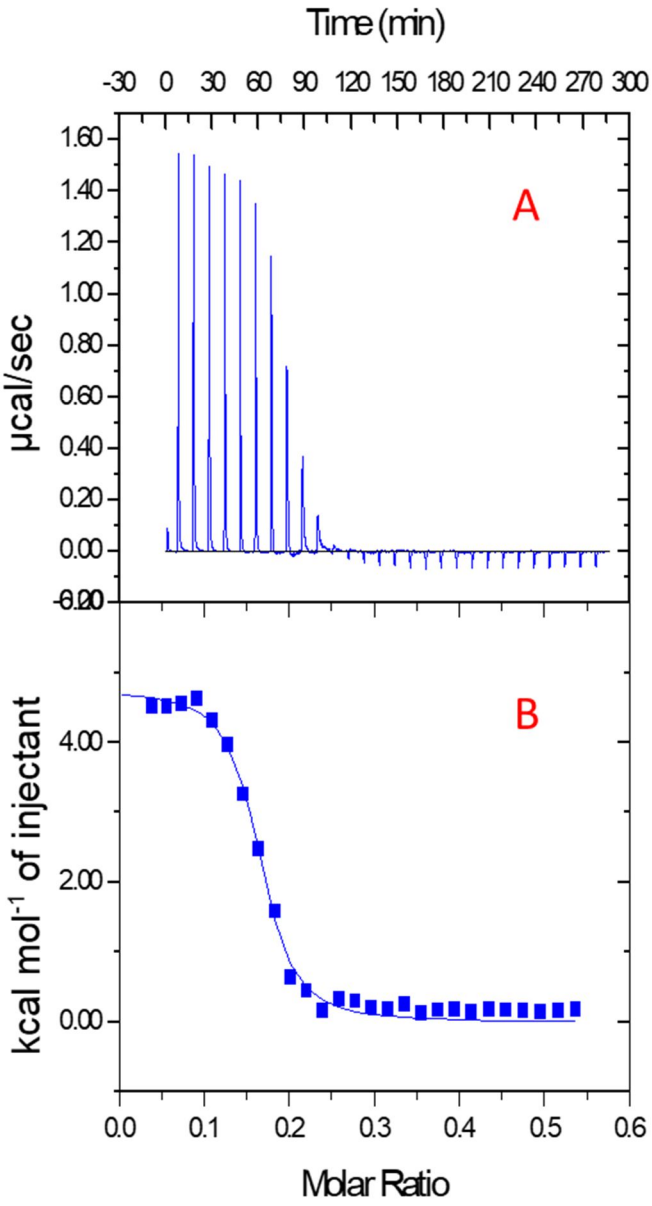

Figure 19. Representative ITC data for the interaction of nanoparticles NP_5 and Eu^{3+} showing (A) 27 consecutive injections of 10 µL of Eu^{3+} (1.5 mM) and the integrated data, with best fitting lines in red, are displayed in part (B) at 25 ºC.

Table 5. Thermodynamic parameters of the complexation reaction of NPs and europium at 25 °C

Entry	Copolymer	N[a]	ΔH (Cal/mol) [b]
NP_1	$PVDPA_{10}$-b-PS_{184}	0.16	3 600
NP_2	$PVDPA_{10}$-b-PS_{260}	0.23	5 100
NP_3	$PVDPA_{10}$-b-PS_{600}	0.60	2 600
NP_4	PS_{112}-b-$PVDPA_{30}$	0.13	2 800
NP_5	PS_{112}-b-$PVDPA_{50}$	0.16	3 300

[a] stoichiometry between NPs and europium. [b] Enthalpy of association.

6. ICP-AES analysis

Using the ITC titration curve as a guide, a series of nanoparticles-europium solutions were prepared at concentrations that corresponded to specific injections on the ITC titration curve using the same solutions as in the ITC experiment (Figure 20). Using ICP-AES, the interaction of 0.6 x 10^{-3} M of PVDPA from NP_2 dispersed in H_2O at pH ~ 5.5 were evaluated on different volume of $Eu(NO_3)_3$ (1.5 x 10^{-3} M) solution, at molar ratios between 0.18 and 0.35. The solution was left for a couple of minutes to settle then filtered to isolate the precipitated complex and the remaining metal species were measured with ICP-AES.

Figure 20B shows the amount of europium in solution after contact with nanoparticles (blue column) against the initial amount of Eu^{3+} in solution (red column), given as the molar ratio (= Eu^{3+}/ PVDPA). The concentrations of free Eu^{3+} dropped from average of 11.238, 12.385 and 20.071 ppm to average of 0.147, 0.318 and 7.163 ppm respectively when NP_2 (PVDPA) was added. Looking at Figure 20B, europium concentration went down from 11.238 ppm to 0.147 ppm before the inflection point (ITC curve, Figure 20A). Theoretically, there is no europium ion present in excess, the polymer (PVDPA) exists primarily free in solution. As soon as metal ions are introduced into the polymer solution, europium concentration went down from 12.385 ppm to 0.318 ppm at the inflection point. The amount of Eu^{3+} in the solution after complexation with nanoparticles decreases from

20.071 ppm to 7.163 ppm when the molar ratio is 0.35, after the inflection point. At this point, we hypothesize that as the metal ion concentration increases because no more free PVDPA in solution to bind with. We see that the molar ratio of Eu^{3+} /PVDPA (NP_1) is ~ 0.2, above which no further europium harvesting is observed, which is consistent with the stoichiometry estimated from the ITC titration.

A)

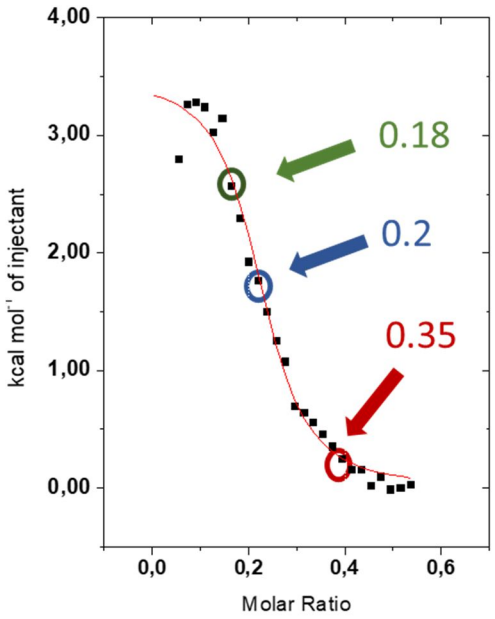

B)

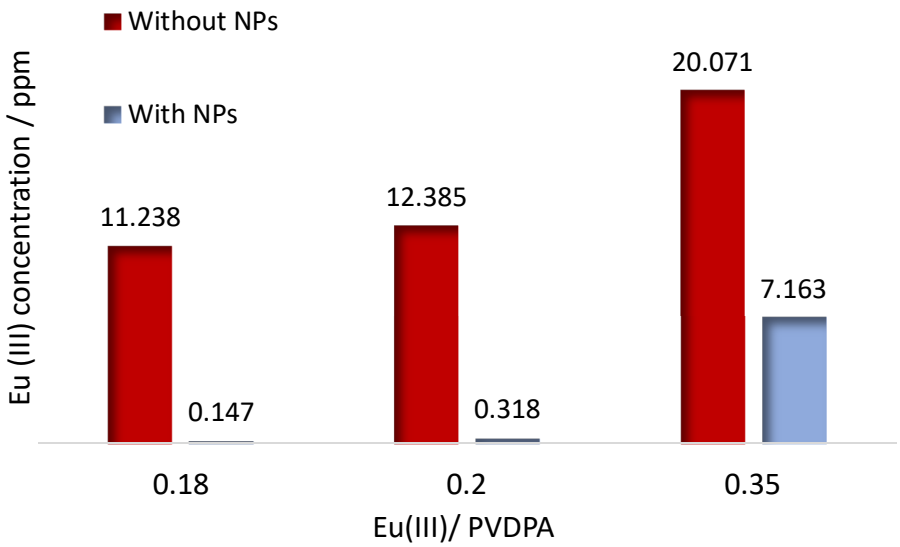

Figure 20. A) ITC thermograph with B) ICP-AES data overlaid under the corresponding ITC injection. B) shows Eu^{3+} concentrations (ppm) before (red) and after (blue) treatment with NP_2

7. Nanoparticles applications

In light of these experiments, nanoparticles can lead to promising material playing an important role in metal binding. Thanks to special properties and the multitude of nanoparticles, they are interest in several areas such as: electronics [31], medicine [32], and several others. Nanoparticles are special materials used across the entire field of life sciences. Here, the focus is made on one of their specific classes, luminescent nanoparticles. They are emerging as interesting candidates with recent explosive growth in various areas as biological imaging [33].

In this work, luminescent nanoparticles have been prepared by adding europium solution to nanoparticles suspension of NP_4 (pH ~ 5.5), where Eu^{3+}/ PVDPA (NP_4) = 0.03, and a red emissive color were immediately observed when exposed to UV excitation (λ = 254 nm) as shown in Figure 21. The resulting nanoparticles, NP_4-Eu^{3+}, were characterized by Dynamic Light Scattering (DLS) to determine both the Hydrodynamic Diameter (D_h) and zeta potential (ζ). Nanoparticles displayed a D_h of 73 nm and ζ of -25 mV indicating that colloids are highly stabilized by electrostatic repulsive force between carboxylate units of PVDPA. The average size of these nanoparticles remained basically unchanged at least within 20 days at 20 °C (Figure S 3). The morphology of the NP_4-Eu^{3+} was further investigated by TEM, which allows for the direct visualization of the spherical particles as seen in Figure S 4.

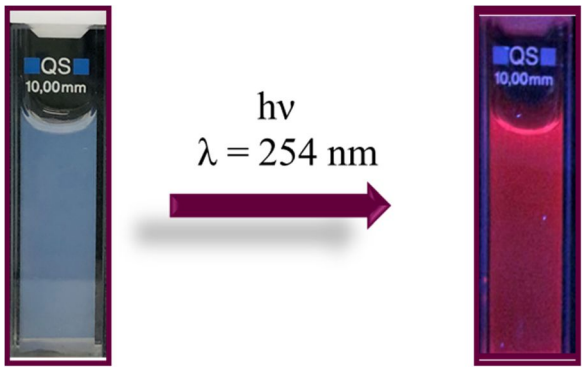

Figure 21. Image of NP_4-Eu^{3+} in water at pH 5.5 under visible light (left) and UV excitation (right).

On the other hand, another potential application for polymeric nanoparticles is their use as chelating ligand for metal extraction. Nanoparticles have been applied as an effective method for metal ion extraction [34], for valuable metal recovery [35].

After synthesis of NPs, the complexation of these NPs with europium has been extensively studied in this work. High uptake capacity of these nanoparticles for europium has been showed. The recovery of europium was evaluated by using ICP-AES, IR, UV-Vis and ITC. Additionally, binding stoichiometry for this series of nanoparticles also appears to be dependent of copolymer chain length. The higher efficiency of trapping europium have been showed with high degree of polymerization of hydrophobic chain (DP = 600)

Based on these observations, a new promising system for REEs scavenging in an aqueous environment was suggested as shown in Figure 22. A commercial dialysis membrane (pore size = 3500 Daltons) was employed in this experiment in which nanoparticles are present. Since dialysis pore sizes are bigger than metal ion diameter, the pollutant metal ion in contaminated water can passed through this membrane however pore sizes small enough to reject these NPs.

An efficient system of nanoparticles for metal extraction process is a system for which the complexation capacity of the nanoparticles is important in large volume of contaminated water. The high surface area of nanoparticles has been considered as an advantage of this system. On the other hand, as metal ions are added into the water, nanoparticles-metal form ionic aggregates as shown in Figure S 5.

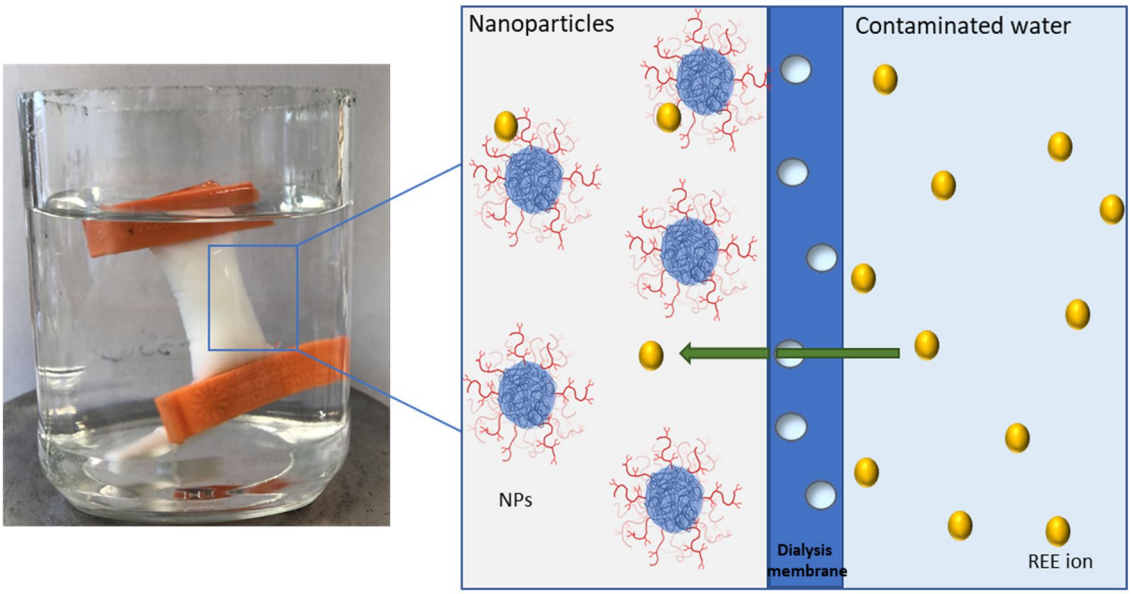

Figure 22. Image of nanoparticles presents in dialysis membrane (left), which dive in water. Schematic illustration of the procedure used for water decontamination (right)

Conclusion

In summary, the effective application of surface active polystyrene-b-poly(4-vinyldipicolinic acid) (PS-b-PVDPA) core-shell nanoparticles in trapping rare-earth metals with a high uptake capacity has attracted our interest in the present research. The motivation behind this study is to obtain the complexation information between the new functional nanoparticles and europium, which proves that it could be a new promising material for lanthanides scavenging, and luminescent nanoparticles preparation in an aqueous environment. By studying the complexation and thermodynamics behavior of these nanoparticles-metal interactions, the impact of chain lengths of each block of copolymer on metal binding with these nanoparticles was demonstrated. The complexation mode of nanoparticles and europium was well verified by extensive characterization using ITC, ICP-AES, TRLFS, ATR-FTIR, and UV-vis analysis. The results presented here will guide the development

of future metal-chelating system for a myriad of applications such as luminescent nanoparticles, and lanthanide harvesting.

Acknowledgment

The authors would like to acknowledge the Lebanese National Council for Scientific Research (CNRS-L) for funding this work. The authors are grateful to Dr François Brisset for performing TEM experiments (ICMMO, Orsay, France)

Reference

[1] G. Charalampides, K. I. Vatalis, B. Apostoplos, and B. Ploutarch-Nikolas, "Rare Earth Elements: Industrial Applications and Economic Dependency of Europe," *Procedia Economics and Finance*, vol. 24, pp. 126–135, 2015, doi: 10.1016/s2212-5671(15)00630-9.

[2] K. Smith Stegen, "Heavy rare earths, permanent magnets, and renewable energies: An imminent crisis," *Energy Policy*, vol. 79, pp. 1–8, Apr. 2015, doi: 10.1016/j.enpol.2014.12.015.

[3] S. Massari and M. Ruberti, "Rare earth elements as critical raw materials: Focus on international markets and future strategies," *Resources Policy*, vol. 38, no. 1, pp. 36–43, Mar. 2013, doi: 10.1016/j.resourpol.2012.07.001.

[4] Y. Ku and I.-L. Jung, "PHOTOCATALYTIC REDUCTION OF Cr(VI) IN AQUEOUS SOLUTIONS BY UV IRRADIATION WITH THE PRESENCE OF TITANIUM DIOXIDE," 2001. [Online]. Available: www.elsevier.com/locate/watres

[5] S. Y. Kang, J. U. Lee, S. H. Moon, and K. W. Kim, "Competitive adsorption characteristics of Co2+, Ni2+, and Cr3+ by IRN-77 cation exchange resin in synthesized wastewater," *Chemosphere*, vol. 56, no. 2, pp. 141–147, 2004, doi: 10.1016/j.chemosphere.2004.02.004.

[6] R. S. Juang, Y. Y. Xu, and C. L. Chen, "Separation and removal of metal ions from dilute solutions using micellar-enhanced ultrafiltration," *Journal of Membrane Science*, vol. 218, no. 1–2, pp. 257–267, Jul. 2003, doi: 10.1016/S0376-7388(03)00183-2.

[7] E. Samper, M. Rodríguez, M. A. de la Rubia, and D. Prats, "Removal of metal ions at low concentration by micellar-enhanced ultrafiltration (MEUF) using sodium dodecyl sulfate (SDS) and linear alkylbenzene sulfonate (LAS)," *Separation and Purification Technology*, vol. 65, no. 3, pp. 337–342, Mar. 2009, doi: 10.1016/j.seppur.2008.11.013.

[8] J. R. Parga *et al.*, "Arsenic removal via electrocoagulation from heavy metal contaminated groundwater in la Comarca Lagunera México," *Journal of Hazardous Materials*, vol. 124, no. 1–3, pp. 247–254, Sep. 2005, doi: 10.1016/j.jhazmat.2005.05.017.

[9] C. A. Bode-Aluko, O. Pereao, G. Ndayambaje, and L. Petrik, "Adsorption of Toxic Metals on Modified Polyacrylonitrile Nanofibres: A Review," *Water, Air, and Soil Pollution*, vol. 228, no. 1, Jan. 2017, doi: 10.1007/s11270-016-3222-3.

[10] P. K. Neghlani, M. Rafizadeh, and F. A. Taromi, "Preparation of aminated-polyacrylonitrile nanofiber membranes for the adsorption of metal ions: Comparison with microfibers," *Journal of Hazardous Materials*, vol. 186, no. 1, pp. 182–189, Feb. 2011, doi: 10.1016/j.jhazmat.2010.10.121.

[11] M. Gergoric, A. Barrier, and T. Retegan, "Recovery of Rare-Earth Elements from Neodymium Magnet Waste Using Glycolic, Maleic, and Ascorbic Acids Followed by Solvent Extraction," *Journal of Sustainable Metallurgy*, vol. 5, no. 1, pp. 85–96, Mar. 2019, doi: 10.1007/s40831-018-0200-6.

[12] S.-G. Teoh, S.-H. Ang, and J.-P. Declercq, "Synthesis and characterization of di-n-butylbis(2,4-dihydroxybenzoato) tin (IV)," 1997.

[13] A. A. Tolba *et al.*, "Synthesis and characterization of poly(carboxymethyl)-cellulose for enhanced La(III) sorption," *Carbohydrate Polymers*, vol. 157, pp. 1809–1820, Feb. 2017, doi: 10.1016/j.carbpol.2016.11.064.

[14] Y. Zhu, Y. Zheng, and A. Wang, "A simple approach to fabricate granular adsorbent for adsorption of rare elements," *International Journal of Biological Macromolecules*, vol. 72, pp. 410–420, Jan. 2015, doi: 10.1016/j.ijbiomac.2014.08.039.

[15] F. M. de Melo, S. da N. Almeida, N. S. Uezu, C. A. O. Ramirez, A. D. dos Santos, and H. E. Toma, "Extraction of Dysprosium Ions with DTPA Functionalized Superparamagnetic Nanoparticles Probed by Energy Dispersive X-ray Fluorescence and TEM/High-Angle Annular Dark Field Imaging," *Journal of Nanoscience and Nanotechnology*, vol. 18, no. 6, pp. 4155–4159, Dec. 2017, doi: 10.1166/jnn.2018.15245.

[16] E. Polido Legaria, M. Samouhos, V. G. Kessler, and G. A. Seisenbaeva, "Toward Molecular Recognition of REEs: Comparative Analysis of Hybrid Nanoadsorbents with the Different Complexonate Ligands EDTA, DTPA, and TTHA," *Inorganic Chemistry*, vol. 56, no. 22, pp. 13938–13948, Nov. 2017, doi: 10.1021/acs.inorgchem.7b02056.

[17] M. Maaz *et al.*, "New insights on Uranium recovery from seawater and aqueous media," *Applied Materials Today*, vol. 18, Mar. 2020, doi: 10.1016/j.apmt.2019.100461.

[18] N. Berri *et al.*, "Surface Grafting of Electrospun Fibers: Multiscale Characterization and Perspective for Potential Applications," *ACS Applied Polymer Materials*, Apr. 2022, doi: 10.1021/acsapm.2c00229.

[19] R. J. Falconer, B. Schuur, and A. K. Mittermaier, “Applications of isothermal titration calorimetry in pure and applied research from 2016 to 2020,” *Journal of Molecular Recognition*, vol. 34, no. 10. John Wiley and Sons Ltd, Oct. 01, 2021. doi: 10.1002/jmr.2901.

[20] R. Ghai, R. J. Falconer, and B. M. Collins, “Applications of isothermal titration calorimetry in pure and applied research-survey of the literature from 2010,” *Journal of Molecular Recognition*, vol. 25, no. 1. pp. 32–52, Jan. 2012. doi: 10.1002/jmr.1167.

[21] W. B. Turnbull and A. H. Daranas, “On the Value of c: Can Low Affinity Systems Be Studied by Isothermal Titration Calorimetry?,” *J Am Chem Soc*, vol. 125, no. 48, pp. 14859–14866, Dec. 2003, doi: 10.1021/ja036166s.

[22] C. G. Sinn, R. Dimova, and M. Antonietti, “Isothermal titration calorimetry of the polyelectrolyte/water interaction and binding of Ca2+: Effects determining the quality of polymeric scale inhibitors,” *Macromolecules*, vol. 37, no. 9, pp. 3444–3450, May 2004, doi: 10.1021/ma030550s.

[23] C. Xu, G. Tian, S. J. Teat, G. Liu, and L. Rao, “Thermodynamic and structural trends in hexavalent actinyl cations: Complexation of dipicolinic acid with NpO22+ and PuO 22+ in comparison with UO22+,” *Chemistry - A European Journal*, vol. 19, no. 49, pp. 16690–16698, Dec. 2013, doi: 10.1002/chem.201302119.

[24] P. Táborský *et al.*, “Spectroscopic characterization of Eu(III) complexes with new monophosphorus acid derivatives of H4dota,” *Journal of Fluorescence*, vol. 15, no. 4, pp. 507–512, Jul. 2005, doi: 10.1007/s10895-005-2824-8.

[25] A. L. Gassner, C. Duhot, J. C. G. Bünzli, and A. S. Chauvin, “Remarkable tuning of the photophysical properties of bifunctional lanthanide tris(dipicolinates) and its consequence on the design of bioprobes,” *Inorganic Chemistry*, vol. 47, no. 17, pp. 7802–7812, Sep. 2008, doi: 10.1021/ic800842f.

[26] S.-G. Teoh, S.-H. Ang, and J.-P. Declercq, “Synthesis and characterization of di-n-butylbis(2,4-dihydroxybenzoato) tin (IV),” 1997.

[27] G. K. Sandi-Iu and S. P. Verma, “TRIORGANOTIN(IV) DERIVATIVES OF FIVE MEMBERED HETEROCYCLIC 2-CARBOXYLIC ACIDS,” 1987.

[28] K. Binnemans, “Interpretation of europium(III) spectra,” *Coordination Chemistry Reviews*, vol. 295. Elsevier B.V., pp. 1–45, Jan. 01, 2015. doi: 10.1016/j.ccr.2015.02.015.

[29] T. Kimura, Y. Kato, H. Takeishi, and G. R. Choppin, “Comparative study on the hydration states of Cm(III) and Eu(III) in solution and in cation exchange resin,” 1998.

[30] J. F. Cawthray, A. L. Creagh, C. A. Haynes, and C. Orvig, “Ion exchange in hydroxyapatite with lanthanides,” *Inorganic Chemistry*, vol. 54, no. 4, pp. 1440–1445, Feb. 2015, doi: 10.1021/ic502425e.

[31] Y. Li, Y. Wu, and B. S. Ong, “Facile synthesis of silver nanoparticles useful for fabrication of high-conductivity elements for printed electronics,” *J Am Chem Soc*, vol. 127, no. 10, pp. 3266–3267, Mar. 2005, doi: 10.1021/ja043425k.

[32] R. Elghanian, J. J. Storhoff, R. C. Mucic, R. L. Letsinger, and C. A. Mirkin, “Selective colorimetric detection of polynucleotides based on the distance-dependent optical properties of gold nanoparticles,” *Science (1979)*, vol. 277, no. 5329, pp. 1078–1081, Aug. 1997, doi: 10.1126/science.277.5329.1078.

[33] H. S. Peng and D. T. Chiu, “Soft fluorescent nanomaterials for biological and biomedical imaging,” *Chemical Society Reviews*, vol. 44, no. 14. Royal Society of Chemistry, pp. 4699–4722, Jul. 21, 2015. doi: 10.1039/c4cs00294f.

[34] T. L. Lin and H. L. Lien, “Effective and selective recovery of precious metals by thiourea modified magnetic nanoparticles,” *International Journal of Molecular Sciences*, vol. 14, no. 5, pp. 9834–9847, May 2013, doi: 10.3390/ijms14059834.

[35] B. Chen, X. Zhao, Y. Liu, B. Xu, and X. Pan, “Highly stable and covalently functionalized magnetic nanoparticles by polyethyleneimine for Cr(vi) adsorption in aqueous solution,” *RSC Advances*, vol. 5, no. 2, pp. 1398–1405, 2015, doi: 10.1039/c4ra10602d.

Supporting information

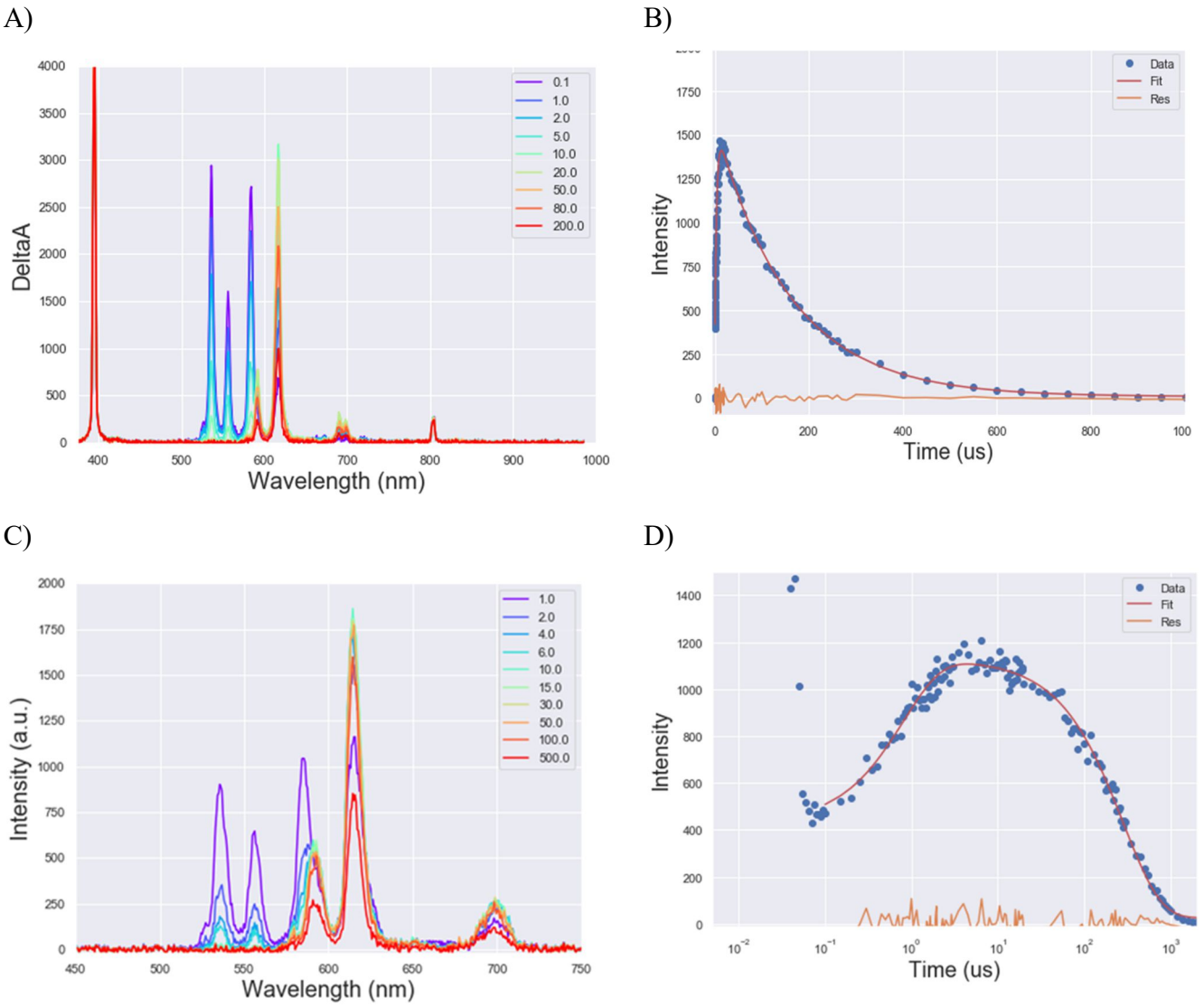

Figure S 1. (A) Luminescence emission spectra, (B) fluorescence decay of $Eu(NO_3)_3$.

(C) Luminescence emission spectra, (D) fluorescence decay of NP_4.

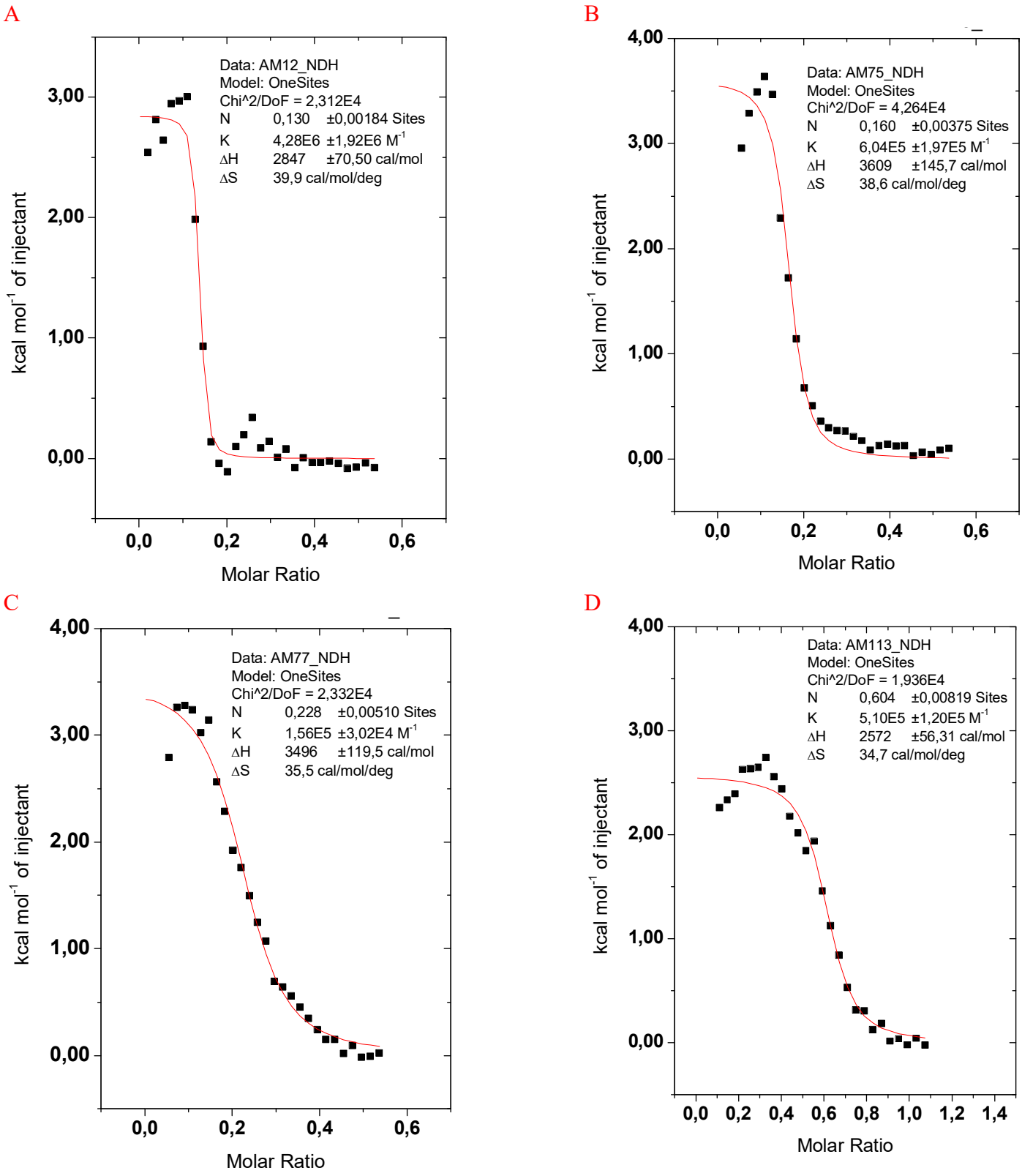

Figure S 2. Representative ITC integrated titration curve of A) NP_4 B) NP_1 C) NP_2 and D) NP_3.

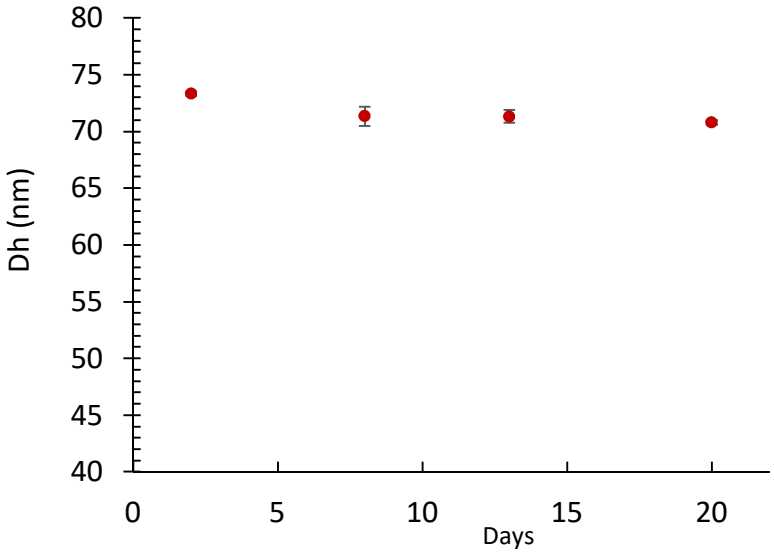

Figure S 3. Stability of nanoparticles (NP_4-Eu^{3+}) with time.

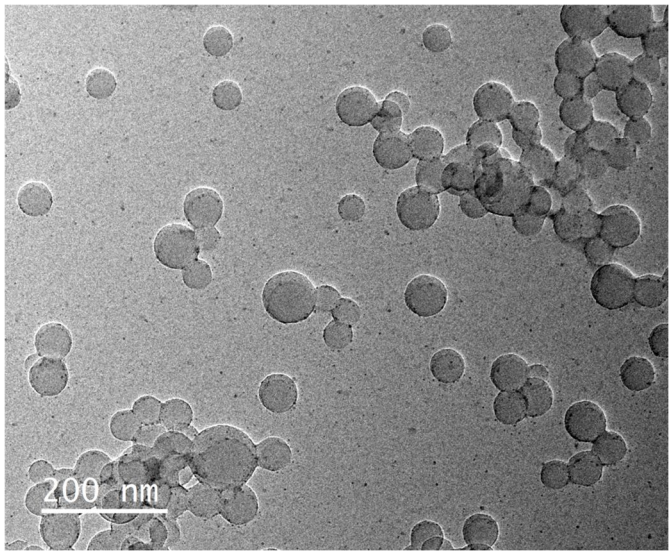

Figure S 4. TEM representative image of NP_4-Eu^{3+}

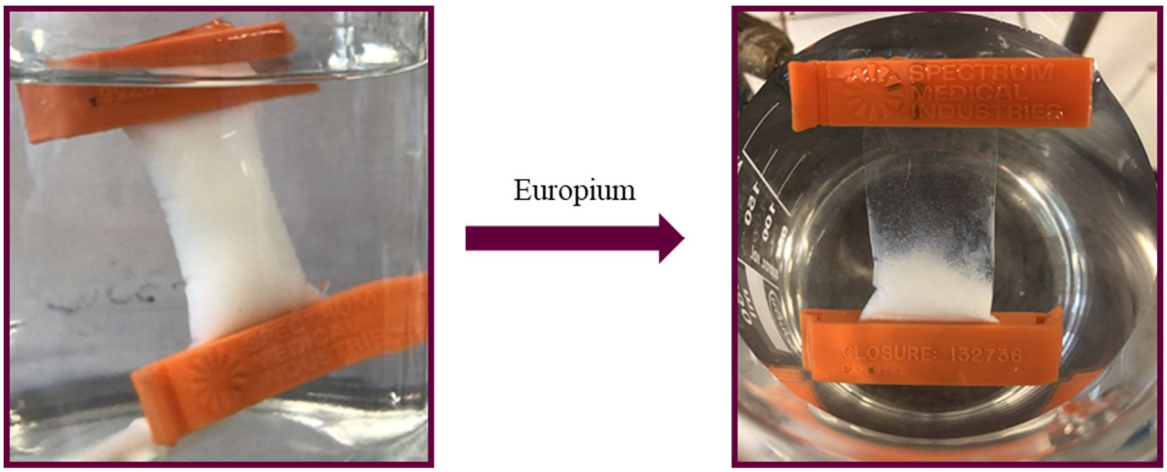

Figure S 5. Image of nanoparticles presents in dialysis membrane (left) dive in pure water. NP_2-europium aggregates after added europium in water (right)

Chapter III. Star polymers

Part I. Synthesis and characterization of star polymers by ATRP via one-pot 'core-first' method using 2 initiators derivatized from calix[6]arene

Abstract

Novel Star-shaped polymers, with multifunctional calixarene-type initiators were synthesized by Atom Transfer Radical Polymerization (ATRP). Two hexafunctional calixarenes derivatives were synthesized in one step and used to initiate the ATRP of 4-vinyl dimethyl dipicolinate (VDPM) by the core-first method called. The effects of the structure of the initiator on the kinetic of the polymers are studied. The polymerization rates exhibited first-order kinetics with respect to the monomer and a linear increase of number average molecular weight (M_n) *vs* monomer conversion was observed of these two systems. The polymers obtained were characterized by NMR spectroscopy, size exclusion chromatography, Dynamic Light Scattering (DLS). Star-like macromolecular that were visualized by Atomic Force Microscopy (AFM) techniques.

Keywords: Star polymers, Atom Transfer Radical Polymerization (ATRP), hexafunctional initiators, calixarenes derivatives.

Introduction

During the last decades the synthesis of polymers, with well-defined composition and architecture have gained a lot of interest. Some of these tailor-made macromolecules, like dendrimers [1], hyperbranched macromolecules [2], star homopolymers [3] and star block copolymers [4] have unusual solution and interfacial properties, because of their unique spatial shapes.

A star polymer is an architectural macromolecule composed of multiple linear chains that are joined at one end of each chain by a junction point. Two mains strategies allow engineering star-shaped macromolecules: the so-called "Arm-first" method and "Core-

first" method. In the first case, arms are synthesized separately and then bounded by polyfunctional crosslinking agents [5][6]. In the second case, arms grow on a multicentre core resulting in macromolecules with well-defined structures in terms of both arm number and length [7]. This variant was found to be efficient for the synthesis of multifunctional initiators for the preparation of polymer stars of high functionality. In light of this, we demonstrate the use of calixarene derivatives as effective initiators for the preparation of well-defined hexafunctional polymer stars. Calix[n]arenes (with n varying from 4 to 8) are a type of phenol-containing macrocycle. They can be synthesized by combining para-substituted phenol and formaldehyde, and their ring sizes can be precisely controlled by synthetic conditions [8]. The hydroxyl groups of theses calixarenes may be easily functionalized, through esterification reaction to prepare the initiators. Calixarenes are well-known and used for their three-dimensional cavities that vary in dimensions: 3.0, 7.6, and 11.7 Å for calix[4]arene, calix[6]arene and calix[8]arene respectively [9]. Calixarene-centred star polymers have been synthesized successfully using living/controlled polymerization techniques [10].

Polymer supported calixarenes can be important in many polymers application. These features are very attractive for medical use such as micellar drug delivery [11][12], biosensor [13] and decontaminating agents for wasted water [14][15].

Several reports have appeared on the controlled preparation of star polymers via ATRP [3][16][17]. Moreover, ATRP has been demonstrated to provide controlled polymerizations of a wide range of monomers like styrene [18][19] and (meth)acrylates [10][11] and with variations in composition and architecture found in block [22], graft [23], star, branched [24], and hyperbranched materials [25].

Several studies have shown that many factors like ligand and metal complexes [26], solvent [27], temperature [28] can affect the rate of polymerization in ATRP. Studies have far concentrated on a variety of linear mono-initiators e.g., ethyl 2-bromoisobutyrate (EtBriB), methyl 2-bromopropionate (MBrP), and 1-phenylethyl bromide (PEBr) by determining the activation rate constants (k_{act}) [29]. In order to better compare and understand the kinetics of ATRP, herein we present the effect of cyclic multi-initiator structure (calix[6]arene) on

the activation process under similar reaction conditions (DMSO at 60 °C) by using size exclusion chromatography (SEC) and NMR as characterization techniques.

The synthesis and characterization of hexafunctional calixarene initiators and their use in the ATRP of 4-vinyl dimethyl dipicolinate (VDPM) is presented. VDPM is derived from chelidamic acid, the carboxylate form of this monomer is known for his strongly chelating capacity to a lot of metals including lanthanides. The study's focus was the effect of the structure of the initiators on their activity. In prior, initiators had to be modified to introduce the chlorine function that subsequently served for the initiation of this monomer by ATRP.

To this aim, two calix[6]arene initiators were applied to study the difference in initiating efficiency between the calixarene derivatives.

Materials and methods

Materials.

CuCl (Aldrich), Tris (2-pyridylmethyl) amine (TPMA, TCI, >98%) used without further purification. Dimethyl sulfoxide (DMSO), Dimethylformamide (DMF) were dried over CaH_2. 4-tert-butylcalix[6]arene (TBC-6) and 4-tert-butylcalix[6]arene-Br (TBC-6-Br) were commercially available reagents purchased in high purity and used without purification.

Methods.

Size exclusion chromatography (SEC) measurements were done with DMF as elution solvent. SEC analysis was performed using a Styragel column (HR 4E, 5 µm, 4.6 x 300 mm) from Waters. PMMA standards were used to estimate the average molar weight and dispersity of analysed samples using RI detector. Dynamic light scattering (DLS) was performed on a Malvern Zetasizer nano ZS instrument equipped with a He-Ne laser beam at a wavelength (λ = 632 nm) and scattering angle of 173°. ^{1}H NMR and ^{13}C NMR measurements were recorded on either a Bruker Avance 360, Bruker 400 or Bruker DRX 400 instrument and data are reported in ppm with the solvent signal as reference. Tapping mode topography and phase imaging was accomplished using di Innova AFM Bruker with NanoDrive v8.02 software. Tapping mode images were acquired using silicon tips from

Nanosensors (PPP NCSTR) with a resonance frequency ranging between 76 and 263 kHz. Images were processed using Gwyddion software, freely available on Internet. The electrospray ionization mass spectrometry (ESI MS) analyses were performed with a Bruker MicroTOF-Q 2009.

Synthesis of the hexafunctional initiator (calix 1)

A procedure described by Angot et al [3] was used to prepare the hexa-arms calixarene derivative. Hexafunctional initiator was prepared by reaction between 2-chloropropionyl chloride and calix[6]arene (TBC-6). In a round flask, equipped with a magnetic stirrer, calix[6]arene (3 g, 2.33 mmol) was suspended in 30 mL of dry THF, then triethylamine (7.7 mL, 55.2 mmol) was added. The reactor was cooled to 0°C in ace/water bath and a solution of 2-chloropropionyl chloride (5.7 mL, 55.2 mmol) dissolved in THF (30 mL) were added dropwise over a period of 1h. The reaction mixture was stirred at room temperature for 24 h. The solution was concentrated and precipitated in ice-cold water. The crude solid was dissolved in DCM and washed successively with aqueous K_2CO_3 solution (1 M) and dried over anhydrous $MgSO_4$ and concentrated. Then the residue was dissolved in a minimum of DCM and precipitated by a dropwise addition at room temperature in diethyl ether, under vigorous stirring, the precipitation was repeated two more times to obtain calix 1 as a white powder (4 g, 89 % yield).

^{1}H NMR (DMSO-d6, 80 °C, 400 MHz) δ ppm: 7.5 to 6.6 (s, 2H, aromatic protons), 5.05 to 4.4 (s, 1H, -CH-), 3.8 to 3.1 (s, 2H, -CH2-), 1.9 to 0.7 (m, 12H, CH_3- and *t*butyl). ^{13}C NMR ($CDCl_3$, 25 °C, 400 MHz) δ ppm: 168.7 (carbonyl), 149.3, 144.3, 129.09, 126.9 (aromatic carbons), 51.8 (CH_3-CH-Cl), 34.7 (-C *t*butyl), 31.6 (-CH_3 *t*butyl), 29.9 (Ar-CH_2-Ar), 21.7 (CH_3-CH- Cl).

MS [ESI(+)]: *m/z* $[M+Na]^+$ calculated for $[C_{84}H_{102}Cl_6NaO_{12}]^+$: 1535.5395 found: 1535.5384.

Synthesis of the hexafunctional initiator (calix 2)

In a round flask, equipped with a magnetic stirrer, TBC-6-Br (0.3 g, 0.196 mmol) and K_3PO_4 (0.3 g, 1.42 mmol) were suspended in 10 mL of 2,2,2 trifluoroethanol and refluxed for 3 days under argon. The reactor was cooled to room temperature, the product is precipitated with 100 mL of water, and recovered by filtration. 0.33g of calix[6]-OSO_2CF_3 was recovered. The obtained product is dissolved in a mixture of 40 mL of dioxane and 5 mL of HCl (37%). The reaction mixture was refluxed for a week. During this period, samples are taken every day to follow the evolution of the reaction. At the end of this period, the product is precipitated with 200 mL of water, and recovered by filtration. Is recovered 0.2 g of calix[6]-C. Yield: 80%

^{1}H NMR ($CDCl_3$, 25 °C, 400 MHz) δ ppm: 7.58 to 7.52 (s, 2H, aromatic protons), 6.95 to 6.86 (s, 1H, -CHCl-), 3.42 to 3.35 (s, 3H, OCH_3), 1.18 to 1.13 (s, 9H, *t*-butyl). ^{13}C NMR ($CDCl_3$, 400 MHz) δ ppm: 151.5, 147.1 133.8, 127,0 (aromatic carbons), 61.7 (O<u>C</u>H$_3$), 51.0 (Ar-<u>C</u>HCl-Ar), 34.5 (<u>C</u> of *t*-butyl), 31.5 (-<u>C</u>H$_3$ of *t*-butyl),

MS [ESI(+)]: *m/z* $[M+Na]^+$ calculated for $[C_{72}H_{90}Cl_6NaO_6]^+$: 1283.4761 found: 1283.4818.

Polymerization procedures of PVDPM:

In a typical polymerization procedure, a schlenck flask was charged with VDPM (175 mg, 0.78 mmol) and calix 1 (2 mg, 0.13 x 10^{-2} mmol). Then, a solution of TPMA (0.37 mg, 0.13 x 10^{-2} mmol) and CuCl (0.128 mg, 0.13 x 10^{-2} mmol) in DMSO (1.5 mL) was added at room temperature and under an argon atmosphere. Before polymerization, the solution was degassed (three freeze-pump thaw cycles) and back-filled with argon. The flask was then placed in an oil bath thermostated at 60 °C and stirred for defined time. The flask was cooled to room temperature; the reaction mixture was dissolved in DCM and then passed through a column of neutral alumina to remove metal salts. The solution was precipitated from an excess of methanol. The solid was filtered off, and dried under vacuum. The polymerisation conversion was determined by ^{1}H NMR.

The same procedure given above is used to the polymerization with calix 2 as initiator.

Results and discussion

Synthesis of calixarene-core hexafunctional initiators

The synthesis of the novel hexa-arm star PVDPM arms polymer needs the use of novel hexa-functional initiators. In this contest, hexafunctional initiators, calix 1 and calix 2, were readily synthesized in one step starting from the TBC-6 and TBCBr-6 respectively. The structures of initiators calix 1 and calix 2 are presented in Scheme 13.

Calix 1 was prepared by the reaction between TBC-6 and 2-chloropropionyl chloride in the presence of triethylamine in THF at room temperature.

The α-chloroester calix 1 was afforded chemically pure, showed by ^{1}H NMR, ^{13}C NMR, and Mass spectrometry. Figure 23 shows the ^{1}H NMR spectrum of calix 1. No residual phenolic protons signal corresponding to the starting BTC-6 was observed, indicating a quantitative esterification. The small peak appearing at 4.7 ppm was assigned to CH_3-CH-Cl protons confirming the esterification reaction, the aromatic and *t*-butyl groups signals around 7 and 1 ppm respectively, were from the calixarene core.

The purified initiators were used in the polymerization of VDPM in the presence of CuCl and TPMA.

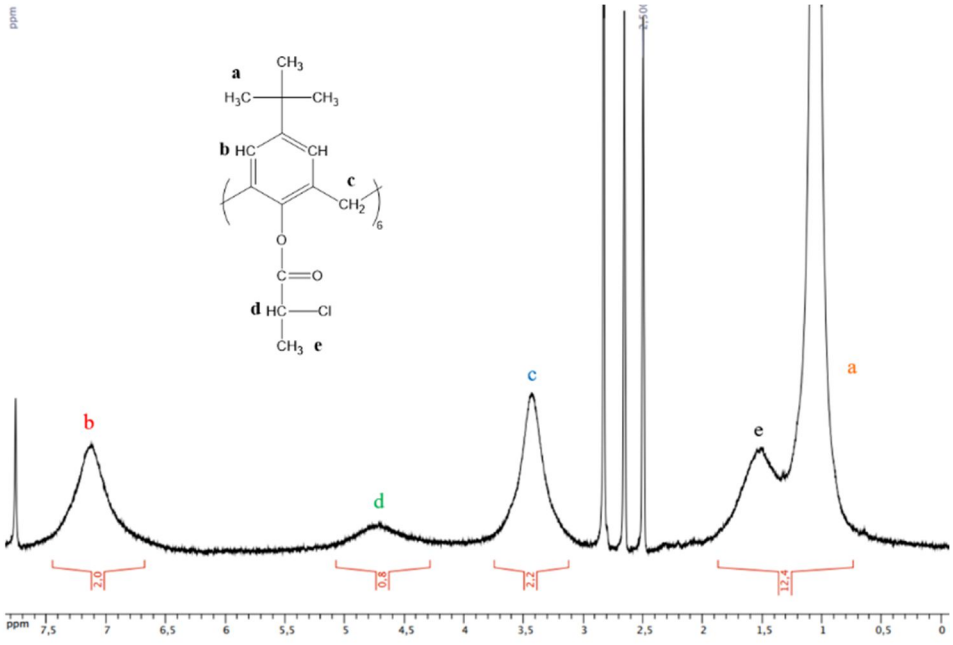

Figure 23. ^{1}H NMR spectrum of calix 1 (DMSO, 400 MHz, 80 °C)

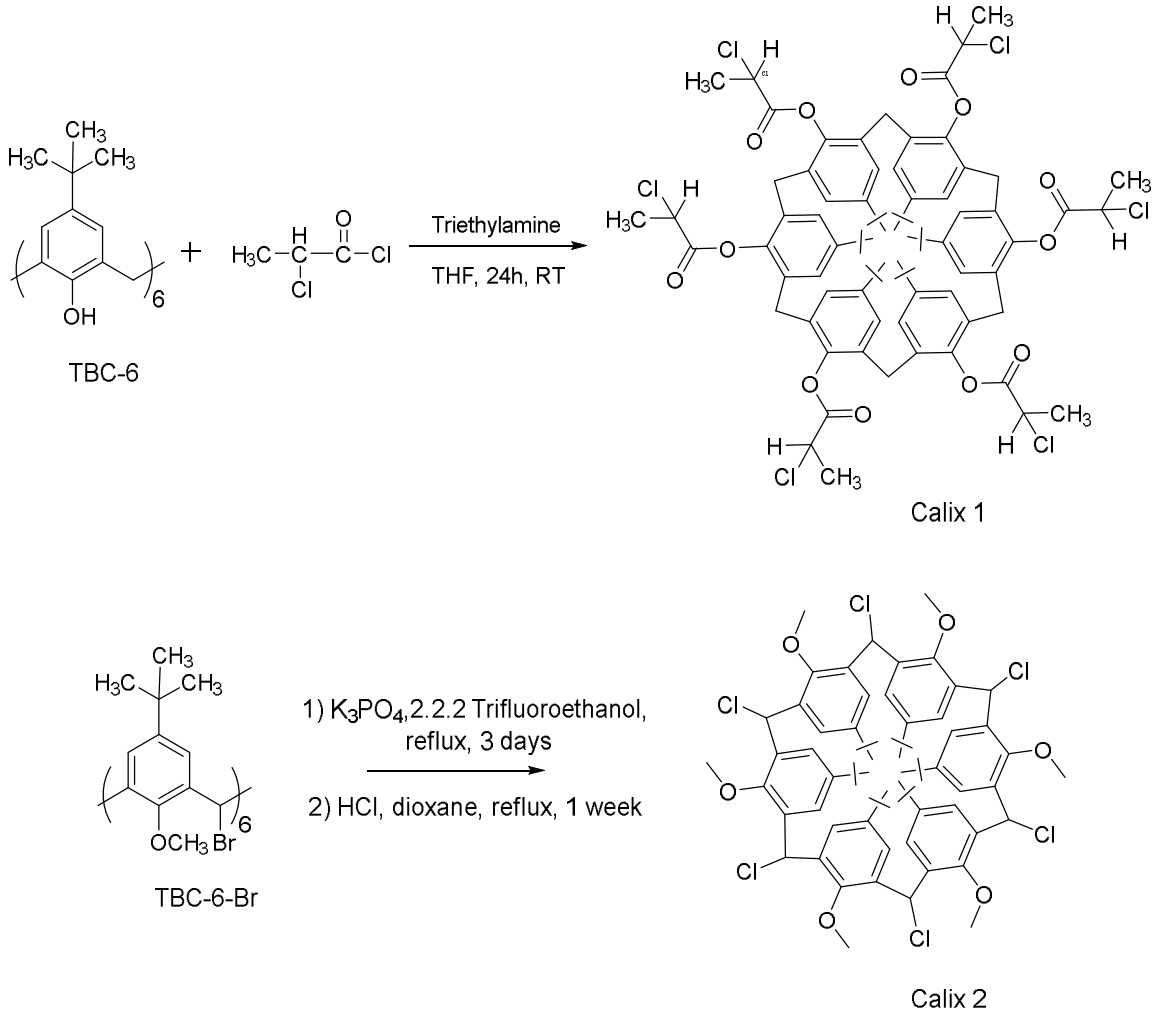

Scheme 13. Synthesis of the calixarene-based hexafunctional initiator (calix 1 and 2)

Synthesis of star-shaped VDPM with multifunctional initiators

6-arms star PVDPM were synthesized using initiators (calix 1 and calix 2), the synthetic route is depicted in Scheme 14. Polymerizations were conducted with ratios of [calix] /[VDPM] /CuCl /TPMA = 1: 600 : 1 : 1, where [calix] and [VDPM] represent initial concentration of initiator and monomer, VDPM, respectively in DMSO at 60 °C. The polymerization occurred smoothly and reached 73% conversion in 2h for calix 1-PVDPM. VDPM polymerization results with calix 1 as initiator are given in Table 6. It shows that the number average molar masses (Mn) increase linearly with conversion. As shown in Table 6, between 10 min and 2 hours of polymerization, VDPM conversion went from 19 to 73 %, giving theoritical Mn (NMR) between 26.7 and 98.4 x 10^3 g/mol and a measured

Mn (SEC) between 16.6 and 30.7 x 10^3 g/mol, correspondingly. As already explained by Angot *et al.* [3], the high values of dispersity due to the star-to-star coupling when the monomer conversion increases. Calix 1-PVDPM polymers afforded high dispersity (Đ > 1.5) under our studied conditions, indicating a star-star coupling reaction during the polymerization.

Using the same reaction conditions that applied to the polymerization of VDPM with the initiator (calix 1), the hexafunctional initiator calix 2 was used to polymerize this monomer. Going from 1 to 8 hours of reaction time and monomer conversions from 18 to 84 %, the calculated Mn (NMR) values go from 25.2 to 114.1 x 10^3 g/mol, correspondingly. However, Mn (SEC) values increase from 5.3 to 19.3 x 10^3 g/mol. Hence, we found that the rate of the polymerization is slow compared to the polymerization based on Calix 1, and it takes longer time (≥ 8h) to achieve a monomer conversion around 84%. SEC technique calibrated by PMMA standards has been used to estimate the average of molar masses and dispersity of analyzed star polymers using a conventional calibration method. Because of the compact nature of branched macromolecules, this method underestimates their molar masses, and thus only gives apparent values [3].

On the other hand, it can be seen from Figure SI 10 that the experimental dispersity values of PMMA standards are much higher than theoretical. The theoritical dispersity ($Đ_{theo}$) values (commercial data given by "Polymer Laboratories") were between 1.01 and 1.16, while, the experminetal results (obtained by SEC) were between 1.28 and 4.24 for a range of molar masses at peak (M_{peak}) of PMMA standards between 1.14-141.5 x 10^3 g/mol. This means that the accuracy of the experimental dispersity values for the whole sample is low and depends on molar masses. Which required the correction of the dispersity values of polymers given by SEC. The error in dispersity value for each polymer (M_{peak}) has been calculated by using the equations of both theoritical and experimental PMMA lines as shown in Figure SI 10. Hence, the error values on dispersity for each sample at M_{peak} have been applied to correct the obtained value by SEC for star polymers.

The experimental and corrected dispersity values of calix 1-PVDPM and calix 2-PVDPM star polymers are given in Table 6 and Table 7, respectively.

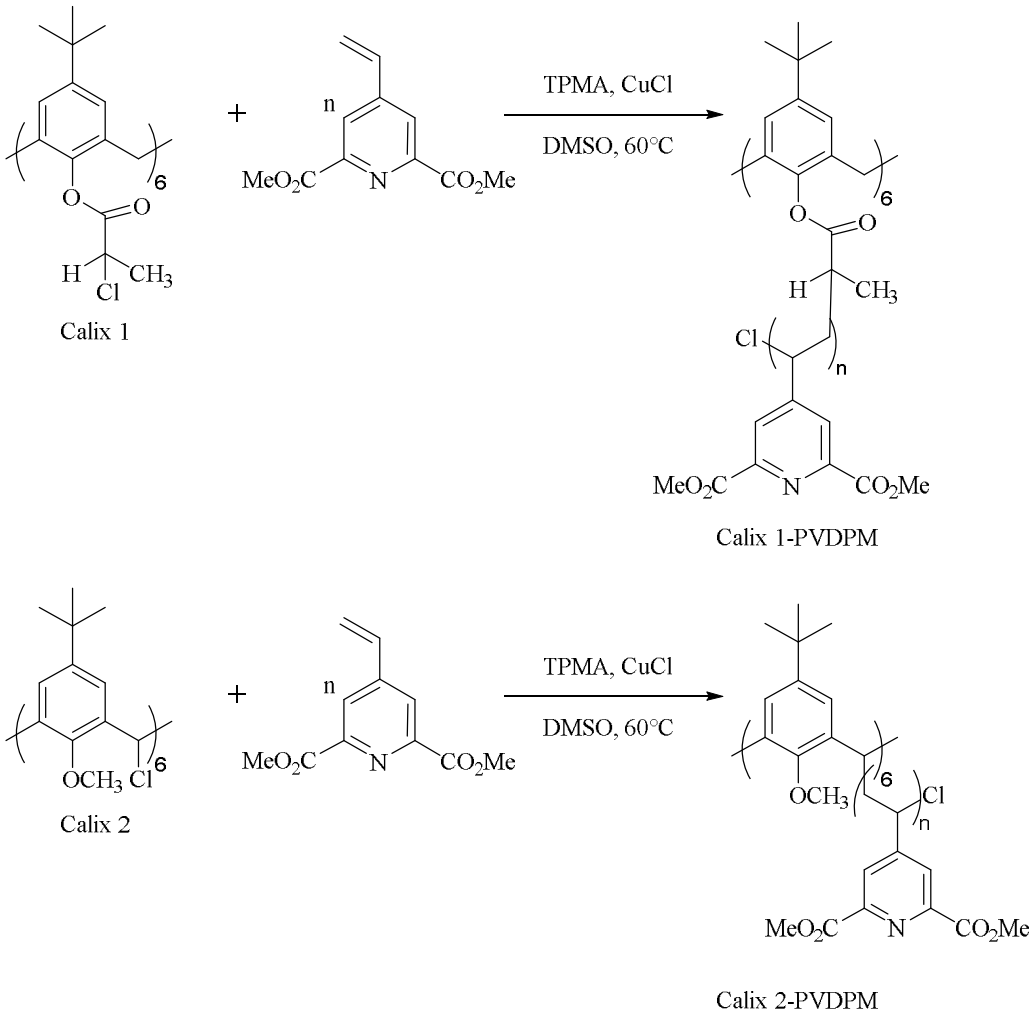

Scheme 14. ATRP synthetic routes of well-defined PVDPM stars by using calix 1 and calix 2

Table 6. ATRP of VDPM at 60 °C with the hexafunctional initiator (calix 1), [M]/[calix 1]= 600

Time (min)	Conversion %	M_n(NMR)[a] 10^3 g/mol	M_n(SEC)[b] 10^3 g/mol	Đ[c]	Đ[d]
10	19	26.7	16.6	6.04	2.73
30	37	50.6	23.3	5.42	2.61
90	65	87.8	23.7	6.30	2.62
120	73	98.4	30.7	3.89	1.68

[a] Determined by ^{1}H NMR in $CDCl_3$. [b] Determined by SEC (DMF as eluent, RI detector). [c] Dispersity (Đ = Mw/Mn) obtained by conventional SEC.[d] Corrected dispersity using the PMMA calibration curve.

Table 7. ATRP of VDPM at 60 °C with hexafunctional initiator (calix 2), [M]/[calix2]

Time (h)	Conversion %	M_n(NMR)[a] 10^3 g/mol	M_n(SEC)[b] 10^3 g/mol	Đ[c]	Đ[d]
1	18	25.2	5.3	2.96	2.13
1.5	27	37.0	6.5	2.96	2.10
6	60	80.9	18.3	2.30	1.38
8	84	114.1	19.6	2.77	1.80

[a] Determined by ^{1}H NMR in $CDCl_3$. [b] Determined by SEC (DMF as eluent, RI detector). [c] Dispersity (Đ = Mw/Mn) obtained by conventional SEC.[d] Corrected dispersity using the PMMA calibration curve.

Figure 24 illustrates the plot of Mn (x 10^3 g/mol) versus conversion (%) for calix 1-PVDPM and calix 2-PVDPM polymers. The polymerization furnished a linear increase in molar masses of star polymers in the function of conversion. The linear for different conversion ratios, indicating that the concentration of the growing radicals stays constant during the polymerization.

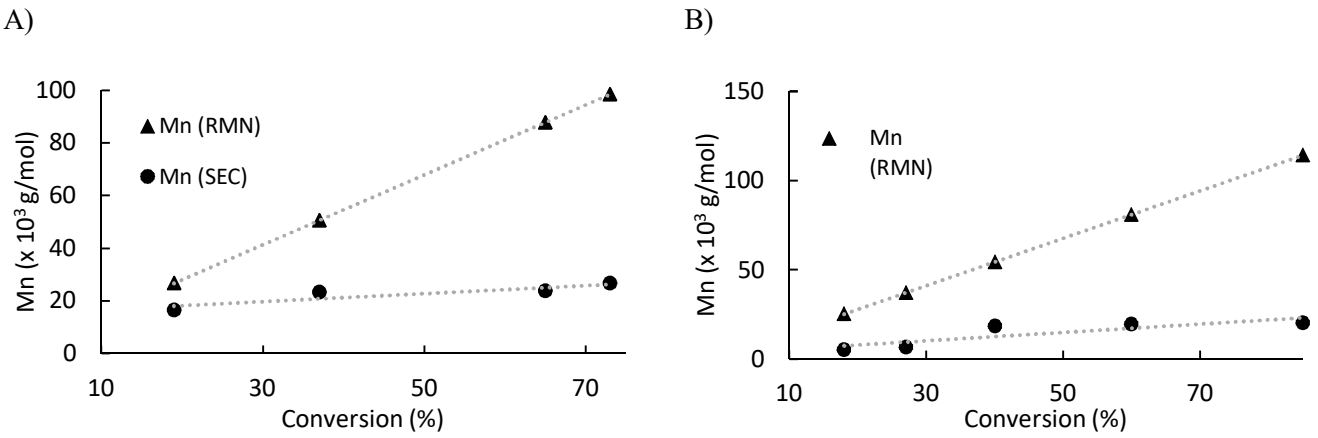

Figure 24. Evolution of molar masses with monomer conversion obtained by SEC and NMR for A) calix 1-PVDPM and B) calix 2-PVDPM star polymers.

SEC profiles at different conversions (Figure 25) indicate that for both hexafunctional, calix 1 and calix 2, polymer systems exhibit the appearance of a shoulder in the high molar mass side of the SEC traces of the stars, which can be attributed to the irreversible coupling of the growing radicals between different stars.

The appearance of an unsymmetrical SEC chromatograms of stars polymers (Figure 25) and the deviation of Mn values around 37% monomer conversion in the case of calix 2-PVDPM (Figure 25A) can be explained by both inter- and intramolecular termination of the growing radicals which is possible in the case of star polymers. Intermolecular termination reactions between two different arms of stars result in an increase of the molar mass. As an example, the coupling reactions between two stars polymers would be constituted of 10 arms instead of 6.

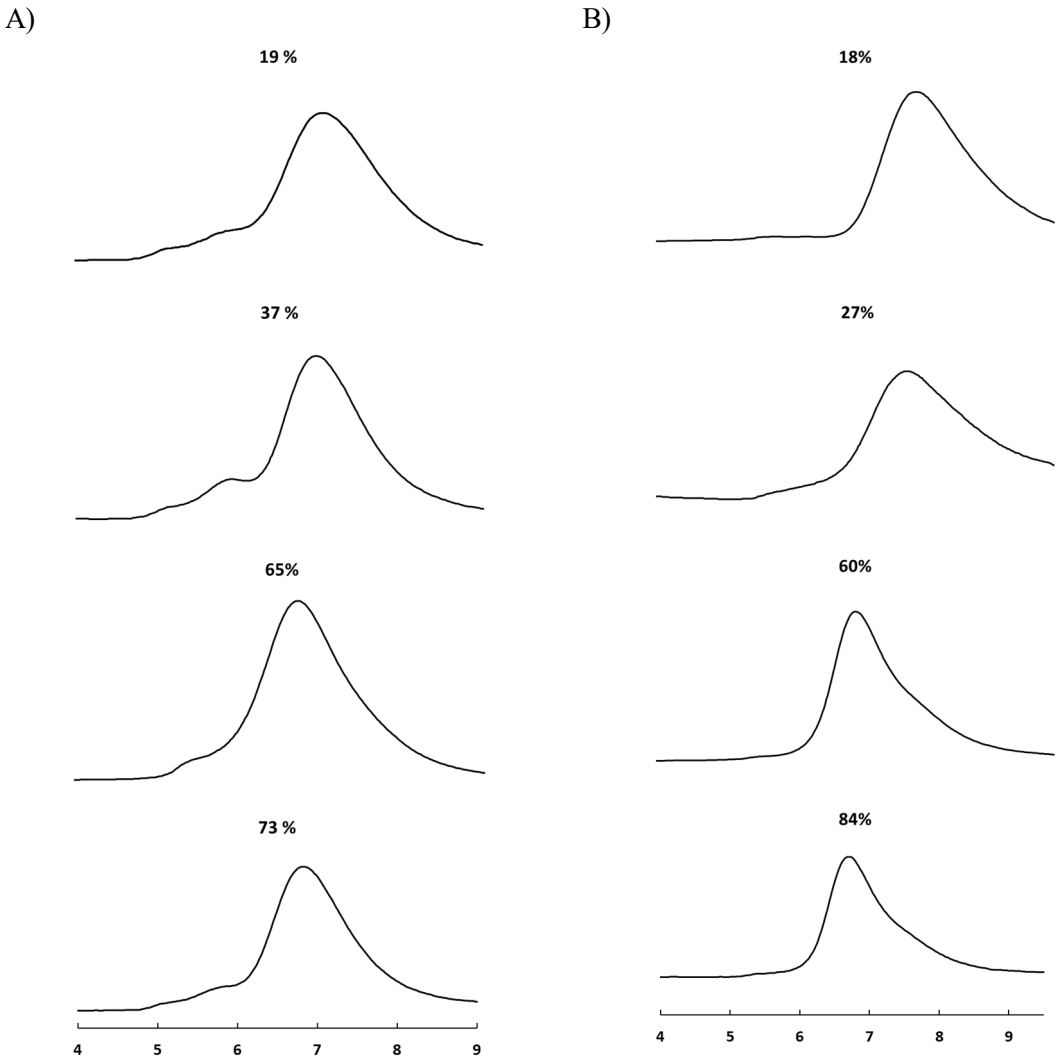

Figure 25. SEC traces (RI detector) of A) calix 1-PVDPM and B) calix 2-PVDPM stars obtained at different conversions.

As shown in Figure 26 the plot of -ln (1-p) versus time is linear for [M]/[calix] ratio equal to 600, indicating a first-order apparent propagation rate constant in the monomer concentration which means the conservation of radicals throughout the reaction.

In a typical transition metal catalysed ATRP the polymerization rate, R_p, can be expressed as shown in eq 1 where k_p is the propagation rate constant, K the equilibrium constant of exchange between active and dormant species and [M], [I], [Mt^nX] and [$Mt^{n+1}X_2$] are the concentrations of monomer, initiator, activator, and deactivator, respectively [30]. As eq 1 shows, the rate has a first-order dependence on both monomer and initiator concentrations.

$$R_p = k_p K[M][I]_o [Mt^n X]/ [Mt^{n+1} X_2] \qquad \text{eq 1}$$

The expression for multifunctional initiators must be modified to account for the number of alkyl halide moieties on each initiating molecule. Eq 2 provides a more general form of the rate expression in which the initiator concentration is multiplied by the number of alkyl halide species per molecule, f.

$$R_p = k_p K f[M][I]_o [Mt^n X]/ [Mt^{n+1} X_2] \qquad \text{eq 2}$$

The success of ATRP depends largely on an appropriate equilibrium between the activation process (k_{act}), generation of radicals due to the detachment of the halogen from R-X, and the deactivation process (k_{deact}) resulting to the formation of alkyl halides. The product of k_p and the equilibrium constant ($K = k_{act}/k_{deact}$) essentially determines the polymerization rate.

The modification in structure of initiator induces enormous change in the rate of ATRP polymerization. Indeed, it defines the nature of radical formed during initiation, which subsequently alter the activation constant, hence, kinetic equilibrium of polymerization. The k_{act} for tertiary, secondary, and primary alkyl halides follows the order of substitution: $3° > 2° > 1°$ which mean tertiary carbon halides are better initiators than secondary ones, which are better than primary carbon halides. In our case, both calix 1 and calix 2 will generate secondary radical. So, in order to investigate the effects that may have played in the increase in the initiation rate of calix 1 compared to calix 2, two main hypotheses are drawn.

First, the effect of initiator chloride position can influence the stabilization of the generated radical. To this aim, it seems interesting to compare the ATRP activation rate constants for various secondary chlorides initiators. Tang and Matyjaszewski found that the secondary benzyl, ester, chloro derivatives follow the relative order 1:1.5. It is worth mentioning that, the k_{act} value for methyl 2-chloropropanoate (MICP) (secondary radical stabilized by a chloroester function) equal to 0.015 M^{-1} s^{-1} 1.5 times higher than value for (1-chloroethyl)benzene (PECl) (secondary radical stabilized by benzyl-substituted chloride function) 0.01 M^{-1} s^{-1} [29]. ATRP will occur fast if the equilibrium constant is high. This is qualitative agreement with the kinetics obtained using calix 1 and calix 2.

On the other hand, it is possible that for systems shapes special effects may affect the reaction kinetic. For example, the observed dependence of the initiator efficiency on propagation rate is probably related to steric hindrances that are due to the spatial proximity of a macrocycle and an active centre [31]. Strandman *et al.* observed a similar effect, with a macrocyclic fragment that affect the efficiency of initiation [32] during the ATRP synthesis of star-shaped polymers based on based on resorcinarene octa-2-bromo-2-methylpropanoate. Moreover, if the initiating groups do not start the polymerization simultaneously and the initiator itself is rigid or sterically hindered, the probability of the unreacted functional groups starting the polymerization probably decreases as the polymerization proceeds. The proximity of the initiating sites also increases the probability of premature termination.

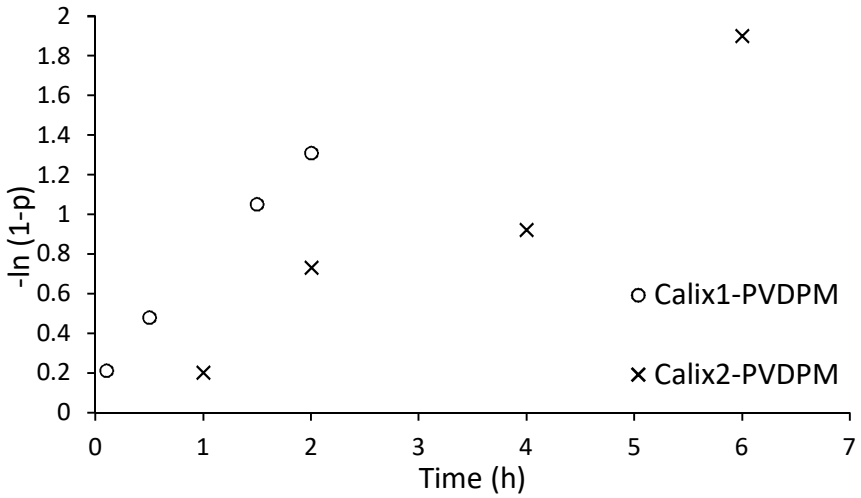

Figure 26. First-order kinetic plot polymerizations of VDPM using calix 1 (○) and calix 2 (×) as initiator at 60 °C.

A)

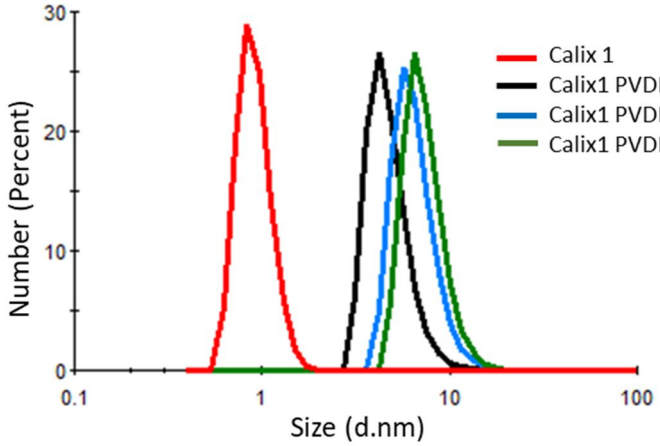

B)

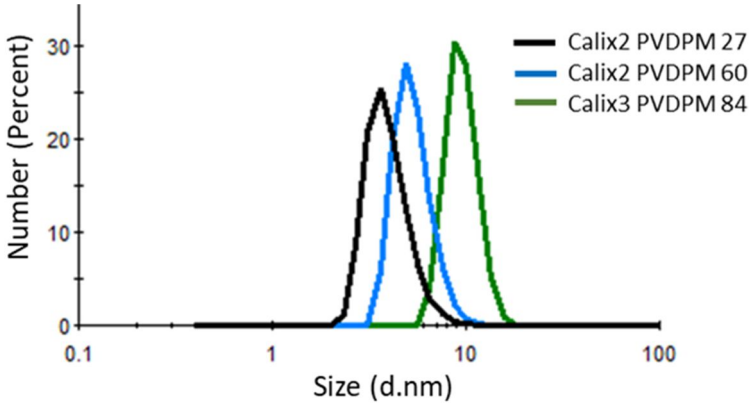

Figure 27. Evolution of the Number-average of hydrodynamic diameter (D_h) as a function of the molar mass for A) calix1 PVDPM and B) calix2 PVDPM in DMF (conc = 1 g/ L).

Next, DLS measurements were carried out to characterize the solutions of calix 1 PVDPM at different monomer conversion. The DLS curves are shown in Figure 27. The hydrodynamic diameter of our polymer-like star were determined at 20 °C using DMF as a solvent. The D_h of the calix 1-PVDPM polymers increased as a result of molar masses as shown in Figure 27A. The D_h of calix 1 before the polymerization was 0.9 nm. The particle dimension increases to 5 nm when the monomer conversion equal to 37 %. For the other star polymers D_h were 6.5 and 7.0 nm for VDPM conversion equal to 65 % and 73 % respectively. Hence, the D_h increases gradually due to the increase in arm chain and coupling reaction between arms chains. The chain extension, which means the degree of chain expansion, is estimated from the D_h and the contour length of the PVDPM unit. Figure 27 B shows the D_h of calix 2-PVDPM polymers at different VDPM conversion.

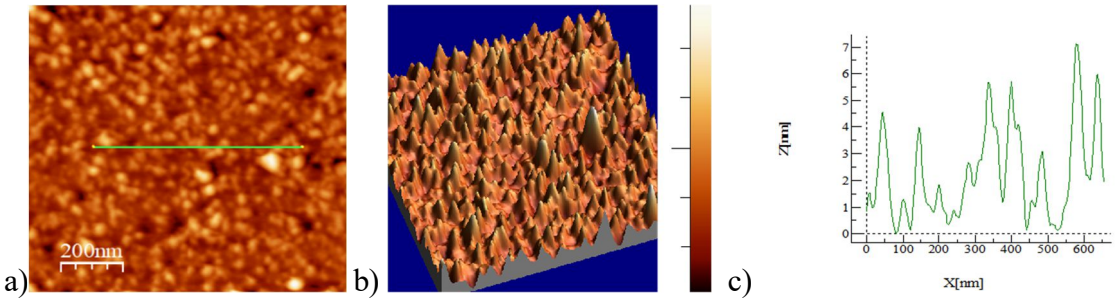

Figure 28. a) AFM topography image, b) 3D reconstruction and c) the profile is heights profile for the coloured line in AFM images) roughness spectrum of calix 1-PVDPM73 on graphene

Figure 28 shows the topography and 3D AFM images obtained for calix 1-PVDPM73. A measured root-mean-square (RMS) roughness of 0.18 nm/µm^2 was observed for bare graphene (Figure SI 11 a). After deposit of calix 1-PVDPM73 in DMF (0.46 g/L) and evaporation of the solvent for 24 h (Figure 28a), RMS roughness increases to 2.19 nm/µm^2. This increase in roughness can be attributed to the formation of a slight layer of polymer built on graphene. (Figure 28b) shows the 3D reconstruction of the polymer layer, this observation proves that smooth, uniform and homogenous surface was obtained after recovering the surface by PVDPM-star polymer. Furthermore, (Figure 28c) shows an average particle diameter of calix 1-PVDPM73 of 4-7 nm, in total agreement with DLS

analysis of calix 1-PVDPM73 in DMF (Figure 27) that have showed the formation of particles with average hydrodynamic diameter of 7 nm.

Figure SI 11 shows the topography and 3D AFM images obtained for calix 1-PVDPM73 at different concentration (0.23 g/L).

Conclusion

Star-shaped polymers with a central calixarene derivatives core and PVDPM arms are synthesized with the use of Atom Transfer Radical Polymerization (ATRP). Two calix[6]arene derivatives were synthesized and characterized. The high activity of the synthesized initiators (calix 1 and calix 2) can be attributed to both carboxy groups (chloroester) and benzyl (calixarene ring), respectively, which contribute to the stabilization of the generated radical. Because initiator's structure is one of the parameters affecting kinetics of ATRP, hence, we studied the structure-activity relationship for the polymerization systems. The polymerization rates exhibited first-order kinetics with respect to the monomer in both cases. SEC, NMR, DLS and AFM were used to characterized the obtained polymers.

References

[1] A. Amirova *et al.*, "Synthesis, Characterization, and Investigation of Thermosensitive Star-Shaped Poly(2-isopropyl-2-oxazolines) Based on Carbosilane Dendrimers," *Macromolecular Chemistry and Physics*, vol. 218, no. 4, Feb. 2017, doi: 10.1002/macp.201600387.

[2] Z. Guan, "Control of Polymer Topology through Transition-Metal Catalysis: Synthesis of Hyperbranched Polymers by Cobalt-Mediated Free Radical Polymerization," 2002, doi: 10.1021/ja025609.

[3] S. Angot, K. S. Murthy, D. Taton, and Y. Gnanou, "Atom transfer radical polymerization of styrene using a novel octafunctional initiator: Synthesis of well-defined polystyrene stars," *Macromolecules*, vol. 31, no. 21, pp. 7218–7225, Oct. 1998, doi: 10.1021/ma980712y.

[4] K. Matyjaszewski, "The synthesis of functional star copolymers as an illustration of the importance of controlling polymer structures in the design of new materials," *Polymer International*, vol. 52, no. 10, pp. 1559–1565, 2003, doi: 10.1002/pi.1339.

[5] J. Roovers, L.-L. Zhouj, P. M. Toporowski, M. van der Zwan, and N. Hadjichristidisi, "Regular Star Polymers with 64 and 128 Arms. Models for Polymeric Micelles?," 1993.

[6] M. Morton, T. E. Helminiak, S. D. Gadkary, and F. Bueche, "Preparation and Properties of Monodisperse Branched Polystyrene," 1962.

[7] K. Matyjaszewski and S. G. Gaynor, "Preparation of Hyperbranched Polyacrylates by Atom Transfer Radical Polymerization. 3. Effect of Reaction Conditions on the Self-Condensing Vinyl Polymerization of 2-((2-Bromopropionyl)oxy)ethyl Acrylate," 1997.

[8] D. Gutsche, "Calixarenes," *Acc. Chem. Res.*, vol. 16, no. 161, 1983.

[9] Y. Zhang, R. A. Agbaria, and I. M. Warner, "Complexation studies of water-soluble calixarenes and auramine O dye," *Supramolecular Chemistry*, vol. 8, no. 4, pp. 309–318, 1997, doi: 10.1080/10610279708034950.

[10] M. P. Kurlykin, A. E. Bursian, M. M. Dudkina, and A. v. Ten'kovtsev, "Synthesis of Star-Shaped Polymers Based on 2-ALKYL-2-Oxazoline with a Calix[8]Arene Central Core and the Study of Their Heat-Sensitive Properties," *Fibre Chemistry*, vol. 47, no. 4, pp. 291–297, Nov. 2015, doi: 10.1007/s10692-016-9681-x.

[11] D. S. Guo, K. Wang, Y. X. Wang, and Y. Liu, "Cholinesterase-responsive supramolecular vesicle," *J Am Chem Soc*, vol. 134, no. 24, pp. 10244–10250, Jun. 2012, doi: 10.1021/ja303280r.

[12] A. M. Shumatbaeva *et al.*, "The pH-responsive calix[4]resorcinarene-mPEG conjugates bearing acylhydrazone bonds: Synthesis and study of the potential as supramolecular drug delivery systems," *Colloids and Surfaces A: Physicochemical and Engineering Aspects*, vol. 589, Feb. 2020, doi: 10.1016/j.colsurfa.2020.124453.

[13] T. C. Gokoglan *et al.*, “A novel architecture based on a conducting polymer and calixarene derivative: Its synthesis and biosensor construction,” *RSC Advances*, vol. 5, no. 45, pp. 35940–35947, 2015, doi: 10.1039/c5ra03933a.

[14] S. Abubakar, T. Skorjanc, D. Shetty, and A. Trabolsi, “Porous Polycalix[n]arenes as Environmental Pollutant Removers,” *ACS Applied Materials and Interfaces*, vol. 13, no. 13, pp. 14802–14815, Apr. 2021, doi: 10.1021/acsami.0c23074.

[15] A. R. Hajipour, S. Habibi, and A. E. Ruoho, “Modification of poly acrylic acid using calix[4]arene derivative for the adsorption of toxic heavy metals,” *Journal of Applied Polymer Science*, vol. 118, no. 2, pp. 818–826, Oct. 2010, doi: 10.1002/app.32246.

[16] K. Matyjaszewski, P. J. Miller, J. Pyun, G. Kickelbick, and S. Diamanti, “Synthesis and characterization of star polymers with varying arm number, length, and composition from organic and hybrid inorganic/ organic multifunctional initiators,” *Macromolecules*, vol. 32, no. 20, pp. 6526–6535, Oct. 1999, doi: 10.1021/ma9904823.

[17] B. Lepoittevin, R. Matmour, R. Francis, D. Taton, and Y. Gnanou, “Synthesis of dendrimer-like polystyrene by atom transfer radical polymerization and investigation of their viscosity behavior,” *Macromolecules*, vol. 38, no. 8, pp. 3120–3128, Apr. 2005, doi: 10.1021/ma048106s.

[18] J.-S. Wang and K. Matyjaszewski, “Controlled"Living" Radical Polymerization. Atom Transfer Radical Polymerization in the Presence of Transition-Metal Complexes,” 1995.

[19] J. Qiu and K. Matyjaszewski, “Polymerization of Substituted Styrenes by Atom Transfer Radical Polymerization,” 1997.

[20] M. Kato, M. Kamigaito, M. Sawamoto, and T. Higashimuras, “Polymerization of Methyl Methacrylate with the Carbon TetrachlorideIDichlorotris-(triphenylphosphine)ruthedum(II)/ Methylaluminum Bis(2,6-di-tert-butylphenoxide) Initiating System: Possibility of Living Radical Polymerization1,” 1996.

[21] K. A. Davis, H. J. Paik, and K. Matyjaszewski, “Kinetic investigation of the atom transfer radical polymerization of methyl acrylate,” *Macromolecules*, vol. 32, no. 6, pp. 1767–1776, Mar. 1999, doi: 10.1021/ma9815051.

[22] D. Taton, E. Cloutet, and Y. Gnanou, “Novel amphiphilic branched copolymers based on polystyrene and poly(ethy1ene oxide),” 1998.

[23] H.-Q. Xie and D. Xie, “Molecular design, synthesis and properties of block and graft copolymers containing polyoxyethylene segments.”

[24] M. Gauthier, L. Tichagwa, J. S. Downey, and S. Gao, “Arborescent Graft Copolymers: Highly Branched Macromolecules with a Core-Shell Morphology,” 1996.

[25] N. Ide and T. Fukuda, “Nitroxide-Controlled Free-Radical Copolymerization of Vinyl and Divinyl Monomers. Evaluation of Pendant-Vinyl Reactivity,” 1997.

[26] W. Tang and K. Matyjaszewski, “Effect of ligand structure on activation rate constants in ATRP,” *Macromolecules*, vol. 39, no. 15, pp. 4953–4959, Jul. 2006, doi: 10.1021/ma0609634.

[27] N. Bortolamei, A. A. Isse, A. J. D. Magenau, A. Gennaro, and K. Matyjaszewski, “Controlled aqueous atom transfer radical polymerization with electrochemical generation of the active catalyst,” *Angewandte Chemie - International Edition*, vol. 50, no. 48, pp. 11391–11394, Nov. 2011, doi: 10.1002/anie.201105317.

[28] K. Matyjaszewski, K. Davis, T. E. Patten, and M. Wei, “Observation and Analysis of a Slow Termination Process in the Atom Transfer Radical Polymerization of Styrene,” 1997.

[29] W. Tang and K. Matyjaszewski, “Effects of initiator structure on activation rate constants in ATRP,” *Macromolecules*, vol. 40, no. 6, pp. 1858–1863, Mar. 2007, doi: 10.1021/ma062897b.

[30] K. Matyjaszewski, T. E. Patten, and J. Xia, “Controlled/"Living" Radical Polymerization. Kinetics of the Homogeneous Atom Transfer Radical Polymerization of Styrene,” 1997.

[31] A. Heise, S. Diamanti, J. L. Hedrick, C. W. Frank, and R. D. Miller, “Investigation of the initiation behavior of a dendritic 12-arm initiator in atom transfer radical polymerization,” *Macromolecules*, vol. 34, no. 11, pp. 3798–3801, May 2001, doi: 10.1021/ma001508p.

[32] S. Strandman, M. Luostarinen, S. Niemelä, K. Rissanen, and H. Tenhu, “Resorcinarene-based ATRP initiators for star polymers,” *Journal of Polymer Science, Part A: Polymer Chemistry*, vol. 42, no. 17, pp. 4189–4201, Sep. 2004, doi: 10.1002/pola.20257.

Supporting information

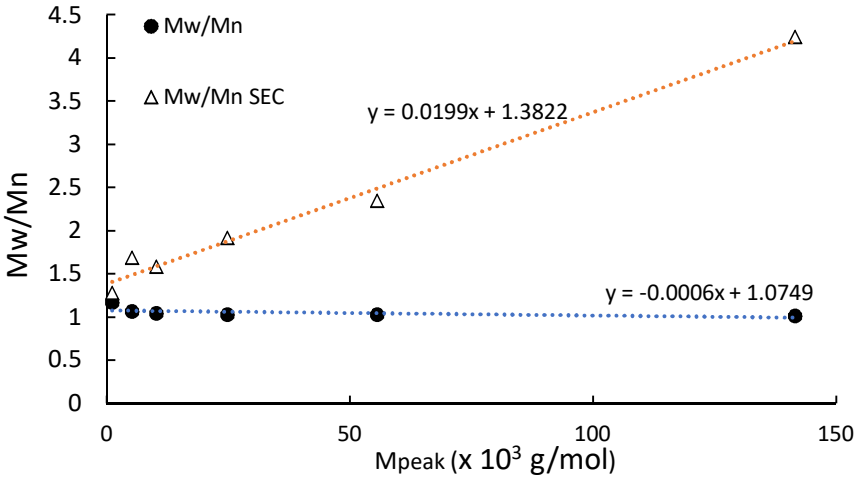

Figure SI 10. Comparaison of the theoritical (●) and experimental (Δ) dispersity of PMMA versus molar masses.

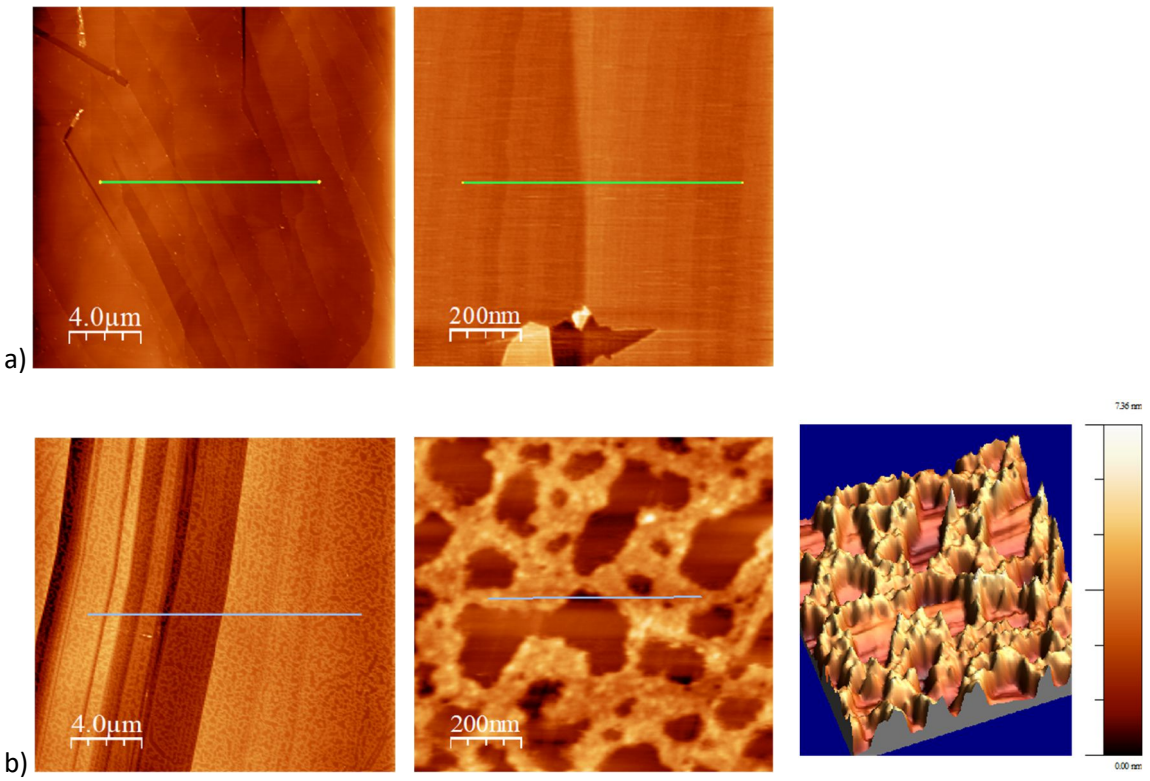

Figure SI 11. a) AFM topography images of clean graphene b) AFM topography of calix 1-PVDPM73 (conc = 0.23 g/ L)(left-middle) and 3D reconstruction (right).

Part II. Star polymers-europium complexation

As mentioned previously in **part I** of this chapter, the carboxylate form of VDPA is known for his strongly chelating capacity to a lot of metals including lanthanides and uranium. After the star polymers preparation, using calix 1 as initiator (calix1-PVDPA), it was important to evaluate their performance (Scheme 15) as a europium scavenger in an aqueous environment.

The complexation of star polymer (calix-PVDPA) with europium has been studied in this dissertation to investigate its capacity in aqueous media decontamination, whose results are presented and discussed in the current part of this chapter.

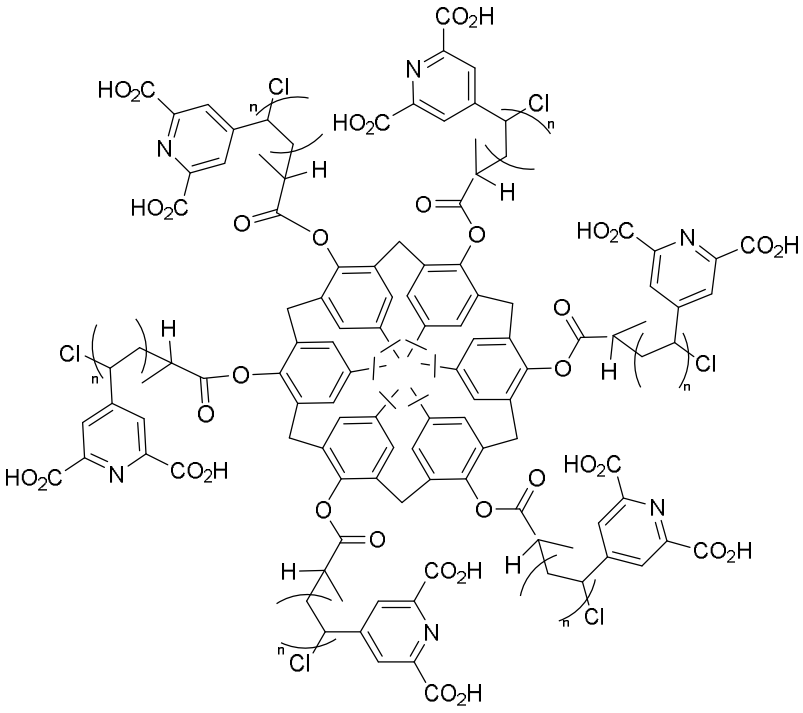

Scheme 15. Calix 1-PVDPA

Depending on pH, dipicolinic acid (DPA) assumes various forms. In the ionic form, DPA is soluble in aqueous solution at a pH above the pKa value 2.22 [1]. However, the first step was the hydrolysis of calix1-PVDPM to get the water-soluble calix1-PVDPA. Polymers were treated in a NaOH (1 M) solution at room temperature and then concentrated HCl was added to precipitate PVDPA, which was isolated by filtration. Scheme 16 Shows the hydrolysis reaction of calix-PVDPM.

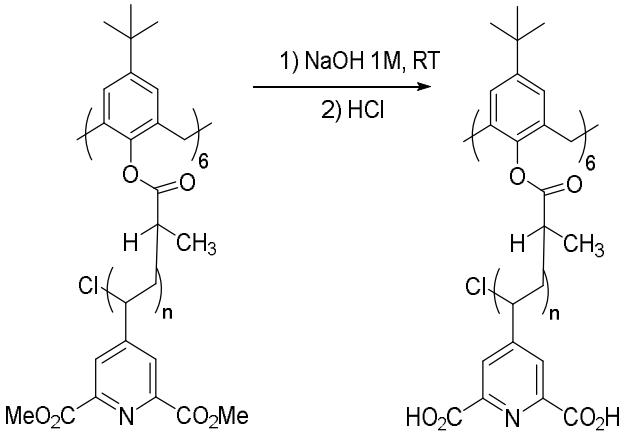

Scheme 16. Calix-PVDPM hydrolysis to calix-PVDPA

Star polymer with lanthanides

In the aim to evaluate the ability of complexation of this polymer with lanthanides, star-polymers have been place with europium (III). The first indication of a spontaneous interaction between calix-PVDPA and europium was observed upon mixing polymer (0.2 mM) (around 2 equivalents of PVDPA) with europium (III) nitrate solution (1.5 mM) (1 equivalent) at room temperature and pH ~ 5.5. Within seconds, a white precipitate was observed, when Eu (III) nitrate solution is added on polymer solution. Under a UV lamp (254 nm) the red fluorescence is seemingly in the solid precipitate as shown in Figure 29. This aggregation is probably due to the formation of complexes with carboxylate groups of PVDPA and europium.

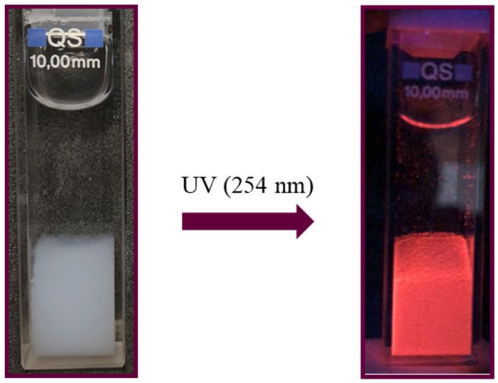

Figure 29. Calix -PVDPA – Eu(III) precipitation from aqueous mixture before (left) and after (right) UV excitation (λ = 254 nm)

In order to investigate the chemical change of polymer before and after the complexation, ATR analyses were performed on both pure polymer and the precipitate.

FTIR analysis

ATR FTIR has been used to rapidly validate chemical environment in polymers before and after the addition of europium. Figure 30 shows clear and broad bands in the range of 3000 - 3600 cm^{-1} can be assigned to the characteristic peaks of O-H stretching vibrations from the water molecules. The bands at 1724, 1240, and 1599 cm^{-1} were related to C=O, C-O and pyridinic C=N stretching vibrations of calix-PVDPA before the complexation. It is seen from this figure (blue spectrum) that after complexation those bands were replaced by bands at 1600 cm^{-1} which correspond to COO^- asymmetrical stretching and a broad band around 1408 cm^{-1} related to COO^- symmetrical stretching proving that carboxylate groups of calix-PVDPA matched the europium ions through these group functions. The separation ($\Delta\nu$) between ν_{as} COO^- and ν_s COO^- can be used to explain the coordination types of carboxyl group in ligand. Therefore the $\Delta\nu$ value of calix-PVDPA-Eu (III) complex is 192 cm^{-1}, smaller than those observed in the spectrum of the free ligand, which implies the presence of bidentate, chelating carboxylate group [2].

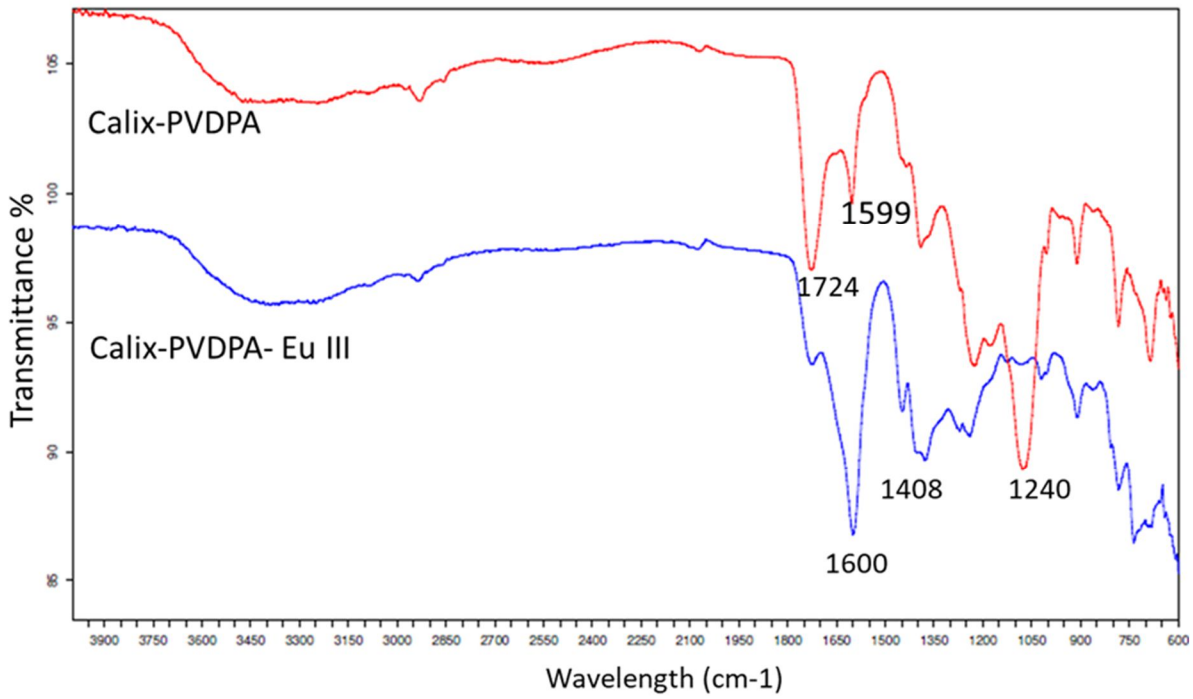

Figure 30. ATR FTIR spectra of calix-PVDPA before (red), and after (blue) complexation

Further characterizations were performed in the next sections in order to confirm the interaction between calix-PVDPA and Eu (III) in water.

Fluorescence spectroscopy: europium environment change

To confirm that the interaction between polymer and lanthanides had been accomplished as intended, fluorescence spectroscopy analysis was conducted. The fluorescence of the europium was measured to help understanding the change in its environment. After laser excitation, Eu(III) exhibits radiative relaxation (fluorescence) emitting light in the visible spectrum. The energy diagram of europium contains features of electronic transition from the lowest excited state, $^5D_0$, to multiple ground states: $^7F_1$, $^7F_2$ and $^7F_4$ as shown in Figure 31. The intensity, splitting and energy of the luminescence bands as well as the relative intensities of the different bands are very sensitive to the symmetry and the detailed nature of the ligand environment [3]. Prior to the test, two different samples of europium solution were prepared, pure europium solution and polymer-europium solution.

The luminescence spectra of Eu(III) solution (1.5 mM) before and after adding 2 equivalents of calix-PVDPA are shown in Figure 31 (right).

The luminescence spectrum is dominated by the $^5D_0 \rightarrow {}^7F_1$ transition at 591 nm, and the $^5D_0 \rightarrow {}^7F_2$ transition at 615 nm is relatively weak for a free Eu^{3+} ion in aqueous solution. On the contrary, the $^5D_0 \rightarrow {}^7F_2$ transition is more intense than the $^5D_0 \rightarrow {}^7F_1$ transition in the Eu^{3+}/ calix-PVDPA solution. This change in intensity could be due to the formation of a Eu(III) complex in solution with calix-PVDPA, which would break the europium ion's symmetry.

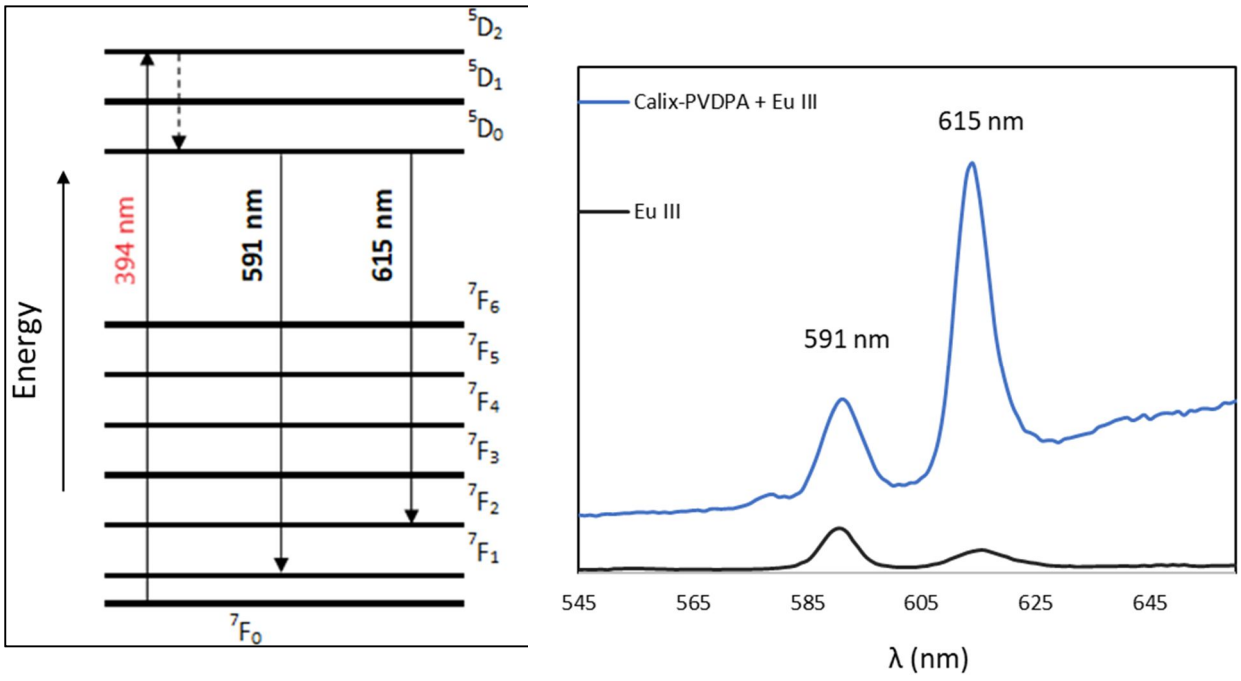

Figure 31. (left) Energy diagram of Eu(III). (right) Emission spectra of Eu(III) solution before (black) and after adding 2 equivalents of calix-PVDPA (blue)

UV-Vis spectroscopy: Influence of complexation on PVDPA band

One of the main goals of this study is to determine the stoichiometry ratio of the complexation between PVDPA function groups and Eu(III). To this aim, the change of absorption of polymer using UV-Vis spectroscopy is evaluated. In a preliminary study, UV-Vis showed that europium solutions don't have useable absorption peaks in the available wavelength range of 200-800 nm. On the other hand, UV absorption spectrum of a calix-PVDPA solution in water has an absorption broad band at around 272 nm. In order to quantify the amount of carboxylate groups that complexes europium, a titration was performed by adding different volume of europium solution (1.5 mM) to calix-PVDPA solutions of a known initial concentration of 0.2 mM. The solutions were then filtrated, and the absorption spectra registered as shown in Figure 32.

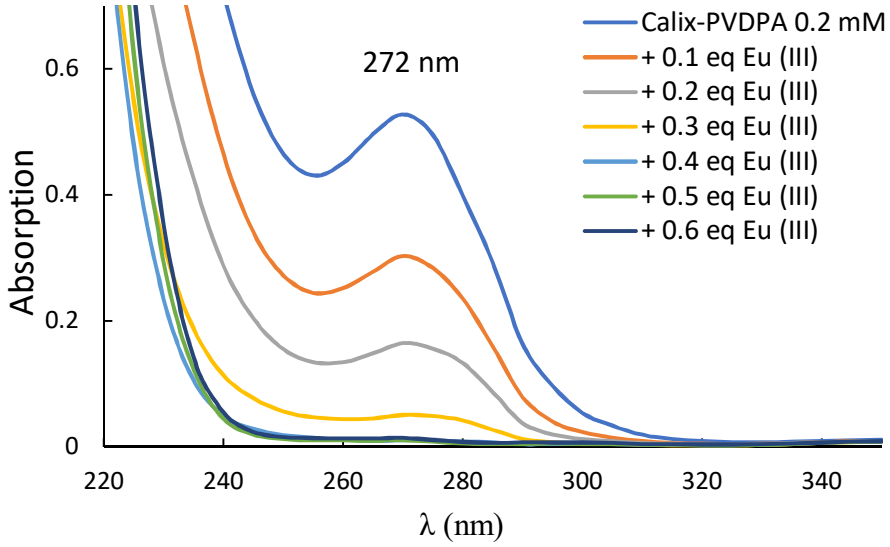

Figure 32. UV absorption spectra of calix-PVDPA interaction with Eu (III)

As presented above the calix-PVDPA absorption spectrum went down when europium was added in increasing ratios, proving again that the precipitate is most probably a strong interaction between polymer and europium. Further measurement was then repeated while looking closely at the PVDPA absorption intensity at 272 nm and with more intermediate steps of added Eu (III).

The absorption analysis points to the complete disappearance of calix-PVDPA peak, corresponds to a stoichiometry ratio of 0.5. The results are shown in Figure 33.

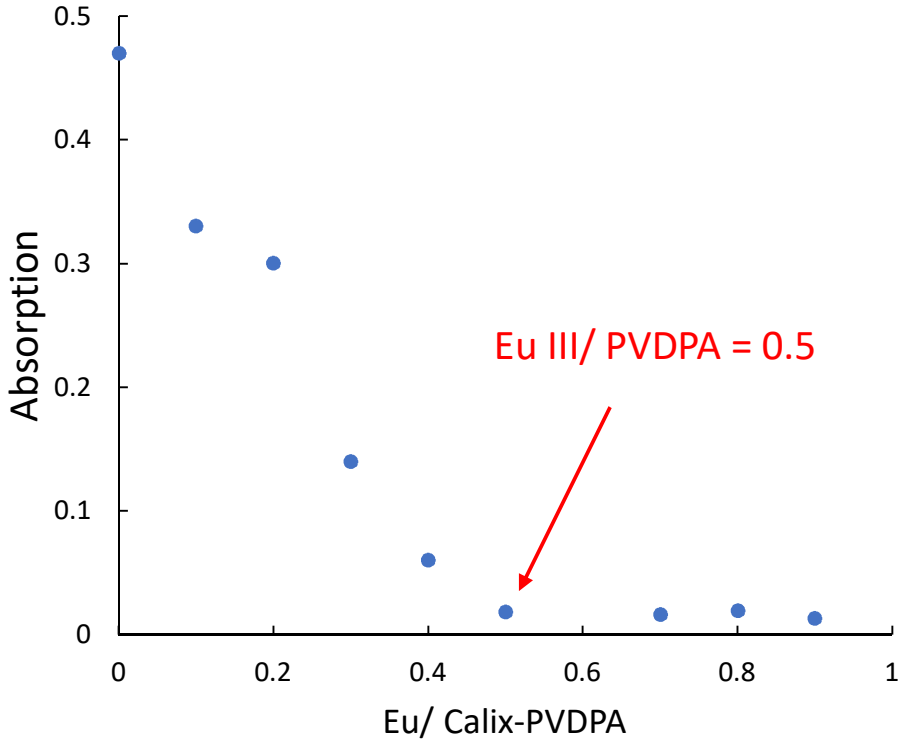

Figure 33. Absorption at 272 nm at variable Eu (III) / calix-PVDPA ratios

ITC: thermodynamic properties of star polymers

Isothermal Titration Calorimetry (ITC) is one of the best methods used to determine the thermodynamic parameters of interactions in solution [4]. It is most often used to study the binding of small molecules (such as medicinal compounds) to larger macromolecules (proteins, DNA etc.) [5]. It is based on the concept that heat can be either absorbed or generated during the process. At constant temperature, a solution containing a metal is added to a cell containing a solution of the ligand (polymer). The interaction between the two partners then results in heat release [4].

The binding of europium (III) to star polymer (calix-PVDPA) was studied using ITC. When metal cations were added into the polymer solution, a heat exchange was found during this experiment. The heat flow peak after each injection of 10 µL of 1.5 mM solution of europium nitrate on calix-PVDPA polymer at 0.6 mM at 25 °C (pH ~ 5.5) is shown in Figure 34. The area underneath each injection peak, equal to the total heat released for that injection is shown in Figure 34 (up). It shows that interaction of calix-PVDPA with europium is an exothermic reaction. Figure 34 (down) shows a typical example of curve fitting which was obtained after integration of heat signals.

This experiment enables the determination of the enthalpy of association (ΔH) and the binding constant (K). Consequently, the ΔH and K of interaction between calix-PVDPA and europium were determined from ITC measurements and were around -8000 ± 800 cal/mol and 5000 ± 1700 L/mol, respectively.

As for fluorescence and UV-Vis titrations, this result proved a strong interaction between calix-PVDPA polymer and europium. In the light of these results, the molar ratio of interaction between PVDPA function groups and europium could be estimate in the range of $0.5 \leq N \leq 0.65$.

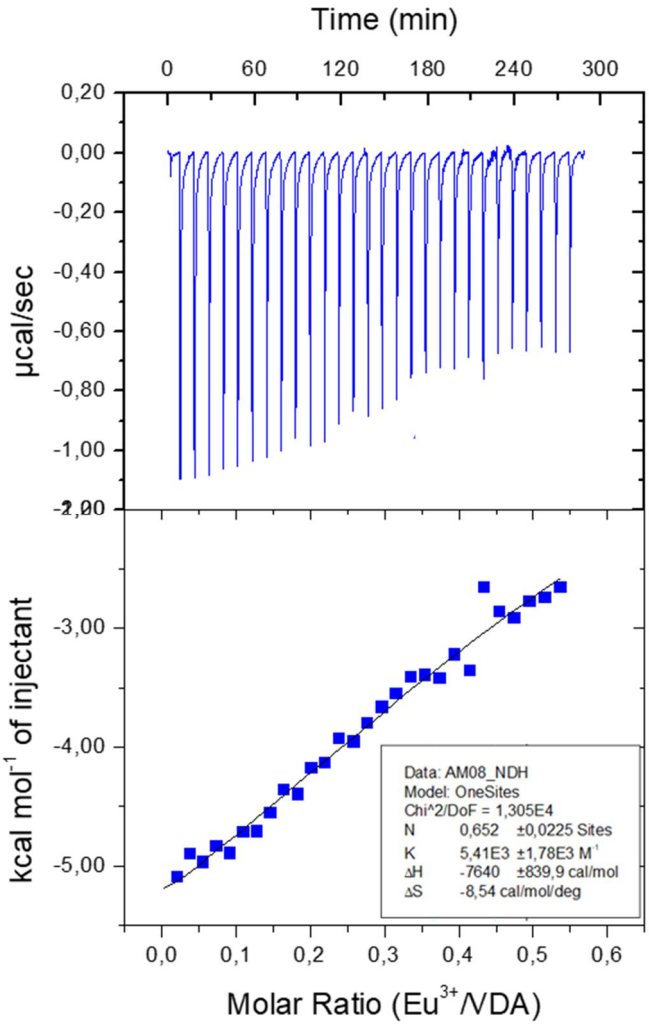

Figure 34. Microcalorimetric titration of calix-PVDPA by europium nitrate. (Up) successive injection at 25 °C of 10 µL of 1.5 mM solution of Eu(III) on a 0.6 mM of polymer. (Down) heat flow against molar ratio.

Conclusion

In conclusion, this sub-section has provided results on the interactions of calix-PVDPA with europium. Calix-PVDPA showed high performance in trapping europium (III) ions in aqueous media. The complexation mode of star polymer and europium was well verified by extensive characterization using ITC, fluorimetry, ATR-FTIR, and UV-Vis analysis.

Reference

[1] D. C. Crans, A. M. Trujillo, S. Bonetti, C. D. Rithner, B. Baruah, and N. E. Levinger, "Penetration of negatively charged lipid interfaces by the doubly deprotonated dipicolinate," *Journal of Organic Chemistry*, vol. 73, no. 24, pp. 9633–9640, Dec. 2008, doi: 10.1021/jo801707y.

[2] G. K. Sandi-Iu and S. P. Verma, "TRIORGANOTIN(IV) DERIVATIVES OF FIVE MEMBERED HETEROCYCLIC 2-CARBOXYLIC ACIDS," 1987.

[3] S. Lis, "L uminescence spectroscopy of lanthanide(III) ions in solution," 2002. [Online]. Available: www.elsevier.com/locate/jallcom

[4] M. E. Martínez Barbosa, L. Bouteiller, S. Cammas-Marion, V. Montembault, L. Fontaine, and G. Ponchel, "Synthesis and ITC characterization of novel nanoparticles constituted by poly(γ-benzyl L-glutamate)-β-cyclodextrin," *Journal of Molecular Recognition*, vol. 21, no. 3, pp. 169–178, 2008, doi: 10.1002/jmr.882.

[5] R. J. Falconer, B. Schuur, and A. K. Mittermaier, "Applications of isothermal titration calorimetry in pure and applied research from 2016 to 2020," *Journal of Molecular Recognition*, vol. 34, no. 10. John Wiley and Sons Ltd, Oct. 01, 2021. doi: 10.1002/jmr.2901.

Chapter IV. Conclusion and perspectives

General conclusions and perspectives

Rare-Earth Elements (REEs) have become increasingly critical components in modern technologies. During the next few years, typical sources of REEs will be insufficient to keep pace with world demand. Additionally, the increase in industrial effluents is causing serious environmental contamination. For example, the direct discharge of toxic organic compounds and metallic ions into water may seriously damage and contaminate environments. Consequently, effective methods for the extraction of these elements have been developed.

This PhD project focused on the synthesis and preparation of new polymeric systems in order to trapp lanthanides from aqueous media using a laboratory synthesized polymer, water soluble, named poly(4-vinyldipicolinic acid) (PVDPA).

The **chapter I** presents an overview on different aspects of the research, it includes major knowledge about sources, distribution, toxicological and economical effects of heavy metals. Additionally, this chapter mainly focused on all the achievements to date of different prospects for heavy metals removal technologies and the advancement and revolution of these techniques. The use of polymer like poly(4-vinyldipicolinic acid) (PVDPA) is an outstanding approach to obtain highly innovative chelating materials. Variable modifications to this type of material, including diblock copolymers, star polymer, have been synthesized and discussed thereafter to improve the capacity of complexation with heavy metals (lanthanides and actinides).

It is therefore fluidly that this project was divided into two main complementary parts. **Chapter II** is divided into two main sections: the first sub-chapter deals with the synthesis of a new class of amphiphilic diblock copolymer polystyrene-b-poly(4-vinyldipicolinic acid), (PS-b-PVDPM) *via* Supplemental Activation Reducing Agent Atom Transfer Radical Polymerization SARA-ATRP. In this part, two different routes for copolymer synthesis have been proposed. Then nanoprecipitation was used to prepare core-shell nanoparticles in aqueous solution using the prepared copolymers. This part of project has allowed for a variety of experiments to be carried out, from copolymer synthesis and

characterization to the preparation of core-shell nanoparticles, including the investigation of their chemical and physical properties.

In the second sub-chapter in **chapter II,** the effective application of surface-active polystyrene-b-poly(4-vinyldipicolinic acid) (PS-b-PVDPA) core-shell nanoparticles in trapping rare-earth metals with a high uptake capacity is the main focus of this research. The motivation behind this study is to obtain the complexation information between the new functional nanoparticles and europium, which proves that it could be a new promising material for lanthanides scavenging, and luminescent nanoparticles preparation in an aqueous environment. By studying the complexation and thermodynamics behavior of these nanoparticles-metal interactions, we have demonstrated the impact of chain lengths of each block of copolymer on metal binding with these nanoparticles. The complexation mode of nanoparticles and europium was well verified by extensive characterizations. The results presented here will guide the development of future metal-chelating system for a myriad of applications such as luminescent nanoparticles, and lanthanide harvesting.

The **chapter III** focuses on the synthesis of novel star-shaped polymers, with multifunctional calix[6]arene-type initiators by Atom Transfer Radical Polymerization (ATRP). Two hexafunctional calixarenes derivatives were synthesized in one step and used to initiate the ATRP of 4-vinyl dimethyl dipicolinate (VDPM) by the core-first method. The effects of the structure of the initiator on the kinetic of the polymers are studied. The polymerization rates exhibited first-order kinetics with respect to the monomer. In the sub-chapter, some of these obtained star polymers have been tested for their complexation properties.

In general, the use of PVDPA polymers is a promising approach for lanthanides and actinides scavenging. Furthermore, another perspective would be to take advantage on many aspects not enough tackled in this thesis. First of all, the obtained amphiphilic block copolymer could be used with a huge range of possibilities such as honeycomb film. Secondly, luminescent nanoparticles merit additional attention. They could offer several unique optical properties for a new class of luminescent drug delivery and alternative to existing bioprobes. They can also serve as optical tags to allow visualization in vitro.

The interactions between PVDPA (nanoparticles or star polymers) and different metals should be further studied.

In order to have an overview of the work presented throughout this manuscript, the main results obtained in the chapter II and III are summarized in the Table 8 below.

To conclude, this work provides new results regarding the metal extraction from aqueous media. Two polymeric systems for metal scavenging have been investigated. Most importantly, inexpensive and simple strategies have been applied in order to keep our approach economically viable. This study may be certainly useful for future work. we hope that this work will open the way to future developments and generate collaborations with experts in different related fields of research, both in academia and industry.

	Scientific issue	Key results
Chapter II	Synthesis and characterization of polymeric nanoparticles, and their metals scavenging capacity	Part I • A new class of PS-b-PVDPM diblock copolymer was successfully synthesized *via* SARA-ATRP. • Two strategies have been used to synthesize the PS-b-PVDPM, thanks to these strategies; the 2 blocks of copolymer with control lengths have been afforded. • Latex nanoparticles have been prepared by nanoprecipitation method. • Deep study of core-shell nanoparticles stability and resistance to many external stimuli (temperature and pH).
		Part II • Detailed study of NPs efficiently for metals trapping in aqueous media. • Complexation and thermodynamics behavior of these nanoparticles-metal interactions have been studied. • Elaboration of luminescent nanoparticles.
Chapter III	Star-shaped polymers and complexation system	Part I • Two hexafunctional calixarenes derivatives have been synthesized. • Novel star-shaped polymers has been synthesized by ATRP. • The effects of initiator structure on the kinetic of the polymers have been studied.
		Part II • Star polymers have been tested for their complexation properties. • Thermodynamics behavior of these star polymer-europium interactions, have been studied.

Table 8. Main results obtained in this PhD project.

Résumé en Français

Au cours des dernières années, la demande en éléments de la famille des métaux lourds (radionucléides et terres rares) a considérablement augmenté en raison de leur utilisation dans de nombreuses technologies telles les véhicules hybrides et les super aimants, car ils possèdent des propriétés physiques, chimiques et magnétiques unique. Au cours de cette thèse, nous avons développé des nouveaux matériaux polymères innovants, le poly(acide 4-vinyldipicolinique) (PVDPA), qui est soluble dans l'eau et qui s'est révélé prometteur pour l'extraction de ces métaux dispersé dans un milieu aqueux.

Au cours de cette thèse, deux systèmes polymères différents ont été préparés : des nanoparticules de type cœur-couronne et des polymères en étoile. Ces nouveaux matériaux ont été obtenus à partir d'un monomère dérivé de l'acide dipicolinique par polymérisation radicalaire contrôlée.

Le chapitre I portant sur les sources, la toxicité et le coût de certains métaux lourds. Un état de l'art dans les sources naturelles et anthropiques de métaux lourds, ses avantages économiques et environnementaux et les technologies utilisées pour la récupération de ces métaux. Ensuite, les principales techniques et stratégies à utiliser dans ce travail ont été passées en revue. Différentes techniques de polymérisation contrôlées ont été décrites, la réaction de polymérisation de type SARA ATRP que nous avons employée dans ce travail a été expliquée et commentée.

Le chapitre II est divisé en deux sections principales: le premier sous-chapitre porte sur la synthèse de nouveaux copolymères à blocs, polystyrène-bloc-poly(4-vinylpyridine-2,6-dicarboxylate de diméthyle) PS-b-PVDPM, et la préparation de nanoparticules dans l'eau basique par la méthode de « déplacement de solvant » qui permet également d'hydrolyser les fonctions esters et d'obtenir in fine des copolymères à blocs amphiphiles, polystyrène-bloc-poly(acide 4-vinylpyridine-2,6-dicarboxylique) PS-b-PVDPA. Cinq copolymères à blocs ont été synthétisés en milieu organique par SARA-ATRP en faisant varier la longueur des différents blocs. Ils ont été caractérisés par CES et par RMN du proton et ATG. Les copolymères ont ensuite été utilisés pour former des nanoparticules à base de PS-b-PVDPA dans l'eau.

La seconde partie de ce chapitre porte sur l'étude de la complexation de l'ion europium (III) par les nouveaux polymères dispersés dans l'eau (principalement sur les PS-b-PVDPA). Des nombreuses techniques d'analyse ont été utilisées (FTIR, fluorimétrie, TRLFS, UV-Vis, ITC et ICP-AES) afin d'obtenir des informations importantes sur la complexation des unités VDPA avec l'Eu^{3+}.

Le chapitre III porte sur la synthèse et la caractérisation de nouveaux polymères en étoile à partir de dérivés commerciaux de calix[6]arène. Après avoir synthétisé et caractérisé deux amorceurs d'ATRP hexafonctionnels, des polymères en étoile à 6 branches de PVDPM ont été synthétisés par ATRP en visant un DP par bras de 100. Les nouveaux polymères ont été caractérisés par CES (et RMN). Les effets de la structure de l'amorceurs sur la cinétique des polymères ont été étudiés. Dans le sous-chapitre, certains de ces polymères étoilés obtenus ont été testés pour leurs propriétés de complexation avec l'Eu^{3+}.

La forte capacité de piégeage des lanthanides dans les milieux aqueux, fait des matériaux à base de PVDPA d'excellents candidats pour différentes applications liées à l'industrie.

Dans cette thèse, nous avons tenté d'apporter une contribution à la résolution de plusieurs défis auxquels l'industrie est confrontée. Nous avons essayé d'éviter des stratégies complexes et coûteuses afin de maintenir notre approche économiquement viable. Nous espérons que ce projet encouragera des développements futurs et générera des collaborations avec des experts de différents domaines de recherche aussi bien dans le milieu académique que dans l'industrie.